

CHARLES UNIVERSITY, PRAGUE

2ND FACULTY OF MEDICINE

and

ACADEMY OF SCIENCES OF THE CZECH REPUBLIC

INSTITUTE OF EXPERIMENTAL MEDICINE



Mgr. Olena Butenko

**Expression and functional characterization of transient receptor
potential vanilloid-related channel 4 (TRPV4) in hippocampal
astrocytes after ischemia/reperfusion**

PhD thesis

Supervisor: Ing. Miroslava Anděrová, CSc.

Prague 2014

Acknowledgements

I would like to express my deep gratitude to my supervisor, Dr. Miroslava Anderova. Her scientific experience and advanced work inspired me throughout my postgraduate studies. Her support greatly helped to advance my research. I am grateful for her careful reading of my thesis and her helpful and constructive comments.

I would also like to thank to all my co-authors for successful collaborations, and to my husband, who has supported me during these years. I am very grateful to my parents, who have supported me throughout my life, and continue to be my greatest inspiration.

Author`s publications:

Publications related to the thesis and contributions of individual co-authors:

1. **Butenko O**, Dzamba D, Benesova J, Honsa P, Benfenati V, V. Rusnakova, S. Ferroni, M. Anderova. (2012) The Increased Activity of TRPV4 Channel in the Astrocytes of the Adult Rat Hippocampus after Cerebral Hypoxia/Ischemia. PLoS ONE. 7(6), IF 4.04

CONTRIBUTIONS:

Hypoxia/ischemia surgery: Butenko O.

Preparation of primary culture of astrocytes: Butenko O., Dzamba D., Honsa P.

Patch-clamp recording *in vitro* and *in situ*: Butenko O.

Calcium imaging *in vitro* and *in situ*: Dzamba D.

RT-qPCR: Rusnakova V.

Western blot: Butenko O., Benesova J.

Immunohistochemical analysis: Butenko O.

Data analysis: Butenko O., Dzamba D.

2. Pivonkova H., Benesova J., **Butenko O.**, Chvatal A., Anderova M. (2010) Impact of global cerebral ischemia on K(+) channel expression and membrane properties of glial cells in the rat hippocampus. Neurochem Int. 57 783-794, IF 3.54

CONTRIBUTIONS:

Hypoxia/ischemia surgery: Butenko O., Pivonkova H.

Patch-clamp recording *in situ*: Butenko O., Pivonkova H.

Western blot: Benesova J.

Immunohistochemical analysis: Pivonkova H.

Data analysis: Butenko O., Pivonkova H.

3. Chvátal A., Anděrová M., Neprašová H., Prajerová I., Benešová J., **Butenko O.**, Verkhatsky A. (2008) Pathological potential of astroglia. *Physiol Res.* 2008; 57(3), IF 1.65

Other author`s publications:

1. Benesova. J., Hock M., **Butenko O.**, Prajerova I., Anderova M., Chvatal A. (2009) Quantification of Astrocyte Volume Changes During Ischemia In Situ Reveals Two Populations of Astrocytes in the Cortex of GFAP/EGFP Mice. Journal of Neuroscience Research 87:96–111, IF 3.38

2. Kozubenko N., Turnovcova K., Kapcalova M., **Butenko O.**, Anderova M., Rusnakova V., Kubista M., Hampl A., Jendelova P., Sykova E. (2010) Analysis of *in vitro* and *in vivo* characteristics of human embryonic stem cell-derived neural precursors. Cell transplantation 19(4):471-86, IF 5.21

Contents

Acknowledgements	2
Author`s publications:	3
List of abbreviations	7
1. INTRODUCTION	11
1.1 Astrocytes	11
1.1.1 Morphology, phylogeny and distribution of astrocytes	11
1.1.2 Antigenic markers of astrocytes.....	13
1.1.3 Passive properties of astrocytes	14
1.1.4 Ion channel expression by astrocytes.....	17
1.1.5 Physiological functions of astrocytes	22
1.2 Cerebral ischemia	27
1.2.1 Pathogenesis of global cerebral ischemia	27
1.2.2 Astrocyte function during global cerebral ischemia	29
1.3 The TRP channels superfamily	31
1.3.1 The TRPV channel subfamily.....	33
1.3.2 TRPV4 channels	35
1.3.3 Activation and regulation of TRPV4 channels	37
1.3.4 TRPV4 in CNS physiology and pathophysiology	39
2. The aims of my PhD thesis experiments:	44
3. MATERIALS AND METHODS	45
3.1 Ethics Statement	45
3.2 Induction of cerebral hypoxia/ischemia in rats	45
3.3 Acute brain slice preparation for electrophysiology.....	46
3.4 Preparation of primary cultures of dissociated astrocytes from the CA1 region of the hippocampus	46
3.5 Solutions and reagents	47
3.6 Patch-clamp recording	49

3.7	Microfluorimetric analysis of intracellular calcium levels.....	51
3.8	Immunocytochemistry/Immunohistochemistry.....	52
3.9	Western Blotting.....	54
3.10	Quantitative PCR analyses.....	55
3.11	Data Analysis and Statistics.....	56
4.	RESULTS.....	57
4.1	Cerebral hypoxia-ischemia induces hippocampal cell damage and development of astrogliosis.....	57
4.2	Increased TRPV4 immunoreactivity in hippocampal astrocytes coincides with the development of astrogliosis.....	70
4.3	TRPV4-mediated intracellular Ca ²⁺ oscillations in reactive astrocytes are augmented <i>in situ</i> after hypoxia/ischemia.....	74
4.4	TRPV4-specific cation currents are up-regulated in reactive astrocytes <i>in situ</i> after hypoxia/ischemia.....	78
4.5	Immunohistochemical and electrophysiological analysis of primary cultured astrocytes isolated from hippocampal CA1 region revealed two distinct types of astrocytes.....	84
4.6	TRPV4-mediated intracellular Ca ²⁺ oscillations are enhanced in primary cultured astrocytes isolated from the ischemic hippocampal CA1 region.....	88
4.7	TRPV4 current activity is significantly increased in cultured astrocytes isolated from the rat hippocampal CA1 region after hypoxia/ischemia.....	90
5.	DISCUSSION.....	94
5.1	Histopathological changes after global cerebral hypoxia/ischemia.....	94
5.2	The correlation of TRPV4 gene expression with development of astrogliosis.....	96
5.3	The role of TRPV4-mediated Ca ²⁺ signalling in astrocytes after hypoxia/ischemia.....	97
6.	CONCLUSION.....	108
7.	REFERENCES.....	110
8.	ATTACHMENTS.....	125

List of abbreviations

$[Ca^{2+}]_e$	extracellular Ca^{2+} concentration
$[Ca^{2+}]_i$	intracellular Ca^{2+} concentration
$[K^+]_e$	extracellular K^+ concentration
$[Na^+]_i$	intracellular Na^+ concentration
4-AP	4-aminopyridine
4 α PDD	4-alpha-phorbol 12,13-didecanoate
AA	arachidonic acid
aCSF	artificial cerebrospinal fluid
aCSF _{0Ca}	artificial cerebrospinal fluid with 0 of extracellular Ca^{2+}
Aldh1L1	aldehyde dehydrogenase 1 family, member L1
AMPA	α -amino-3-hydroxyl-5-methyl-4-isoxazole-propionate
APQ	aquaporin channel
ATP	adenosine-5'-triphosphate
BBB	blood-brain-barrier
BLAST	Basic Local Alignment Search Tool
BSA	bovine serum albumin
CaM	calmodulin
Casp 3	caspase 3
CBF	cerebral blood flow
CFT1-LCFSN	human airway epithelial cells
CFTR	cystic fibrosis transmembrane conductance regulator
ClC	voltage-dependent Cl^- channel
CICA	calcium-activated Cl^- channel
C_m	membrane capacitance
CNS	central nervous system
Cx	connexin
DAG	diacylglycerol
DAPI	4',6-diamidino-2-phenylindole
DMEM	Dubelcco's Modified Eagle Medium
DMSO	dimethyl sulfoxide
dNTP	deoxyribonucleotide triphosphate
DRG	dorsal root ganglion
EAAT1	excitatory amino acid transporter 1
EAAT2	excitatory amino acid transporter 2
EDTA	ethylene-diamine-tetraacetic acid

EET	epoxyeicosatrienoic acid
ER	endoplasmic reticulum
Ext	extracellular solution
FBS	fetal bovine serum
FJB	Fluoro-Jade B
GABA	γ -aminobutyric acid
GFAP	glial fibrillary acidic protein
GLAST	glutamate transporter
Gln	glutamine
Glu	glutamate
GluR	glutamate receptor
GluT	glutamate transporter
GPCR	G-protein-coupled receptor
GS	glutamine synthase
H/I	hypoxia/ischemia
HEK293	human embryonic kidney 293 cells
Iba1	ionized calcium binding adaptor molecule 1
IL-1	Interleukin 1
Int	intracellular solution
IP ₃	inositol trisphosphate
IP ₃ R	inositol trisphosphate receptor
IR	input resistance
K _A	fast activating and inactivating outward K ⁺ current
KA	kainite receptor
K _{DR}	delayed outwardly rectifying K ⁺ current
K _{IR}	inwardly rectifying K ⁺ current
Lac	lactate
LY	Lucifer Yellow
MCT	monocarboxylate transporter
MTP	mitochondrial transition pore
Na _v	voltage-gated Na ⁺ channel
NCX	sodium-calcium exchanger
NG2	NG2 chondroitin sulfate proteoglycan
NGS	normal goat serum
NMDA	N-methyl-D-aspartate
ORA	outwardly rectifying astrocyte
ORG	outwardly rectifying glia

PARP-1	poly (ADP-ribose) polymerase 1
PB	phosphate buffer
PBS	phosphate buffered saline
PCNA	proliferating cell nuclear antigen
PFA	paraformaldehyde
PG	passive glia
PKA	protein kinase A
PKC	protein kinase C
PLA ₂	phospholipases A ₂
PLC	phospholipase C
PLL	poly-L-lysine
PMA	phorbol 12-myristate 13-acetate
PTB	pentobarbital
Pyr	pyruvate
RLT	RNeasy Lysis buffer
ROS	reactive oxygen species
RR	ruthenium red
RT-qPCR	reverse transcription quantitative polymerase chain reaction
S100 β	beta-subunit of cytoplasmic calcium-binding protein
SD	standard deviation
SDS	sodium dodecyl sulphate
SNARE	soluble N-ethylmaleimide-sensitive factor attachment protein receptor
SR-101	Sulforhodamine 101
TEA	tetraethylammonium
TG	trigeminal ganglion
TM	transmembrane-spanning segment
TNF α	tumor necrosis factor alpha
TRP	transient receptor potential channel
TRPA	transient receptor potential ankyrin channel
TRPC	transient receptor potential canonical channel
TRPM	transient receptor potential melastatin channel
TRPML	transient receptor potential mucolipin channel
TRPN	transient receptor potential no mechanoreceptor potential C channel
TRPP	transient receptor potential polycystin channel
TRPV	transient receptor potential vanilloid channel
TTX	tetrodotoxin
TUNEL	terminal deoxynucleotidyl transferase-mediated 2'-deoxyuridine 5'-

	triphosphate-biotin nick end labeling
VGCC	voltage-gated Ca ²⁺ channel
VRA	variably rectifying astrocyte
VRAC	volume-regulated anion channel
VRG	variably rectifying glia
V _{rest}	resting membrane potential

1. INTRODUCTION

1.1 Astrocytes

Astrocytes are the most abundant glial cells in the central nervous system (CNS), which account for 50% of the total cellular volume and 90% of the number of brain cells (Verkhatsky and Butt, 2007; Wang and Bordey, 2008). Classically, astrocytes are viewed as homogeneous cell population; they have a star-shaped morphology, extend multiple processes and they surround neighboring neurons and blood vessels (Verkhatsky and Butt, 2007).

1.1.1 Morphology, phylogeny and distribution of astrocytes

Astroglial cells are divided into several types based on their morphological features and spatial distribution in the CNS. The main group contains astrocytes, which have classic stellate or star-shaped morphology: protoplasmic astrocytes and fibrous astrocytes. The protoplasmic astrocytes are found mainly in grey matter, while fibrous astrocytes reside in white matter. Protoplasmic astrocytes have multiple bushy processes (approximately 50 μm long) (Fig. 1), which enwrap synapses and contact blood vessels (Wang and Bordey, 2008).

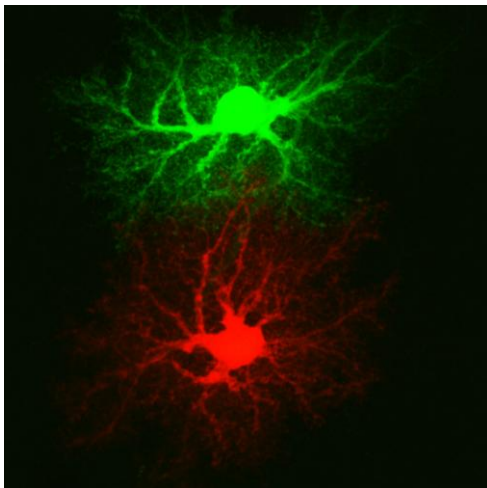


Figure 1. Morphology of adjacent protoplasmic astrocytes in rat hippocampal CA1 region; visualized by intracellular injection of Alexa 488 (green) and Alexa 568 (red) (Bushong et al., 2004)

Fibrous astrocytes are characterized by stellate morphology with less branched, thin and long processes (more than 300 μm), which envelop nodes of Ranvier by their endfeet. According to another independent nomenclature, astrocytes *in vitro* and *in situ* are divided into two categories: type 1 and type 2 astrocytes. This classification is based on the type of progenitor cells, which give rise to a certain cell type. The type 1 astrocytes originate from astrocytic

lineage, whereas type 2 astrocytes develop from bipotential progenitor cells (termed O-A2), which can produce astrocytes type 2 or oligodendrocytes (Montgomery, 1994). Another large group of astroglial cells are the radial glia. These cells are present in developing brain and have long radial processes, which play a role in scaffolding and guiding the migration of newborn neurons (McDermott et al., 2005). In addition, there are several types of specialized astroglial cells localized in specific regions of CNS, such as Müller glia of the retina, Bergmann glia of the cerebellum, tanycytes of the hypophysis and periventricular organs, pituicytes of the neurohypophysis and perivascular and marginal astrocytes of the pia mater (Metea and Newman, 2006; Verkhratsky and Butt, 2007).

During CNS evolution, the number and complexity of astrocytes increase. In the leech, for example, ganglion contains 20-30 neurons and one astrocyte. In the nematode *Caenorhabditis elegans*, the ratio of neurons to astrocytes is 6:1, while in rodents, the neuron-astrocyte ratio is 3:1 (Nedergaard et al., 2003; Verkhratsky and Butt, 2007). Astrocyte to neuron ratio in human cortex is 1.4:1 (Nedergaard et al., 2003).

Cortical and hippocampal astrocytes are organized in non-overlapping spatial microdomains. Each domain contains one single astrocyte contacting synapses and blood vessels in its vicinity. The astroglial domains are interconnected at the astrocytic endfeet via gap junctions into astroglial syncytium (Fig. 2). Every astrocyte domain contains about 140 000 synapses in rodent hippocampus and about 200 000 synapses in human brain (Mitterauer, 2010; Oberheim et al., 2008).

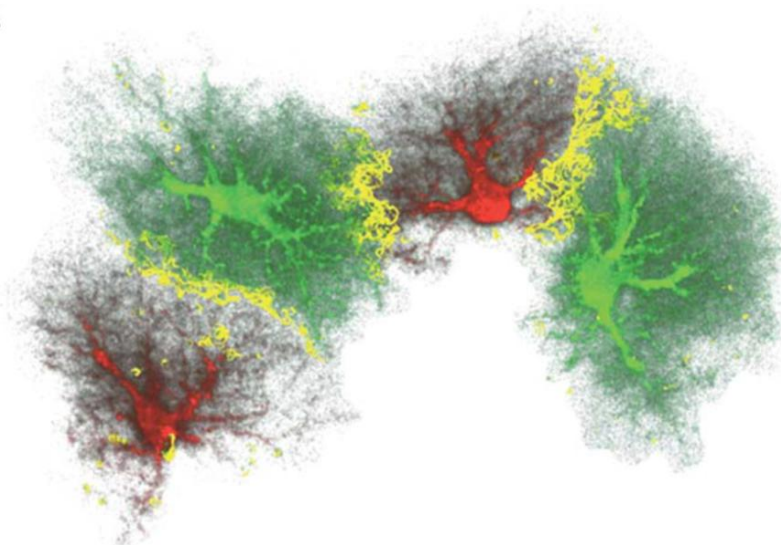


Figure 2. The domains of the astrocytes. Inter-digitation of fine cellular processes in a 3D reconstruction of dye filled astrocytes in the dentate gyrus of the hippocampus. The yellow zone indicates the border area, where cellular processes of two adjacent astrocytes interdigitate (Pekny et al., 2007).

A functional gap junction channel is composed of two connexons in the membranes of neighboring astrocytes. Each connexon comprises six symmetrical subunits, termed connexins. Astrocytes predominantly express four connexins Cx43, Cx30, Cx26 and Cx45, which form homotypic (the same connexins) or heterotypic (different connexins) gap junction channels (Mitterauer, 2010; Verkhratsky and Butt, 2007). The injection of fluorescent dye Lucifer Yellow (LY) into a single astrocyte results in fluorescent detection of 50-100 neighboring astrocytes. The coupling of astrocytes via gap junctions provides synchronization of astrocytic signalling, calcium wave propagation, and spatial buffering of potassium.

1.1.2 Antigenic markers of astrocytes

Astrocytes are characterized by the expression of intermediate filament proteins, components of cytoskeleton, such as glial fibrillary acidic protein (GFAP), vimentin, or nestin. While vimentin and nestin are inherent to immature astrocytes, the GFAP is the principal intermediate filament protein of mature astrocytes (**Fig. 3**) (Eliasson et al., 1999; Eng et al., 2000).

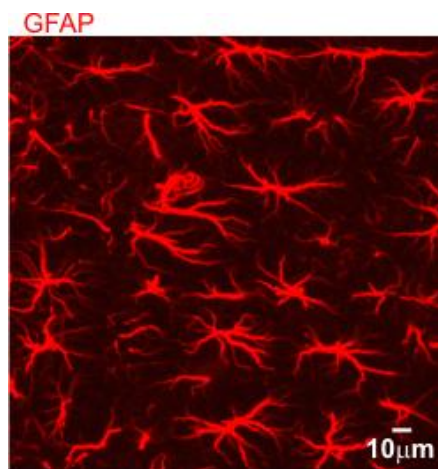


Figure 3. GFAP-positive astrocytes in the rat hippocampal CA1 region (Butenko unpublished data).

Commonly, GFAP is used as an astrocyte-specific marker that can be detected by immunocytochemistry using specific antibodies against GFAP. The normal level of GFAP expression in astrocytes varies depending on the area of the brain. For example, every Bergmann glia in the cerebellum expresses GFAP, whereas in the cortex and the hippocampus only 15-20 percent of mature astrocytes are GFAP-positive (Verkhratsky and Butt, 2007). Another commonly used marker for mature astrocytes is β -subunit of cytoplasmic calcium-binding protein (S100 β), associated with membrane and cytoskeleton (Rothermundt et al., 2003; Brozzi et al., 2009). In astrocytes, S100 β protein acts as Ca^{2+} sensor and plays a role in

cytosolic Ca^{2+} buffering (Sen and Belli, 2007). In normal brain, the levels of S100 β and GFAP proteins gradually increase with age in rodents and humans (Eng et al., 2000; Rothermundt et al., 2003). In addition, numerous studies showed that the expression of these proteins is markedly up-regulated in reactive astrocytes under pathological conditions (Eliasson et al., 1999; Brozzi et al., 2009; Middeldorp and Hol, 2011).

The other markers of mature astrocytes include glutamate transporters GLT-1 and GLAST (in human astrocytes termed EAAT2 and EAAT1), glycogen granules and glutamine synthase (GS). Additional antigenic markers of astrocytes include aquaporin 4 channels (APQ4) and inwardly rectifying K^+ channels, such as Kir4.1. Some of these markers are expressed by the majority of astrocytes in the brain (GLT-1) whereas others are found only in a subpopulation of astrocytes (Kir4.1 channels) (Wang and Bordey, 2008; Higashi et al., 2001). Recently, microarray analyses have identified new highly specific astroglial marker aldehyde dehydrogenase 1 family member L1 (Aldh1L1), with a substantially broader pattern of astrocyte expression than the traditional astrocyte marker GFAP (Cahoy et al., 2008). Interestingly, the astrocytes of neonatal and juvenile brain are immunoreactive for a chondroitin sulfate proteoglycan NG2, which is also a marker of oligodendrocyte progenitor cells (Volterra and Meldolesi, 2005; Wang and Bordey, 2008).

1.1.3 Passive properties of astrocytes

Traditionally, astrocytes have been described as homogeneous population of non-excitabile cells, unable to generate action potential under physiological conditions characterized by highly negative resting membrane potential and low input resistance. However, during the past decades different investigators described astrocytic heterogeneity with respect to ion channel expression and membrane current profiles *in situ*.

One of the first classification systems based on electrophysiological study *in situ*, describes two types of astrocytes termed “passive” and “complex”, which differ in their voltage-activated current pattern. Passive astrocytes display symmetrical non-decaying K^+ currents during depolarizing and hyperpolarizing voltage steps and are GFAP-positive, whereas complex cells show the voltage-activated outward K^+ currents and expression of S100 β (Steinhauser et al., 1994; Walz, 2000). Later, D`Ambrosio and colleagues described three electrophysiologically distinct types of astrocytes termed “complex”, “inwardly rectifying” and “linear” astrocytes. In the CA1 region of the hippocampus the linear

astrocytes are the most numerous cells and are characterized by extensive cell coupling (D'Ambrosio et al., 1998). Another two studies of Zhou and co-authors also revealed the existence of three major current profiles of hippocampal astrocytes: outwardly rectifying glia (ORG or ORA), variably rectifying glia (VRG or VRA) and passive glia (PG) (Fig. 4, see Table 1). ORG display voltage-gated Na^+ currents, delayed outwardly rectifying K^+ currents (K_{DR}) and fast activating and inactivating outward K^+ currents (K_{A}). They are found predominantly in juvenile brain, where 76% of ORG express NG2 and 24% express GLAST. VRG express K_{A} currents and inwardly rectifying K^+ currents (K_{IR}). Until juvenile period VRG-type express GLAST, however in adult brain almost 100% of VRG are NG2-positive (Zhou et al., 2006).

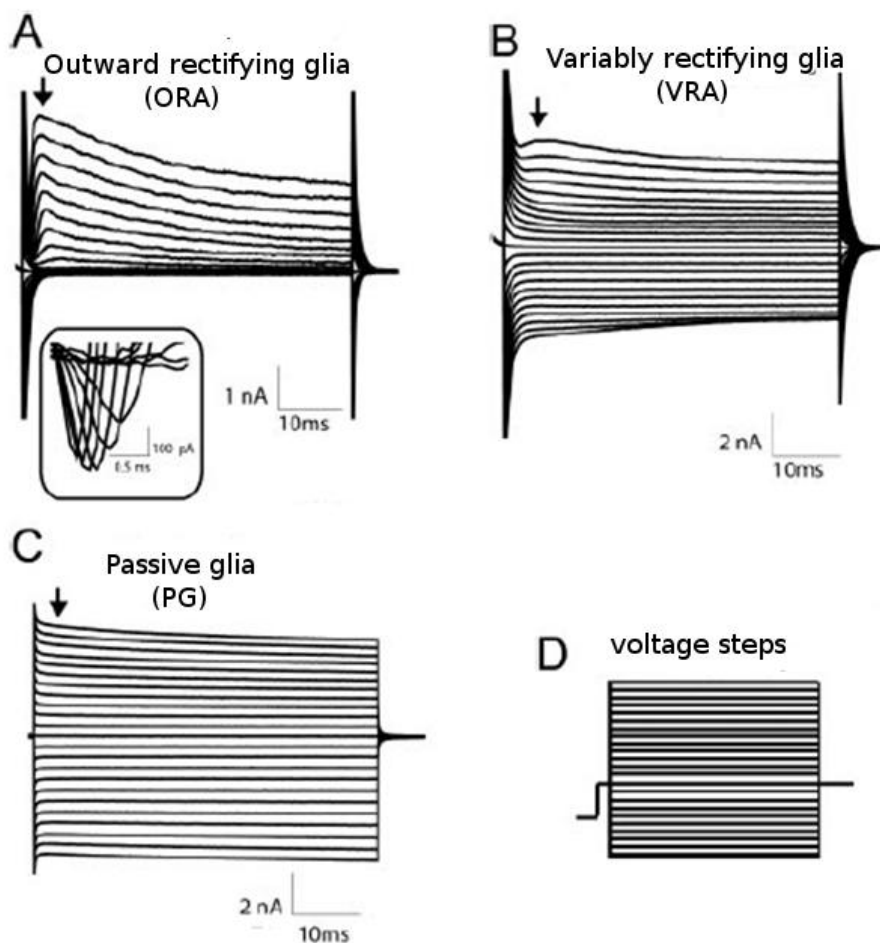


Figure 4. (A–C) Three whole-cell current profiles recorded from morphologically identified astroglia. (A) Outwardly rectifying glia (ORG) are characterized by activation of inwardly rectifying Na_v currents (see *inset*) and fast activating/inactivating outwardly rectifying K^+ (K_{A}) and delayed outwardly rectifying K^+ (K_{DR}) currents, which are induced by membrane depolarization. **(B)** Variably rectifying glia (VRG); show a combined expression of outward K_{A} , K_{DR} , and inwardly rectifying K^+ currents. **(C)** Passive glia (PG) are distinguished by the predominant expression passive K^+ currents. **(D)** voltage protocol for whole-cell voltage-clamp recording in astrocytes, cells were held at -70 mV (Zhou et al., 2006).

Similar to previous studies Zhou and colleagues showed that PG in the mature brain are the dominant electrophysiological subtype; they are characterized by large passive K^+ conductance with linear current-voltage relationship and lack of voltage-activated ion channels. Passive glia also show immunoreactivity for GLAST and GFAP, which are the markers of mature astrocytes. The expression of large passive K^+ currents is correlated with functional maturation of hippocampal astrocytes. Thus, PG firstly appear at P4 and their number increases with progress of maturation. Passive glia display highly negative resting membrane potential (ranging from -80 to -90 mV) close to K^+ equilibrium (Nernst) potential ($E_K = -90$ mV) and low membrane resistance (see **Table 1**) (Zhou et al., 2006). Numerous studies have shown that the resting K^+ conductance of passive hippocampal astrocytes is underlain by inwardly rectifying Kir4.1 and several members of two-pore domain K^+ channels, such as weakly inwardly rectifying channels TWIK-1 and outwardly rectifying TREK-1 and TREK-2 (Zhou et al., 2009; Tang et al., 2009; Wang and Bordey, 2008). In addition, the dominant passive conductance in astrocytes *in situ* also originates from intensive astrocytic coupling within the nervous tissue via gap junctions (Zhou and Kimelberg, 2000).

Table 1. Passive membrane properties of electrophysiologically identified glia and interneurons *in situ*

Cell Type	Membrane Potential, mV	Membrane Capacitance, pF	Membrane Resistance, $M\Omega$
ORG	-45.9 ± 17.2 (111)	24.5 ± 15.4 (111)	870.3 ± 705.7 (111)
VRG	-71.8 ± 12.7 (134)	74.4 ± 54.3 (134)	114.6 ± 112.4 (134)
PG	-72.8 ± 8.3 (275)	2897.7 ± 13041.0 (275)	6.3 ± 12.2 (216)
Neuron	-53.8 ± 8.2 (15)	34.1 ± 25.4 (10)	147.2 ± 170.0 (10)

The values in each column represent means \pm SD and the numbers in parentheses are the cell numbers used to calculate each value. Abbreviations: ORG, outwardly rectifying astrocyte; VRG, variably rectifying astrocyte; PG, passive glia (Zhou et al., 2006).

Besides electrophysiological phenotype, classification of hippocampal astrocytes are also based on the expression of glutamate transporters and ionotropic glutamate receptors. Matthias and colleagues showed the presence of two distinct populations of hippocampal glia *in situ*, designated as GluR cells and GluT cells. The GluR hippocampal astrocytes possess

short and thin processes and display complex current profile. Interestingly, the application of glutamate or AMPA induces rapidly-activated current in GluR cells, whereas the D-aspartate, a substrate of glutamate transporters, does not. In contrast to the GluR cells, the GluT cells display morphological and electrophysiological patterns of mature protoplasmic astrocytes. In addition, GluT cells showed numerous widely branched processes and are characterized by more negative resting membrane potential and passive current profile. Notably, the GluT cells display glutamate uptake current, whereas the functional AMPA receptors are absent. Thus, Matthias revealed two different types of glia, which express either functional AMPA-type glutamate receptors or glutamate transporters (Matthias et al., 2003).

Taken together, astrocytes *in situ* display heterogeneous electrophysiological properties, which are correlated with maturation stages and morphology.

1.1.4 Ion channel expression by astrocytes

Astrocytes express various types of voltage-gated K^+ channels including K_A , K_{DR} and K_{IR} . K_A and K_{DR} channels are activated by depolarization of membrane to potentials more positive than -40 mV. In hippocampal astrocytes *in situ* as well as in freshly isolated astrocytes, the sustained outward current is sensitive to selective K_{DR} channel blocker - tetraethylammonium (TEA) or to Cs^+ and the transient K_A outward current is blocked by 4-aminopyridine (4-AP) (Bordey and Sontheimer, 1997). K_A and K_{DR} might have influence on proliferation activity due to their high expression in immature astrocytes (Verkhatsky and Steinhäuser, 2000). The K_{IR} channels in astrocytes maintain negative resting membrane potential and provide high K^+ permeability. All K_{IR} channels are activated by membrane hyperpolarization from -60 mV to -180 mV and blocked by extracellular application of Cs^+ or micromolar concentration of Ba^{2+} . Interestingly, strong immunoreactivity of Kir4.1 is detected in astrocytes surrounding synapses and blood vessels. Such specific distribution of astrocytic Kir4.1 in the brain with elevated K^+ might correspond to spatial potassium buffering function (Higashi et al., 2001).

Voltage-gated Na^+ channels (Na_v) have been found in astrocytes *in situ* as well as cultured and freshly isolated astrocytes. However, the percentage of astrocytes expressing Na_v decreases with postnatal development, which might be linked with cell proliferation and differentiation in early postnatal stages. Astrocytic Na_v current is activated by depolarizing voltage steps more positive than -40 mV and rapidly inactivates. It can be inhibited by the Na^+

channel-specific toxin tetrodotoxin (TTX) (Bordey and Sontheimer, 1997; Sontheimer et al., 1996) and electrophysiological studies revealed TTX-sensitive and TTX-resistant Na^+ channels in astrocytes. Voltage-clamp recordings in cultured astrocytes showed that protoplasmic astrocytes express Na_v current, which is highly sensitive to TTX, whereas fibrous astrocytes displayed TTX-resistant Na^+ current. The mature hippocampal astrocytes show only TTX-sensitive Na^+ current (Verkhratsky and Steinhauser, 2000). In addition, Na^+ influx can occur also via Na^+/K^+ ATPase, Na^+ -dependent transporters, such as $\text{Na}^+/\text{HCO}_3^-$ and $\text{Na}^+/\text{K}^+/\text{Cl}^-$ cotransporters and Na^+/H^+ and $\text{Na}^+/\text{Ca}^{2+}$ exchangers (Kirischuk et al., 2012; Takuma et al., 1994; Rojas et al., 2007). The Na^+ influx through astroglial membrane is also associated with Na^+ -dependent neurotransmitter transporters, such as GLT-1 and GLAST, and γ -aminobutyric acid (GABA) transporters of the GAT-1, 3 subtypes. The increased intracellular Na^+ concentration ($[\text{Na}^+]_i$) reduces uptake of glutamate and results in the accumulation of excess glutamate in synaptic cleft. Moreover, increases in $[\text{Na}^+]_i$ stimulate Ca^{2+} entry and K^+ uptake (Kirischuk et al., 2012).

Astrocytes express several types of chloride and other anion channels (Kimelberg et al., 2006; Sik et al., 2000). The majority of studies concerning Cl^- channel expression has been done on cultured astrocytes. There are five distinct families of astrocytic Cl^- channels: voltage-dependent Cl^- channels (CICs), calcium-activated Cl^- channels (CICAs), cystic fibrosis transmembrane conductance regulator (CFTR), GABA- and glycine-activated Cl^- channels (Walz, 2002) and volume-regulated anion channels (VRAC) (Kimelberg et al., 2006). The main physiological role of Cl^- channels in astrocytes is water homeostasis and cell volume regulation. Many studies (Walz, 2002; Parkerson and Sontheimer, 2003; Kimelberg, 2005) showed the activation of astroglial chloride channels upon swelling and their involvement in cell volume regulatory processes. In addition, cell swelling activates release of ATP and excitatory amino acids taurine, glutamate and aspartate via chloride channels, modulating synaptic transmission and neuronal excitability in pathological states (Fig. 5) (Mongin and Kimelberg, 2005; Verkhratsky and Steinhauser, 2000).

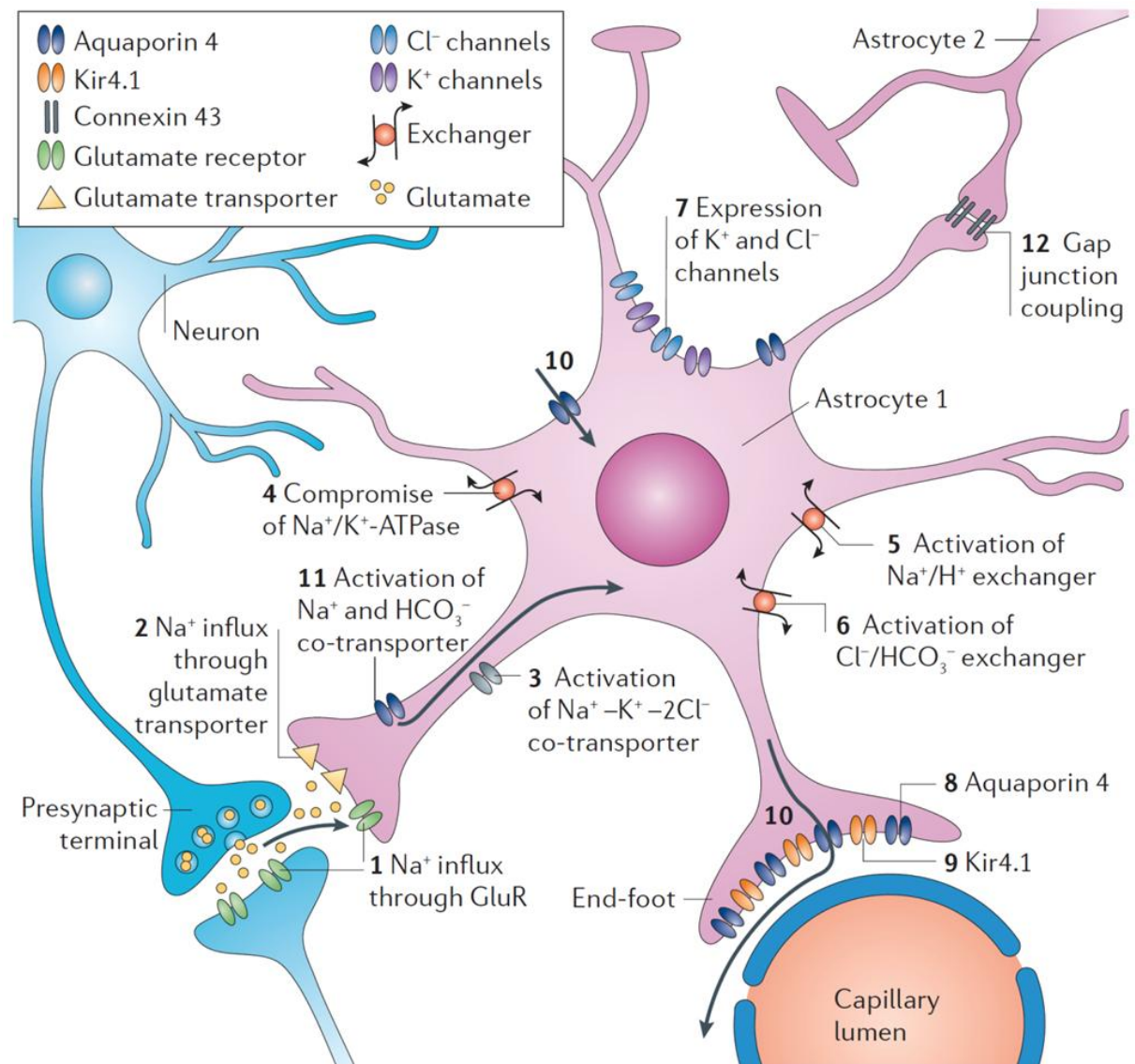


Figure 5. Swelling-related mechanisms. Glial swelling after exposure to glutamate could result from Na^+ influx, which drives glutamate transporters (1, 2). High extracellular concentrations of K^+ ($[\text{K}^+]_e$) could cause swelling through $\text{Na}^+-\text{K}^+-2\text{Cl}^-$ co-transporters (3). Astroglial swelling involves many of the mechanisms also observed in other cell types, including compromise of the $\text{Na}^+/\text{K}^+-\text{ATPase}$ (4), activation of Na^+/H^+ exchanger (5), $\text{Cl}^-/\text{HCO}_3^-$ exchangers (6). Various K^+ and Cl^- channels are expressed in swelling astrocytes (7). The aquaporin 4 (AQP4) (8) is exclusively expressed by astrocytes. The enrichment of AQP4 in astroglial end-feet surrounding blood vessels suggests that it regulates not only astrocyte volume, but also the exchange between vascular and interstitial compartments, as well as the size, shape and diffusion characteristics of the extracellular space. The co-localization of AQP4 (8) and Kir4.1 (9), the conspicuous changes in extracellular volume during spatial K^+ buffering and the observation that K^+ clearance is delayed in animals that lack perivascular AQP4 indicate that AQP4 is crucial to activity-dependent K^+ buffering. Accordingly, activity-driven increases of $[\text{K}^+]_e$ cause depolarization of adjacent astrocytes, which favors astroglial uptake of Na^+ and bicarbonate (HCO_3^-) through Na^+ and HCO_3^- cotransporters (11). The resulting increase in intracellular osmolarity drives water into astroglia through AQP4 channels. Spatial buffering of ions and water handling is also dependent on astrocyte gap junctional coupling (12) (Seifert et al., 2006).

In astrocytes, maintaining of ion and cell volume homeostasis involves water transport, which is provided by specialized water channels - aquaporins. The AQP4 is a widely distributed aquaporin in the brain and expressed primarily in astrocytes. AQP4 is concentrated in astrocytic endfeet adjacent to capillaries, in perisynaptic astroglial endfeet or in endfeet surrounding nodes of Ranvier, where it is co-localized with Kir4.1 channels and gap junction protein Cx43 (**Fig. 5**). Such strategic localization enables water redistribution and clearance of increased extracellular K^+ through astroglial syncytium during normal neuronal activity ([Amiry-Moghaddam and Ottersen, 2003](#); [Zelenina, 2010](#)). Under the pathological states, such as ischemia, trauma or inflammation, alterations in AQP4 expression result in the brain edema formation. Recent studies revealed that AQP4-null mice are more protected from cytotoxic brain edema after hyponatremia than non-transgenic mice due to reduction of water influx across the blood-brain-barrier (BBB) ([Papadopoulos and Verkman, 2007](#)). Also, Yang and colleagues demonstrated that over-expression of AQP4 in transgenic mice accelerates cytotoxic brain edema formation by increasing water influx into the brain ([Yang et al., 2008](#)). Furthermore, the studies on rats demonstrated that up-regulation of AQP4 occurs after a focal cortical contusion injury ([Sun et al., 2003](#)). Recently, the expression of AQP9 has been discovered in reactive astrocytes in infarct region after middle cerebral artery occlusion as well as after global cerebral ischemia. Interestingly, the maximal expression of AQP4 in astrocytic endfeet occurs 1 hour and 48 hours after the stroke and it is correlated with two periods of maximal hemispheric swelling. In contrast, AQP9 channels are activated in 24 hours after the stroke and are not associated with astrocytic swelling. Thus, these experimental data confirmed that AQP4 plays a key role in water transport and participates in astroglial swelling evoked by ischemia or stroke ([Badaut, 2010](#)).

Astrocytes also control intracellular Ca^{2+} level and maintain Ca^{2+} homeostasis. In astrocytes, elevated cytosolic Ca^{2+} ($[Ca^{2+}]_i$) can spread through astroglial syncytium via gap junctions and thus underlie interglial communication. Various types of plasmalemal Ca^{2+} -permeable channels ensure Ca^{2+} entry into astrocytes. There are two groups of voltage-gated Ca^{2+} channels (VGCCs): 1) low-voltage activated (T-type) and 2) high-voltage activated (L-, N-, P-, Q-, R-type). Electrophysiological and pharmacological experiments showed functional expression of VGCCs in cultured cortical astrocytes as well as freshly isolated hippocampal astrocytes ([Papura et al., 2011](#); [Alberdi et al., 2005](#)). Astroglial VGCCs are activated by membrane depolarization, which can be associated with increased level of extracellular K^+ concentration ($[K^+]_e$) during neuronal activity under physiological as well as pathophysiological conditions.

Astrocytes express ionotropic and metabotropic glutamate receptors, which modulate intracellular Ca^{2+} level (Lalo et al., 2006). The ionotropic glutamate receptors are classified based on their specific agonists into three groups: α -amino-3-hydroxy-5-methyl-4-isoxazolepropionic acid (AMPA), N-methyl-D-aspartate (NMDA) and kainate (KA) receptors. The astroglial AMPA receptors, which are expressed in the cortex, the hippocampus and the cerebellum, are devoid of GluA2 subunit, which makes them permeable for Ca^{2+} (Parpura et al., 2011). Despite the wide spatial distribution of glial AMPA receptors their physiological contribution is limited due to the rapid desensitization. In contrast, the NMDA receptors have a high Ca^{2+} permeability and provide a sustained Ca^{2+} entry without desensitization. Nevertheless, astroglial NMDA receptors are different from those in neurons. They display very weak sensitivity to Mg^{2+} block, which allows their activation at negative membrane potentials (Parpura et al., 2011; Verkhratsky et al., 2009; Parpura and Verkhratsky, 2012). Kainate receptors have been identified on mRNA and protein level in astrocytes in the corpus callosum (Garcia-Barcina and Matute, 1996). *In vitro* as well as *in vivo* studies revealed that astrocytes express metabotropic glutamate receptors, mainly mGluR3 and mGluR5. The astrocytic mGluR3 expression level increases in reactive gliosis after brain injury, epilepsy, multiple sclerosis and persistent inflammation (Durand et al., 2013).

Astrocytes express various types of functional ionotropic P2X and metabotropic P2Y purinoreceptors, which are involved in glial Ca^{2+} signalling. In cortical astrocytes P2X₁, P2X₅ and P2X₇ receptor subtypes are identified and hippocampal astrocytes show expression of P2X₁₋₄, P2X₆ and P2X₇ subtypes (Verkhratsky et al., 2009; Lalo et al., 2011). The ligand-gated P2X receptors provide ATP-induced direct Ca^{2+} and Na^+ entry through the membrane, which depolarizes the cell and activates VGCCs. Among the diversity of metabotropic G-protein-coupled P2Y receptors, P2Y₁ and P2Y₂ receptor subtypes are the most abundantly expressed by astrocytes (Scemes and Giaume, 2006). The activation of P2Y receptors stimulates production of intracellular inositol trisphosphate (IP_3) triggering release of Ca^{2+} from endoplasmic reticulum (ER) (Verkhratsky et al., 2009; James and Butt, 2002). It has been also shown that activated P2Y₁ receptors induce Ca^{2+} signals in cultured astrocytes as well as in Müller cells *in situ*, which provide the propagation of Ca^{2+} waves through gap junction (Li et al., 2001; Verkhratsky et al., 2009; James and Butt, 2002). Under pathological conditions such as ischemia, upregulation of P2X_{2,4,7} and P2Y_{1,2} receptors might participate in cytosolic Ca^{2+} overload, which may initiate glial protective or apoptotic pathways (Franke et al., 2012).

Besides all membrane proteins described above, astrocytes also express amino acid transporters for example: GABA and glutamate, and also adrenergic, serotonergic, muscarinic, and peptidergic receptors. Interestingly, astrocytes can regulate the receptor expression in response to changes in surrounding environments. For instance, in response to pathological stimuli astrocytes can increase expression of epidermal growth factors receptors, chemokines and cytokines (Porter and McCarthy, 1997; Wang and Bordey, 2008).

1.1.5 Physiological functions of astrocytes

Astrocytes are highly complex cells involved almost in all processes in the CNS. The functions of astrocytes are closely interrelated with their structure and biochemical and biophysical properties.

Astrocytes play a housekeeping role in the brain and are involved in maintaining extracellular homeostasis. First of all, astrocytes are the main support cells and serve as a scaffold for neuronal distribution and regulation of synaptogenesis. Astrocytes envelop synapses and regulate synaptic activity via release of neurotransmitters. Astrocytic endfeet surrounding blood vessels form BBB and regulate cerebral blood flow (Kimelberg and Nedergaard, 2010).

One of the main housekeeping functions of astrocytes is maintenance of K^+ homeostasis. In 1960s Kuffler and co-authors demonstrated that astrocyte membrane is highly permeable for K^+ and normal neuronal activity causes depolarization of astrocytes due to K^+ influx. These observations underlined the spatial K^+ buffering hypothesis. It suggests that astrocytes take up the locally increased K^+ ions from extracellular space and redistribute them via gap junction through the astroglial syncytium to regions with low extracellular K^+ concentration (Fig. 6) (Kuffler et al., 1966). The authors proposed that astroglial K^+ flow is driven by the difference between membrane potential of an astrocyte and K^+ equilibrium potential. Later studies indicated that the clearance of increased $[K^+]_e$ is achieved by K^+ diffusion through K_{IR} channels, predominantly via Kir4.1 channels, as their conductance increases in response to $[K^+]_e$ elevation (Kofuji and Newman, 2004; Leis et al., 2005). Furthermore, different studies demonstrated involvement of Na^+/K^+ pump and passive K^+/Cl^- uptake in the mechanism of K^+ clearance in astrocytes *in situ* (Leis et al., 2005; Walz and Wuttke, 1999; D'Ambrosio et al., 2002).

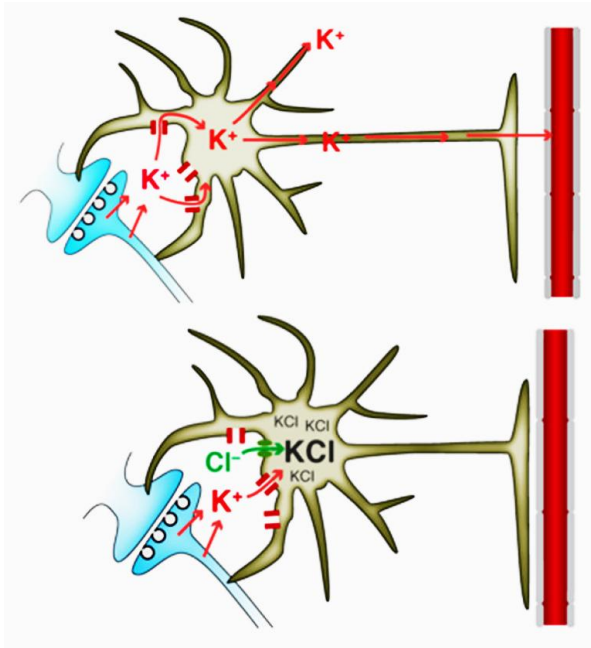


Figure 6. Schematic diagram of the two major mechanisms proposed to be involved in astrocytic buffering of excess extracellular K^+ concentration ($[K^+]_e$). In K^+ siphoning (upper image), potassium ions diffuse via gap junctions and are released distant to the site of uptake and may increase local blood flow. In the second proposed mechanism of astrocytic K^+ buffering (lower image), K^+ and Cl^- are taken up in equivalent amounts and accumulate locally in astrocytes (Kimelberg and Nedergaard, 2010).

Next pivotal function of astrocytes is the maintenance of glutamate homeostasis in synapses. In the brain astrocytes protect neurons from excitotoxicity by the clearance of extracellular glutamate, which predominantly occurs via Na^+ -dependent glutamate transporters GLAST and GLT-1 (Nedergaard et al., 2002; Oberheim et al., 2012). In astrocytes glutamate is rapidly converted to glutamine by glutamine synthetase and released into extracellular space. Glutamine is non-toxic amino acid and is absorbed by neighboring neurons, where it is again converted to glutamate by glutaminase (Fig. 7).

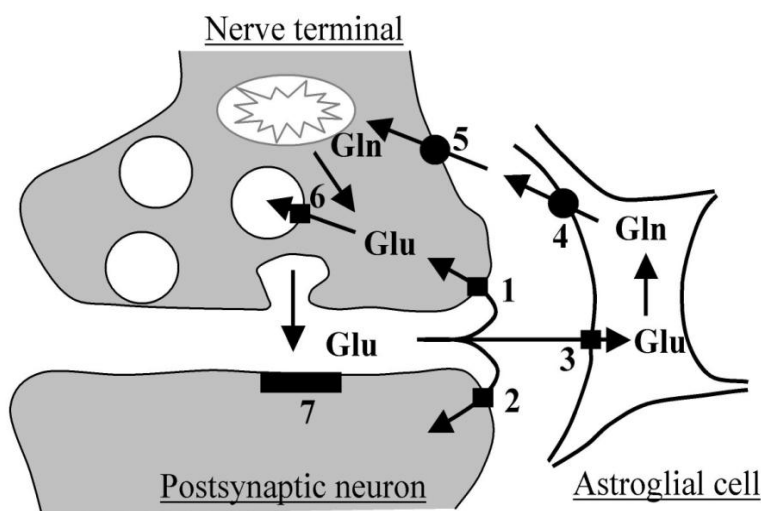


Figure 7. Glutamate (Glu) uptake and Glu/glutamine (Gln) cycle. Glu released from the nerve terminal by exocytosis is taken up by neuronal Glu transporter present presynaptically (1) and postsynaptically (2) and by glial Glu transporter (3). Glu/Gln cycle is one type of Glu recycling, but the significance is still unclear *in vivo*. Astrocytes detoxify Glu by converting it to Gln. Gln is subsequently released from the glial cells by glial Gln transporter (4) and taken up by neuronal Gln transporter (5). Neurons convert Gln back to Glu, which is loaded into synaptic vesicles by vesicular Glu transporter (6). (7), postsynaptic Glu receptors (Tao et al., 2005).

transporter (5). Neurons convert Gln back to Glu, which is loaded into synaptic vesicles by vesicular Glu transporter (6). (7), postsynaptic Glu receptors (Tao et al., 2005).

In astrocytes, glutamate uptake is coupled with activation of glycolysis. The Na^+ influx, which accompanies glutamate uptake, activates Na^+/K^+ ATPase. In astrocytes, the increase in Na^+/K^+ pump activity stimulates glucose uptake and its glycolytic processing, which results in ATP production required for pump activity and production of lactate. Lactate is an essential source of energy for neurons and mechanism of its production, release from astrocytes and its involvement in neuronal activity associated with synaptic transmission is described in the model of “astrocyte-neuron lactate shuttle” (Fig. 8) (Magistretti, 2006; Fillenz, 2005; García-Cáceres et al., 2012).

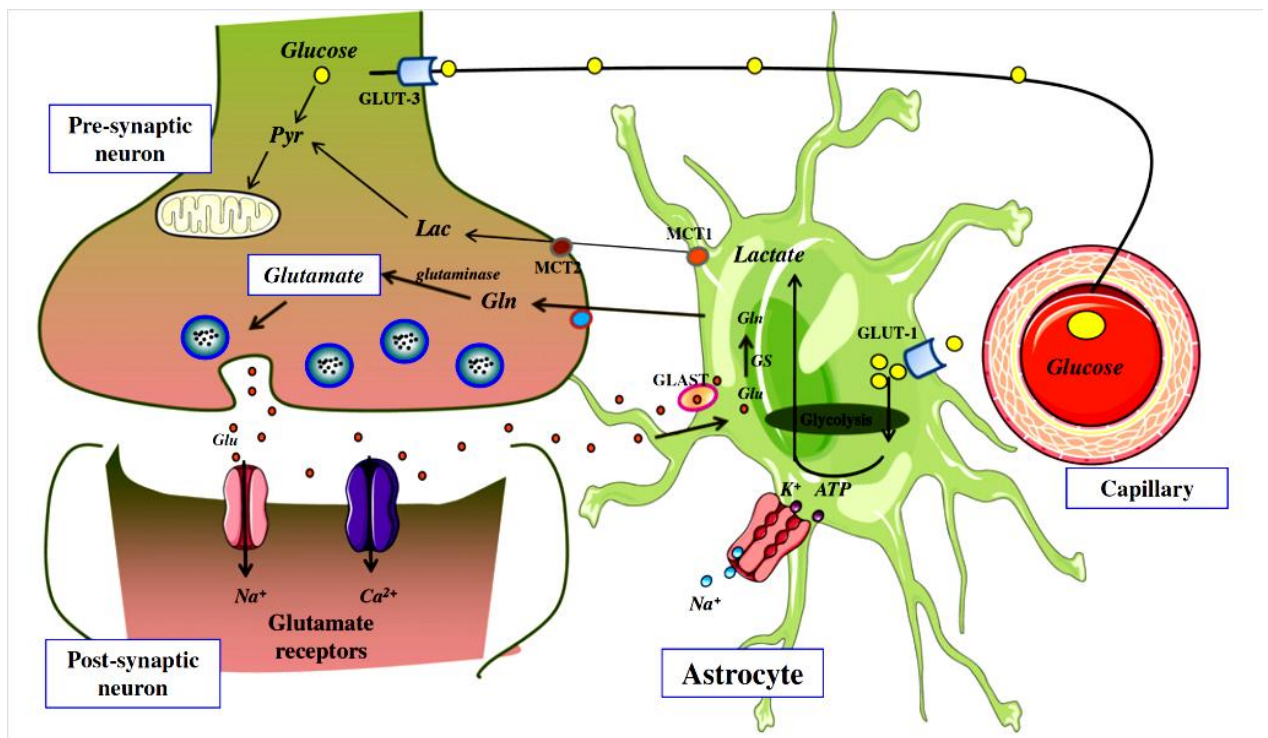
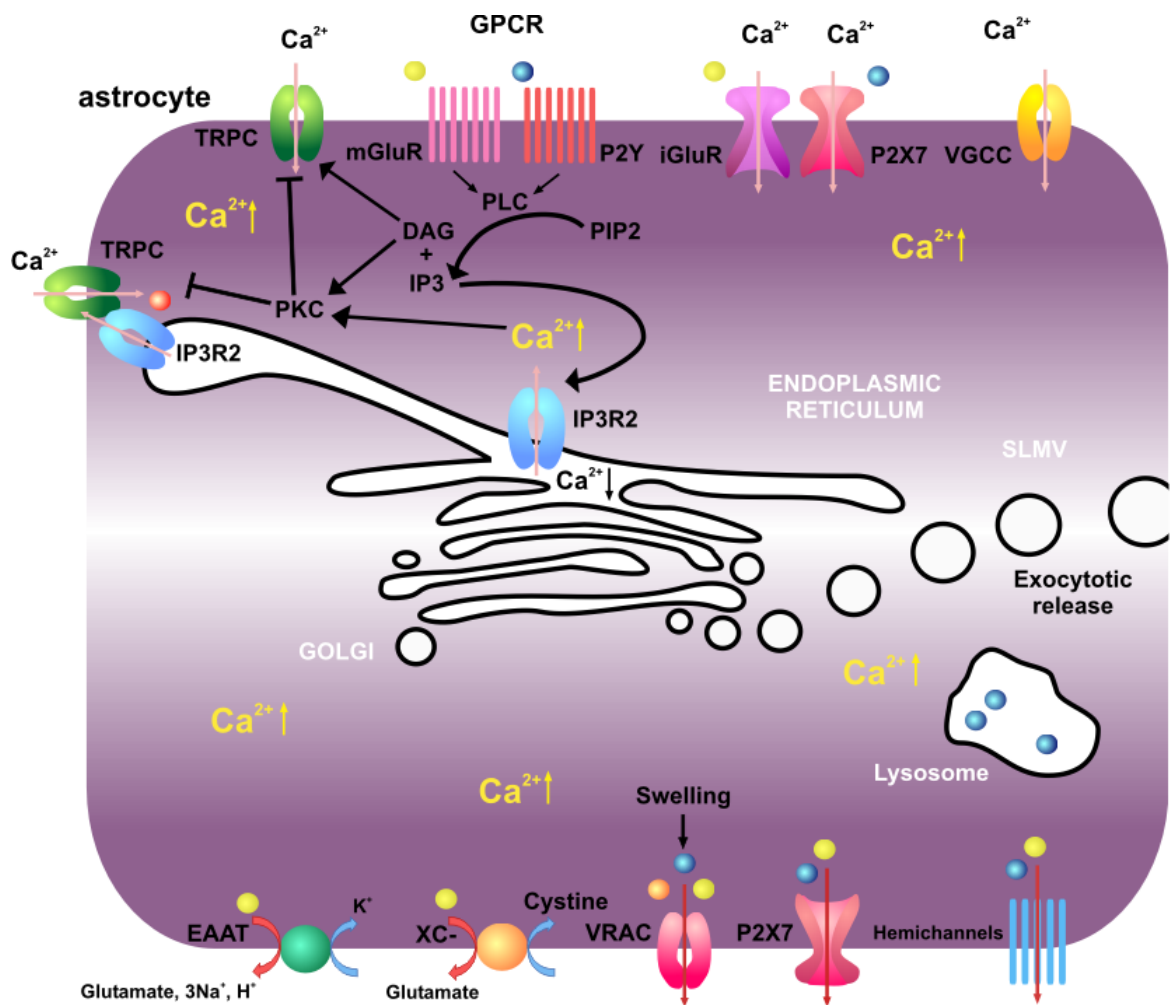


Figure 8. Schematic representation of glucose and glutamate transport, metabolism and secretion by astrocytes and neurons. The glutamate/glutamine cycle is tightly coupled to glucose oxidation in astrocytes, which then release lactate to be taken up by neurons and be oxidized. Abbreviations: Lac - lactate; Pyr - pyruvate; GLAST - glutamate/aspartate transporter; Glu - glutamate; GLUT - glucose transporter; GS - glutamine synthetase; GLN - glutamine; MCT - monocarboxylate transporter (García-Cáceres et al., 2012).

Astrocytes also possess mechanisms for controlling intracellular Ca^{2+} levels. Large body of evidence showed that astrocytes *in vitro* as well as *in situ* are able to respond to neuronal activity with the increases of cytosolic Ca^{2+} and moreover, they are able to spread Ca^{2+} signals into adjacent astrocytes (Cornell-Bell et al., 1990; Dani et al., 1992; Porter and McCarthy, 1997; Simard and Nedergaard, 2004; Wang et al., 2006). Current evidences indicate two types of astrocytic Ca^{2+} signalling: Ca^{2+} oscillation and propagating Ca^{2+} waves

(Takano et al., 2009). Ca^{2+} oscillations are repetitive increases in cytosolic Ca^{2+} concentration within single cell, which can be induced by several transmitters such as glutamate, GABA and ATP or by removal of extracellular Ca^{2+} via Ca^{2+} -permeable channels in cell membrane (Takano et al., 2009). On the other hand, the mechanism of astroglial Ca^{2+} oscillations results from the release of Ca^{2+} from internal stores through canonical phospholipase C (PLC) pathway. The mechanism of PLC pathway includes the activation of metabotropic G-protein-coupled receptor (GPCR), phospholipase C (PLC)-dependent production of diacylglycerol (DAG) and IP_3 from the membrane phospholipids. IP_3 binds to inositol trisphosphate receptors (IP_3Rs) on the membrane of endoplasmic reticulum (ER) and activates Ca^{2+} release from the ER. These Ca^{2+} increases generate Ca^{2+} spikes or Ca^{2+} oscillations (**Fig. 9**) (Nedergaard et al., 2003). The Ca^{2+} waves are mainly associated with activation of G-protein coupled purinergic receptors and plasmalemmal VGCC, and they spread through astroglial syncytium via gap junctions for a long distance. It has also been demonstrated that Ca^{2+} can enter through newly discovered transient receptor potential cationic channels (Ben Achour et al., 2010). Under physiological conditions spontaneous astroglial Ca^{2+} oscillations and subsequent release of neurotransmitters can modulate neuronal activity and regulate cerebral vasculature (Takano et al., 2009; Zonta et al., 2003; Straub and Nelson, 2007). Moreover, the astroglial Ca^{2+} signalling plays a crucial role in astrocytic activation following CNS injury (Takano et al., 2009; Nedergaard et al., 2003).


















- | | | | |
|---|--|---|--|
|  | Glutamate |  | VGCC (voltage-gated calcium) |
|  | ATP |  | TRPC (transient receptor potential channel C-type) |
|  | D-serine |  | P2Y (metabotropic purinergic receptor) |
|  | Calcium influx factor (CIF) |  | mGluR (metabotropic glutamate receptor) |
|  | VRAC (volume-regulated anion channel) |  | P2X (ionotropic purinergic receptor) |
|  | Hemichannels |  | iGluR (ionotropic glutamate receptor) |
|  | EAAT (excitatory amino acid transporter) |  | IP3R2 (inositol 3,4,5-triphosphate receptor 2) |
|  | XC- (glutamate-cystine exchanger) | | |

Figure 9. Mechanism of Ca²⁺ increase in astrocytes. The most widely accepted mechanism for astrocytic Ca²⁺ increase is dependent on GPCR activation. GPCR activation leads to the depletion of intracellular Ca²⁺ stores via the canonical PLC/InsP₃R pathway. In addition, the products of phosphatidylinositol 4,5-bisphosphate (PIP₂) hydrolysis by PLC, InsP₃ and DAG, gate Ca²⁺ entry through TRPCs. Alternatively, extracellular calcium can enter through-activated ionotropic receptors (iGluR or P2X), or through VGCCs. Transmitters can be released via Ca²⁺-dependent and -independent mechanisms. Ca²⁺-dependent vesicular exocytosis has been proposed as the main source of secreted astrocytic glutamate and D-serine. Glutamate, D-serine and ATP appear to be released from synaptic-like microvesicles (SLMVs), while ATP is also released from lysosomes by exocytosis. Besides, Ca²⁺ elevations can also lead to ATP and glutamate release through hemichannels and the ATP via purinoreceptor channel P2X7. Ca²⁺-independent mechanisms include reversal of glutamate transporters (excitatory amino-acids transporters, EAATs) and transmitter efflux through volume-regulated anion channels (VRACs) (for ATP, glutamate and D-serine) or the glutamate–cystine exchanger XC (Ben Achour et al., 2010).

1.2 Cerebral ischemia

Cerebral ischemia is either caused by occlusion of blood vessels supplying the brain or by systemic decrease of cerebral blood flow (CBF), both resulting in brain damage. Global ischemic injury is caused by transient cardiac arrest, shock and asphyxia, while focal ischemia (stroke) occurs in consequence of thrombosis or embolism (Harukuni and Bhardwaj, 2006; VanGilder et al., 2012; Verkhratsky and Butt, 2007). The area of focal cerebral ischemia resulting from the regional reduction of CBF consists of “infarction core” with severely reduced blood flow, which is surrounded by “penumbra”, a zone with residual circulation (Harukuni and Bhardwaj, 2006). Within the area of ischemic “core” the necrotic cell death occurs very rapidly during the first minutes; however, within the “penumbra” cell death is delayed and happens mostly via apoptotic pathway (Lo et al., 2003; Doyle et al., 2008). Global cerebral ischemia is characterized on cellular level by subchronic and selective hippocampal CA1 pyramidal neuronal death, microglia activation and development of reactive astrocytes (Lipton, 1999; Abe et al., 1995; Anderova et al., 2011). The period of reperfusion (CBF restoration) can also be potentially damaging due to increase of reactive oxygen species (ROS) or cerebral edema formation (Harukuni and Bhardwaj, 2006).

1.2.1 Pathogenesis of global cerebral ischemia

Global cerebral ischemia and reperfusion are characterized by cascade of pathogenic events that progress over time. After the onset of ischemia the inhibition of ATP synthesis results in the depletion of ATP stores within two minutes (Small et al., 1999; Doyle et al.,

2008). Such energy breakdown leads to the loss of ion gradients, uncontrolled entry of Ca^{2+} and Na^+ followed by neuronal membrane depolarization and excessive release of glutamate into the extracellular space. Under physiological conditions the excess glutamate is taken up by astrocytes; however, under ischemic conditions the glutamate re-uptake is compromised or even reversed, which leads to dramatic increase of extracellular concentration of glutamate. Elevated extracellular glutamate concentration induces prolonged and sustained activation of Ca^{2+} permeable channels, ultimately resulting in amplification of Ca^{2+} influx (Small et al., 1999; Harukuni and Bhardwaj, 2006). Calcium overload and excitotoxicity initiate the mitochondrial dysfunction and excessive generation of mitochondrial ROS. High level of ROS induces further damage by oxygenizing cellular proteins, lipids, nucleic acids and carbohydrates. Moreover, ROS and further Ca^{2+} overload induce formation of non-specific mitochondrial transition pores (MTP) in inner membrane and the opening of MTP results in loss of membrane potential, mitochondrial swelling and disruption of outer mitochondrial membrane. Consequently, the MTP opening allows free efflux of mitochondrial Ca^{2+} and pro-apoptotic proteins such as cytochrom C and pro-caspases into cytoplasm (Lo et al., 2003; Verkhatsky and Butt, 2007). Additionally, ischemia activates nitric oxide synthase, which leads to increased production of nitric oxide (NO) and together with superoxide the strong oxidant peroxynitrite (ONOO^-) is generated. The oxidative stress and nitric oxide are linked with DNA damage and excessive activation of poly-(ADP-ribose) polymerase-1 (PARP-1) results in ATP depletion, cell starvation and death (**Fig. 10**) (Doyle et al., 2008; Lo et al., 2003; Szeto, 2006).

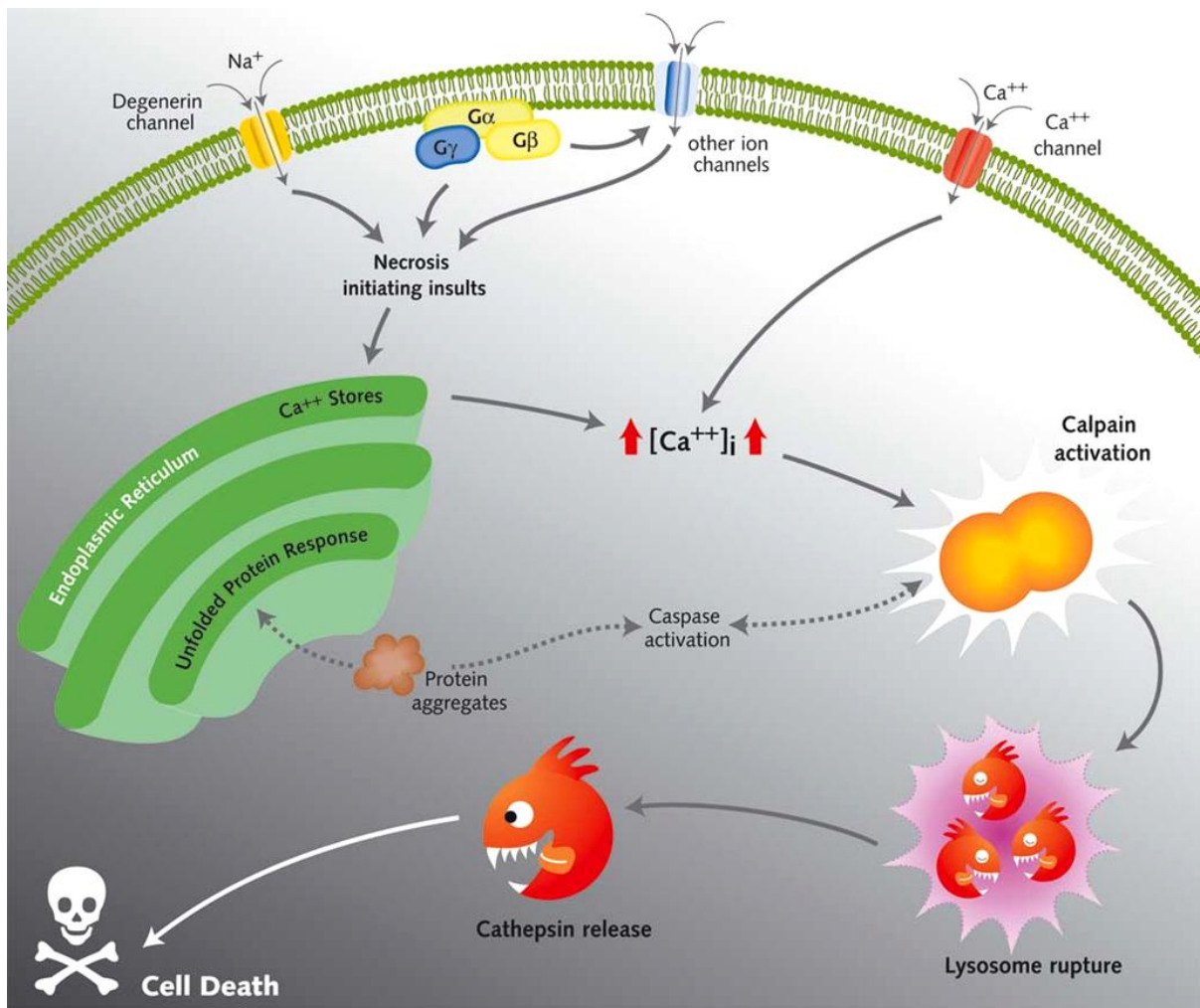


Figure 10. A likely death scenario. Many diverse initiating conditions that trigger necrosis may provoke a net increase in the cytoplasmic calcium concentration ($[Ca^{2+}]_i$), either by stimulating uptake of extracellular calcium or by facilitating the release of calcium stores from the endoplasmic reticulum. Calcium could, in turn, signal the mobilization of executioner cathepsin proteases and other hydrolases through calpain activation. Calpains have also been implicated in the activation of proapoptotic caspase proteases (Syntichaki and Tavernarakis, 2002).

1.2.2 Astrocyte function during global cerebral ischemia

The most vulnerable and sensitive cells to global cerebral ischemia are hippocampal CA1 pyramidal neurons and neurons in *hilus* of *dentate gyrus* (Small et al., 1999). The neuronal cell death is associated with glutamate excitotoxicity, which results in massive Ca^{2+} influx through NMDA receptors. The increased $[Ca^{2+}]_i$ activates numerous proteolytic enzymes, which induce neuronal necrotic cell death. On the other hand, astrocytes are more resistant to ischemic shock; they are able to maintain metabolic and structural integrity longer than neurons (Gurer et al., 2009). They respond to ischemia by transformation into

“activated” state defined as reactive astrogliosis, which has positive as well as negative impact on the neighboring nervous tissue (Small et al., 1999). The astrocytes become activated after the induction of inflammatory mediators, which are released in ischemic region. Activated astrocytes synthesize *de novo* and release inflammatory mediators, such as tumor necrosis factor α (TNF α), interleukin-1 β (IL-1 β), prostaglandins, arachidonic acid (AA) and oxygen free radicals. In addition, activated microglia release the proinflammatory cytokines TNF α , stromal cell-derived factor-1 α and prostaglandins in extracellular space that amplify astroglial activation (Liu et al., 2011).

During the first days after the onset of ischemia reactive astrocytes form glial scar, which surrounds the damaged brain tissue and prevents damage propagation. On the other hand, hypertrophied reactive astrocytes contribute to the extracellular space volume decrease by forming compact glial scar, which consequently limits regeneration of axons or entry of inflammatory cells, and it enhances accumulation of glutamate and inflammatory molecules, which may amplify cell damage (Fig. 11) (Barreto et al., 2011).

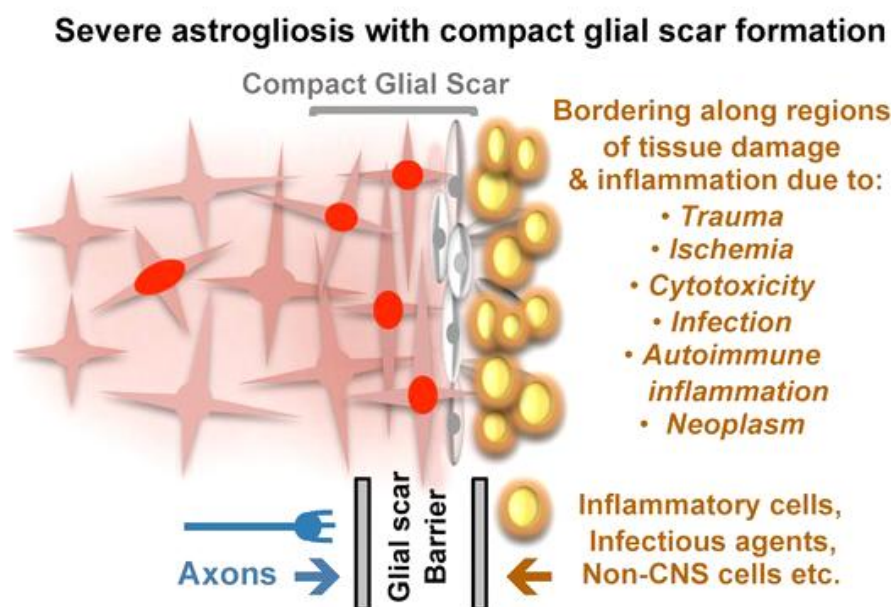


Figure 11. Severe reactive astrogliosis with compact glial scar formation occurs along borders to areas of overt tissue damage and inflammation, and includes newly proliferated astrocytes (with red nuclei in the figure) and other cell types (gray in the figure) such as fibromeningeal cells and other glia, as well as deposition of dense collagenous extracellular matrix. In the compact glial scar, astrocytes have densely overlapping processes. Mature glial scars tend to persist for long periods and act as barriers not only to axon regeneration but also to inflammatory cells, infectious agents, and non-CNS cells in a manner that protects healthy tissue from nearby areas of intense inflammation (Sofroniew and Vinters, 2010).

Despite the ischemic shock reactive astrocytes are able to supply neuronal energy needs in the brain by anaerobic production of lactate. However, long term anaerobic glycolysis can promote further ischemic damage due to increased lactic acidosis (Rossi et al., 2007). In the early stages after ischemia astrocytes are also able to take up the glutamate via specific astroglial Na^+ /glutamate co-transporters, thus protecting neurons from the extensive glutamate excitotoxicity (Rossi et al., 2007). Nevertheless, under conditions of severe ischemia, the reversal of glutamate transporters due to Na^+ accumulation in the astrocyte cytoplasm leads to glutamate release and an additional damage of the tissue (Leis et al., 2005). During ischemia the elevation of extracellular K^+ triggers astroglial K^+ uptake and distribution of K^+ through gap junctions, which results in spreading the death messengers through the astroglial syncytium. Thus, persistent massive influx of K^+ contributes to the waves of depolarization termed “spreading depression,” which expand the area of infarction zone (Chen and Swanson, 2003). Furthermore, high $[\text{K}^+]_e$ induces swelling of astrocytes via activation of K^+ channels and aquaporins, namely AQP4 (Badaut et al., 2002). The ischemia-induced astrocyte swelling is accompanied by activation of Cl^- and VRAC channels, which mediate the efflux of glutamate and other amino acids, and contribute to astrocyte volume recovery (Benfenati and Ferroni, 2010).

Moreover, there is considerable evidence that $[\text{Ca}^{2+}]_i$ oscillations and propagating $[\text{Ca}^{2+}]_i$ waves evoked by focal ischemia can spread through the astroglial syncytium over long distances and cause damage in the distal CNS regions (Nedergaard et al., 2010). Despite the fact that the large number of studies described the phenomenon of astroglial Ca^{2+} influx evoked by acute brain injury, the molecular identity of the ion channels and receptors involved in this event is still a subject of an intensive research. It has been suggested that in astrocytes the massive and uncontrolled plasmalemal Ca^{2+} entry after hypoxia/ischemia could be mediated by the activation of voltage-gated Ca^{2+} channels (Latour et al., 2003), NMDA receptors (Lalo et al., 2006), ATP-activated P2X_7 and P2Y receptors (Cotrina and Nedergaard, 2009) and the reversed operation of the $\text{Na}^+/\text{Ca}^{2+}$ exchanger (Matsuda et al., 2001).

1.3 The TRP channels superfamily

The **T**ransient **R**eceptor **P**otential (TRP) ion channels contain a large superfamily of cationic channels, which function as polymodal cell sensors.

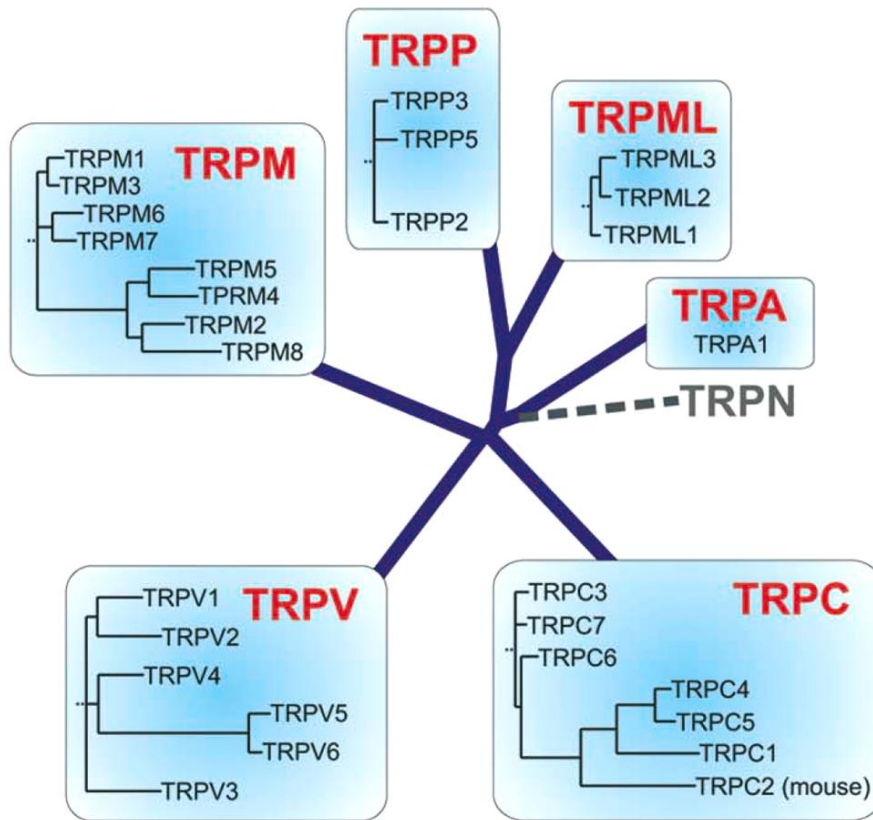


Figure 12. Phylogeny and architecture of TRP channels. Phylogenetic relationships between members of the human TRP channel superfamily. The multiple-alignment phylogenetic tree illustrates the relation between the different TRP subfamilies. Phenograms were generated independently for each subfamily. Note that TRPC2 is a pseudogene in primates and that TRPN channels have not been identified in mammals (Voets et al., 2005).

The TRP channels were first defined in 1969, when mutant *trp* gene in *Drosophila melanogaster* photoreceptors was discovered showing a transient response to light stimuli in fly eye (Voets et al., 2005; Owsianik et al., 2006). Based on the amino acid homology TRP superfamily can be classified into seven subfamilies: TRPC (Canonical), TRPV (Vanilloid), TRPM (Melastatin), TRPP (Polycystin), TRPML (Mucolipin), TRPA (Ankyrin) and TRPN (no mechanoreceptor potential C) (Fig. 12) (Nilius et al., 2005; Voets et al., 2005). The molecular structure of all TRPs contains six putative transmembrane-spanning segments (TM1-TM6) with intracellular NH₂ and COOH termini and pore loop between TM5 and TM6. TRP domains assemble into homo- or heterotetrameric functional channel with cation permeable central pore (Owsianik et al., 2006) (Fig. 13).

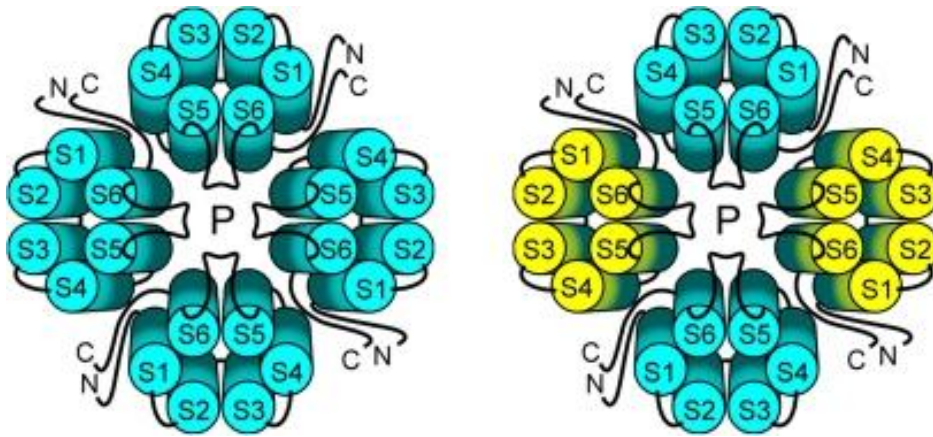


Figure 13. The quaternary structure of TRP channels allows homo- or heteromeric configurations. The four-fold symmetry of TRP channel subunit assembly offers the potential of forming homo- (**left**) or heteromeric (**right**) channel complexes. Since each of the four subunits contributes to the central pore, regulatory and biophysical properties might be altered in heteromeric channel complexes compared to their respective homooligomers. First evidence of TRP channel heteromers was obtained for the eye-specific TRP/TRPL channel complexes in *Drosophila melanogaster*. The selectivity and promiscuity of mammalian TRP channel assembly was, however, largely elusive (Schaefer M. Retrieved from: http://www.uni-leipzig.de/~pharma/main/research/schaefer/TRP_multimerisation.html)

Most TRPs are non-selective cation channels, which are permeable mainly for Ca^{2+} and less for Na^+ , with permeability ratios ($P_{\text{Ca}}/P_{\text{Na}}$) between ~ 1 and ~ 10 , except for Na^+ -permeable (TRPM3 α 1, TRPM4, TRPM5; $P_{\text{Ca}}/P_{\text{Na}} < 0.05$) channels and Ca^{2+} -permeable (TRPM3 α 2, TRPV5, TRPV6; $P_{\text{Ca}}/P_{\text{Na}} > 100$) channels. The TRP channels are activated by wide range of stimuli including intracellular or extracellular messengers, temperature change, chemical, mechanical or osmotic stress and some of them are sensitive to intracellular Ca^{2+} store depletion (Nilius et al., 2007; Ramsey et al., 2006). According to their activation these channels are involved in variety of physiological functions, such as sensory transduction, pheromone signalling, mechanosensation, temperature sensation, nociception, osmoregulation and ion homeostasis, particularly of Ca^{2+} and Mg^{2+} (Gees et al., 2010).

1.3.1 The TRPV channel subfamily

The mammalian TRPV channel subfamily is divided into six members - TRPV1-6 and they are widely expressed in the nervous system. The TRPV1-4 members are activated by the broad range of stimuli and involved in thermo-, mechano- and osmosensation. They are permeable mainly for Ca^{2+} , with permeability ratio $P_{\text{Ca}}/P_{\text{Na}}$ between ~ 1 and ~ 10 . The first described and the most studied TRPV1 channels are activated by capsaicin – the active

component of chilli pepper, noxious heat (see **Table 2**), H^+ and endocannabinoid lipids, such as anandamide and eicosanoids (Nilius et al., 2007). TRPV1 channels are expressed in hippocampal pyramidal neurons in CA1, CA3 areas and in *dentate gyrus* (Kauer and Gibson, 2009). Moreover, they are localized in dorsal root ganglion (DRG), trigeminal ganglion (TG) and peripheral nerve terminals, where they are implicated in nociception (**Fig. 14**) (Pedersen et al., 2005; Cao et al., 2009).

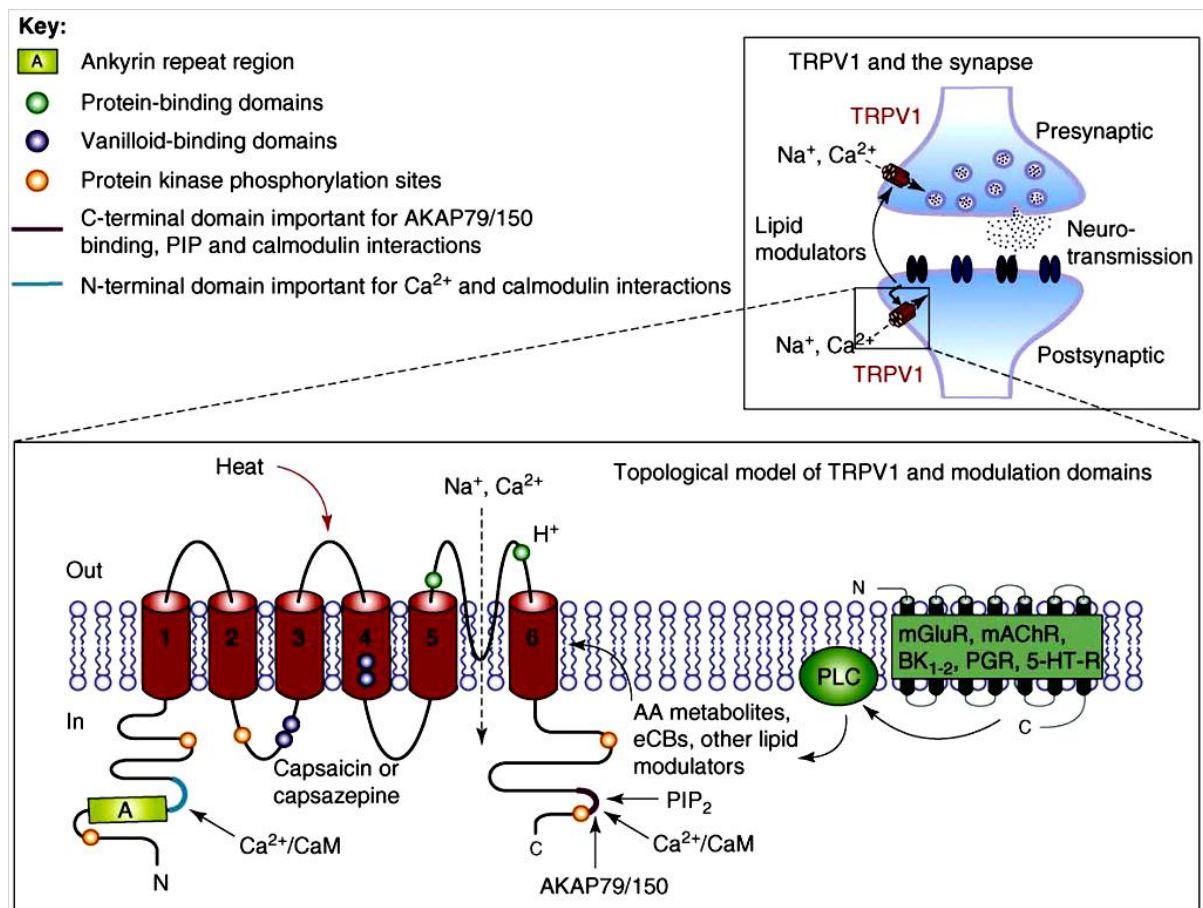


Figure 14. Diagram of the structure of the TRPV1 channel. The structures of TRPV1, TRPV2, TRPV3 and TRPV4 are similar. The N-terminal tail has multiple ankyrin repeats with a calmodulin-binding site, whereas the C-terminal tail has consensus sequences for several protein kinases, scaffolding proteins and second messengers. Numerous G-protein coupled receptors (GPCRs), primarily acting via activation of phospholipase C activate TRPV1 channels. Phospholipase C metabolites including arachidonic acid metabolites, endocannabinoids and other lipids activate the channel. Inset: potential sites of TRPV1 channels in pre- and postsynaptic membranes, where they can alter synaptic transmission and plasticity. Abbreviations: 5-HT-R - 5-hydroxytryptamine receptor; AA - arachidonic acid; BK - bradykinin receptor; CaM - calmodulin; eCB - endocannabinoid; mAChR - muscarinic acetylcholine receptor; mGluR - metabotropic glutamate receptor; PGR - progesterone receptor; PIP - phosphatidylinositol phosphate; PIP₂ - phosphatidylinositol 4,5-bisphosphate; PLC - phospholipase C (modified scheme from Kauer and Gibson, 2009).

Table 2. Thermosensitivity of TRPV channels

TRPV:	Activation temperature
TRPV1	$\geq 43^{\circ}\text{C}$ (Grandl et al., 2010)
TRPV2	$\geq 52^{\circ}\text{C}$ (Leffler et al., 2007)
TRPV3	$>30-33^{\circ}\text{C}$ (Smith et al., 2002)
TRPV4	$25-37^{\circ}\text{C}$ (Nilius et al., 2004)

The TRPV2 channels show ~50% homology to TRPV1 channels and are activated by heat or swelling via protein kinase A (PKA) pathway. TRPV2 are detected in the cerebral cortex where they co-localize with TRPV1 (Kauer and Gibson, 2009). TRPV2 are also localized in DRG neurons and probably participate in high-threshold noxious heat sensation. TRPV3 channels are also weakly Ca^{2+} permeable channels and they are expressed in DRG and trigeminal ganglion (TG) neurons and in hippocampal pyramidal neurons, the cortex, the thalamus, the striatum and the cerebellum (Ramsey et al., 2006; Kauer and Gibson, 2009; Gees et al., 2010). Recently, Shibasaki and co-authors showed that cerebellar astrocytes strongly express TRPV2 protein. Furthermore, they demonstrated TRPV2 cation current and $[\text{Ca}^{2+}]_i$ elevations in astrocytes in response to high temperature ($>48^{\circ}\text{C}$) and endogenous ligand lysophosphatidylcholine (Shibasaki et al., 2013). TRPV4 channels are expressed in the cerebellum, basal ganglia, the hippocampus and ependymal cells of the choroid plexus in lateral ventricles. TRPV4 channels are activated by moderate temperature ($25 - 37^{\circ}\text{C}$) and constitutively opened at normal body temperature (Nilius et al., 2004; Kauer and Gibson, 2009). The TRPV5 and TRPV6 are exclusively selective for Ca^{2+} ($P_{\text{Ca}}/P_{\text{Na}} > 100$) and display strong inward rectification. These channels are regulated by intra- and extracellular Ca^{2+} . In addition, TRPV5 and TRPV6 are able to form homo- or heterotetrameric channels; they are highly expressed in the small intestine, kidneys and epithelial cells, however, there are no evidence of their presence in the nervous tissue (Nilius et al., 2007; Ramsey et al., 2006).

1.3.2 TRPV4 channels

TRPV4 (OTRPC4; VR-OAC) cation channels display the 45% sequence identity with TRPV1 (Fig. 14). The TRPV4 channels consist of 871 amino acids, and each subunit contains six transmembrane segments with a pore forming loop between TM5 and TM6 and COOH and NH_2 intracellular termini (Fig. 15). The NH_2 terminus contains six ankyrin repeats, which

can be involved in association of NH₂ termini into tetrameric structure (Everaerts et al., 2010). Moreover, these repeats anchor TRPV4 channel to cytoskeleton and provide link for its activation (Nilius et al., 2004).

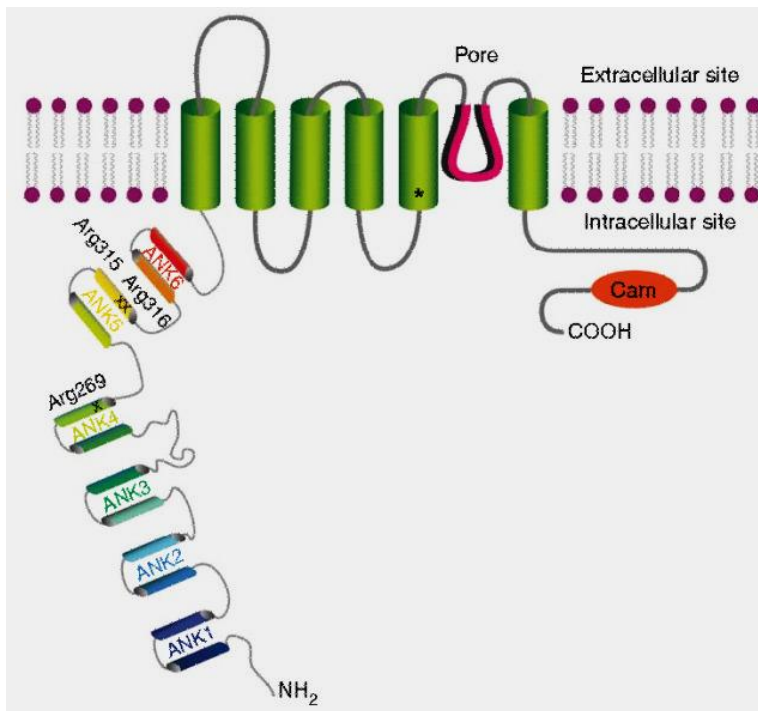


Figure 15. Schematic model of TRPV4. The TRPV4 protein is composed of a cytosolic N-terminal region and six transmembrane domains (green), including the pore region (magenta) and an intracellular C-terminal tail. The N-terminal region contains the ankyrin repeat domain (ARD), which consists of six ankyrin repeats (ANK), highlighted here in different colors (ANK1–6) (Auer-Grumbach et al., 2010).

TRPV4 channels are predominantly permeable for Ca²⁺ and less for Na⁺ and Mg²⁺ with ratio $P_{Ca}/P_{Na} \sim 10$ and $P_{Na}/P_{Mg} \sim 3$. The current-voltage (I-V) relationship displays slight outward rectification in Ca²⁺ containing extracellular solution and TRPV4 current reversal at ~ 0 mV (Fig. 16) (Owsianik et al., 2006; Everaerts et al., 2010).

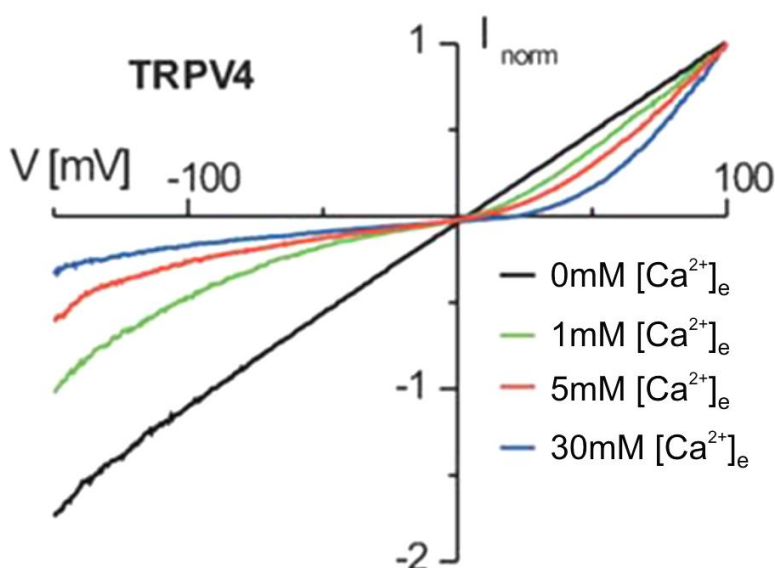


Figure 16. Functional properties of the TRPV4 pore. Current-voltage relationship for TRPV4 whole cell currents normalized to +100 mV in the presence of different [Ca²⁺]_e. Note the Ca²⁺-dependent outward rectification representing the low-affinity block of inward currents through TRPV4 by [Ca²⁺]_e (Owsianik et al., 2006).

1.3.3 Activation and regulation of TRPV4 channels

In native tissue TRPV4 channels display basal spontaneous activity, which is dependent on extracellular $[Ca^{2+}]_e$ and results in increased $[Ca^{2+}]_i$. In the absence of $[Ca^{2+}]_e$ the spontaneous TRPV4 activity is strongly reduced (Plant and Strotmann, 2007).

TRPV4 is originally identified as osmotically and swelling activated channel. The mechanism of hypotonicity and swelling-induced TRPV4 activation includes phospholipases A₂ (PLA₂) pathway and AA and epoxyeicosatrienoic acids (EETs) formation. Arachidonic acid released from membrane phospholipids following cell swelling activates TRPV4 channels and induces Ca^{2+} influx (Fig. 17) (Watanabe et al., 2003; Nilius et al., 2004; Plant and Strotmann, 2007).

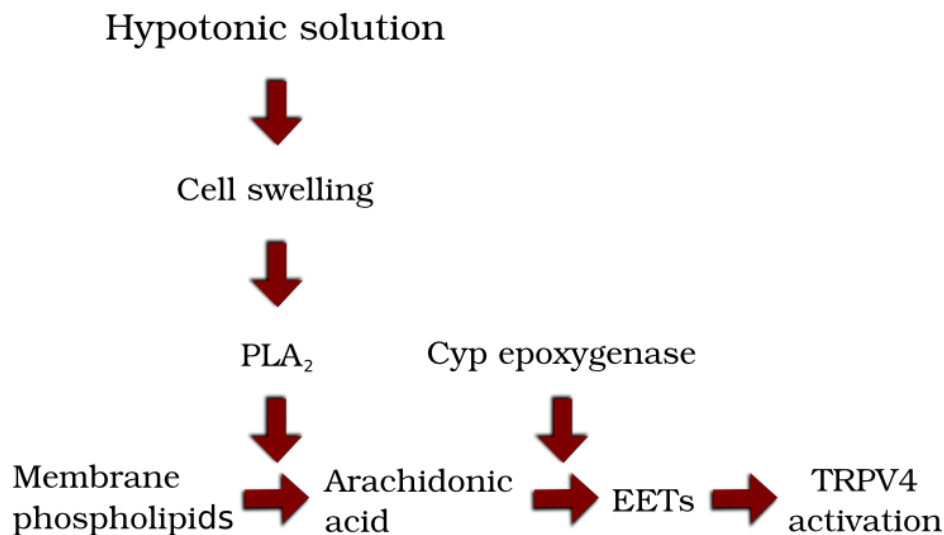


Figure 17. Hypotonicity-induced TRPV4 activation. Abbreviations: PLA₂, phospholipases A₂; Cyp epoxygenase, cytochrome 450; EETs, epoxyeicosatrienoic acids (Plant and Strotmann, 2007).

Besides moderate heat, the TRPV4 channels are activated also by specific synthetic agonists (*N*-((1*S*)-1-[[4-((2*S*)-2-[[2,4-dichlorophenyl)sulfonyl]amino]-3-hydroxypropanoyl]-1-piperazinyl]carbonyl]-3-methylbutyl)-1-benzothiophene-2-carboxamide (GSK1016790A) and phorbol ester derivate 4- α -phorbol 12, 13-didecanoate (4 α PDD) (Fig. 18) (Thorneloe et al., 2008). 4 α PDD as well as EETs directly activate TRPV4 channels (Stevens, 2011; O'Neil and Brown, 2003). The 4 α PDD-induced current is slowly-activated, transient and progressively desensitizing after repetitive administration (Vriens et al., 2009). Other phorbol 12-myristate 13-acetate (PMA) is structurally similar to 4 α PDD, but it has 10 to 50-fold lower effect on TRPV4 activation (Nilius et al., 2004).

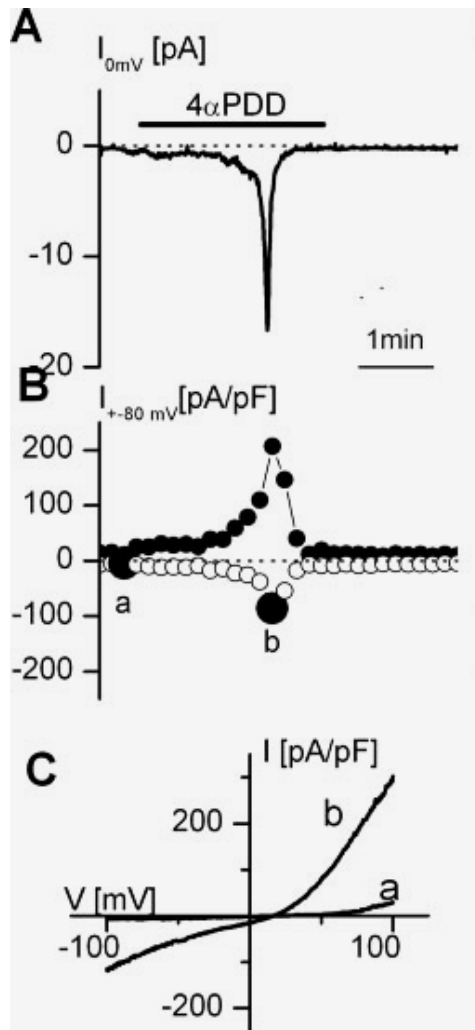


Figure 18. Activation of TRPV4 by phorbol ester derivative 4- α -phorbol 12, 13-didecanoate (4 α PDD). (A) At a holding current of 0 mV, application of 1 μ M 4 α PDD induced an inward current (I) that typically appeared with some delay and rapidly inactivated in the presence of extracellular Ca^{2+} . (B) Time course of currents at -80 and +80 mV measured from repetitively applied voltage ramps from -100 to +100 mV (holding potential 0 mV). (C) current-voltage (I-V) relationships measured at times indicated by *a* and *b* in B. Note the outward rectification in the presence of extracellular Ca^{2+} (Nilius et al., 2004).

TRPV4 channel activity as well as of other TRPs is modulated by changes in $[Ca^{2+}]_i$ or $[Ca^{2+}]_e$. The application of 4 α PDD in the presence of extracellular Ca^{2+} activates TRPV4 current, while the increase in $[Ca^{2+}]_i$ reduces TRPV4 activity. The replacement of the extracellular Ca^{2+} by Ba^{2+} or Sr^{2+} also reduces TRPV4-mediated current (Watanabe et al., 2003). TRPV4 current is inhibited by widely used TRP antagonist, such as ruthenium red (RR), which reversibly inhibits inward, but not outward current, and also by non specific inhibitors such as Gd^{3+} and La^{3+} . Moreover, TRPV4 current is inhibited by specific antagonists such as RN-1734, RN-9893 and HC-067047 (Vriens et al., 2009; Vincent et al., 2009; Everaerts et al., 2010).

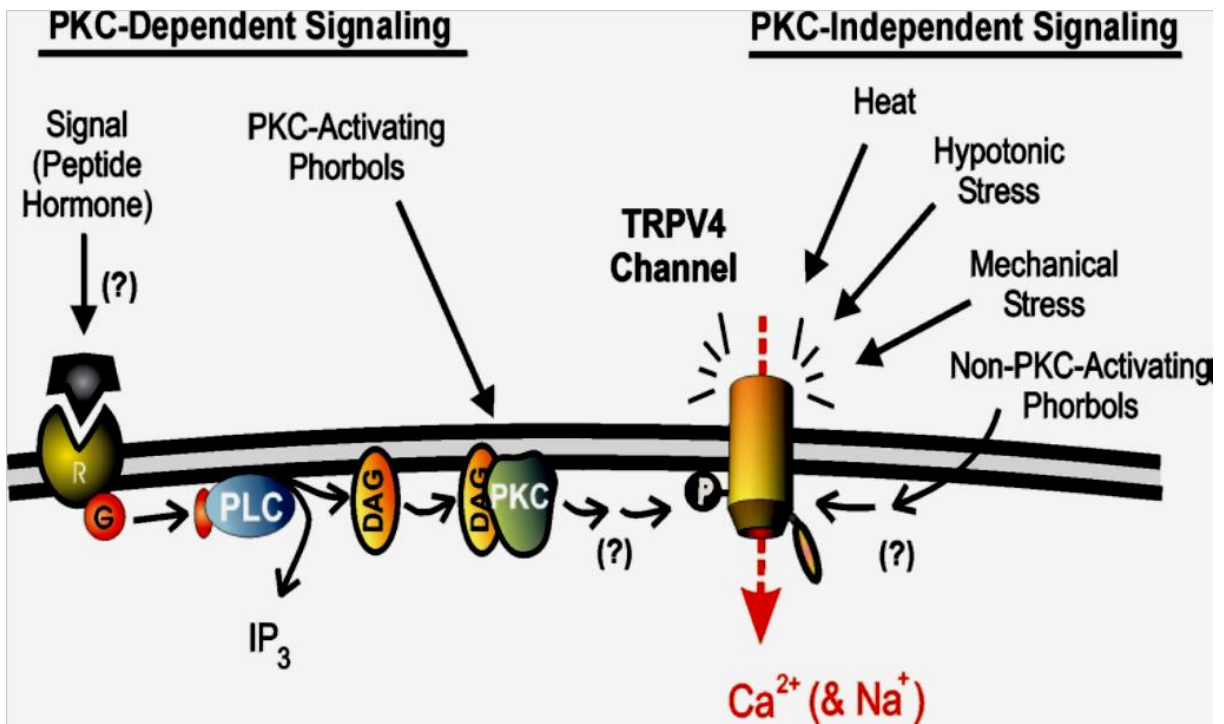


Figure 19. Molecular model showing potential converging pathways regulating TRPV4 channels as a representative example of molecular integration of microenvironmental stimuli. TRPV4 channels are permeable to calcium and monovalent cations, such as sodium. The channel appears to be regulated by at least two pathways, one protein kinase C (PKC)-dependent, the other PKC independent, although other pathways are likely to be involved in the channel activation. The range of stimuli for the two pathways is indicated. Abbreviations: R - hormone/ligand receptor; G - G protein; PLC - phospholipase C; DAG - diacylglycerol; IP₃ - inositol trisphosphate; P - potential phosphorylation site; ? – potential signalling pathways controlling activation of TRPV4 (O’Neil and Brown, 2003).

1.3.4 TRPV4 in CNS physiology and pathophysiology

TRPV4 channels are widely expressed in the CNS and the peripheral nervous system and they are implicated in a broad variety of functions from sensory detection to signal transduction (Kauer and Gibson, 2009; Nilius et al., 2004).

It has been shown that in the brain TRP channels are expressed predominantly in neurons. In DRG neuronal co-cultures Cao and co-authors described the co-expression of TRPV1 and TRPV4 and they demonstrated that 4αPDD induces an increase in $[Ca^{2+}]_i$. They showed that TRPV1 and TRPV4 channel activation occurs via PKC and suggested the role of TRPV1 and TRPV4 in nociception (Cao et al., 2009). The TRPV4 channels are also identified in hippocampal neurons, in which Shibasaki and colleagues found a strong expression of TRPV4 channels under physiological conditions. This study showed that TRPV4 channels are

activated at physiological body temperature ($\sim 37^{\circ}\text{C}$) and mediate neuronal depolarization, which suggests their role in regulation of neuronal activity. Moreover, the data indicated that at physiological body temperature TRPV4-mediated neuronal depolarization triggers neuronal firing via activation of NMDA receptors (Shibasaki et al., 2007). Recently, it was demonstrated that temperature-sensitive TRP channels in neurons are also involved in CNS pathology, such as ischemia. Lipski and co-workers demonstrated the expression of TRPM2/TRPM7 and TRPV3/TRPV4 in neurons of the CA1 subfield of the hippocampus and suggested their involvement in oxidative stress (Lipski et al., 2006). The most recent study on the hippocampal pyramidal neurons showed that activation of TRPV4 channels potentiates NMDA receptors, increases calcium overload and may contribute to glutamate excitotoxicity during stroke. Moreover, it has been shown that inhibition of TRPV4 channels provides neuroprotective effect against cerebral ischemia (Fig. 20) (Li et al., 2013).

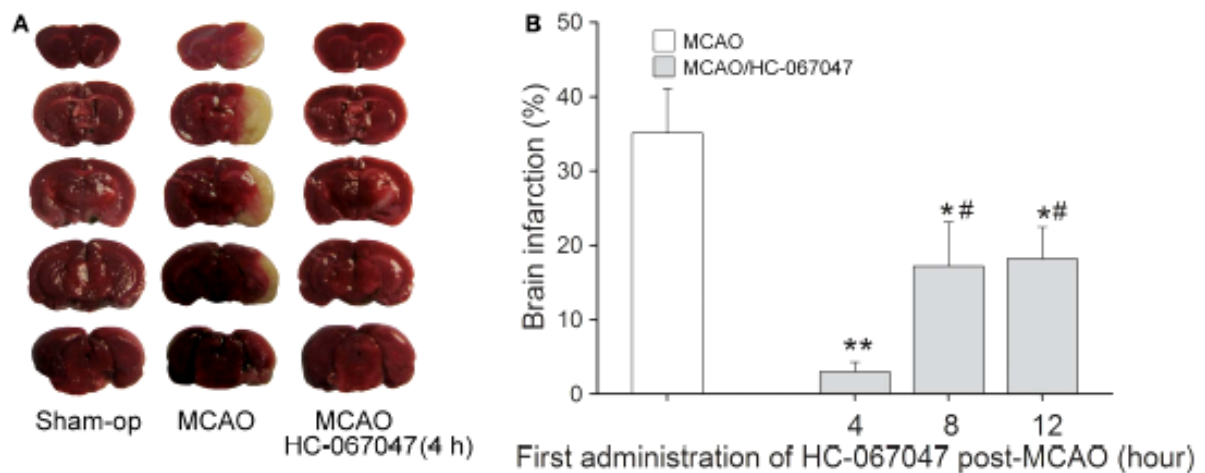


Figure 20. TRPV4 antagonist reduces brain damage after focal cerebral ischemia. (A) Representative photographs of cerebral infarction in middle cerebral artery occlusion (MCAO) mice treated with HC-067047. The treatment with HC-067047 (HC-4 h) after stroke significantly reduced the MCAO-induced cerebral infarction. (B) Time-window of neuroprotective effect of HC-067047. Bar graphs show the mean infarct volume percentage in MCAO mice that were treated with HC-067047 starting 4, 8 and 12 h post-MCAO. ** $P < 0.01$ and * $P < 0.05$ vs. vehicle-treated MCAO mice, # $P < 0.05$ vs. HC-4 h (Li et al., 2013).

Recently, Benfenati and colleagues demonstrated that primary cultured astrocytes as well as rat cortical astrocytes of strongly express TRPV4 channels (Benfenati et al., 2007). They observed that TRPV4-mediated intracellular Ca^{2+} elevation and typical TRPV4 current in cultured astrocytes are activated by $4\alpha\text{PDD}$ or hypotonicity and they are blocked by Ca^{2+} -free solution or by specific TRPV4 inhibitor (Fig. 21). In addition, in cultured astrocytes

TRPV4 channels are sensitive to hypotonic stress, and by forming a molecular complex with aquaporins, they were suggested to participate in regulating cell volume recovery (Benfenati et al., 2011; Benfenati and Ferroni, 2010; Liu et al., 2006). In the most recent study, Dunn and co-authors showed that TRPV4-mediated Ca^{2+} entry in astrocytic endfeet contributes to regulation of cerebral microcirculation. Moreover, they found that TRPV4-mediated plasmalemmal Ca^{2+} entry activates IP_3R , thus amplifying Ca^{2+} signals and initiating Ca^{2+} waves. Interestingly, the $[\text{Ca}^{2+}]_i$ increase in astrocytic endfeet stimulates release of vasoactive substances and causes vasoconstriction of adjacent arterioles, while lower $[\text{Ca}^{2+}]_i$ inhibits TRPV4 activity, thus, producing vasodilation (Dunn et al., 2013).

A recent study on organotypic slices of the juvenile hippocampus confirmed TRPV4 channel expression in astrocytes (Fig. 22, 23) and revealed their involvement in oxidative stress-induced cell death. The authors demonstrated that the application of RR or Gd^{3+} reduces astrocytic damage, thus suggesting involvement of TRPV4 channels in astroglial pathophysiology (Bai and Lipski, 2010).

However, to the best of our knowledge, the role of astrocytic TRPV4 channels during *in vivo* ischemic injury has not yet been defined. The present study was undertaken to address the pathophysiological role of TRPV4 channels in adult rat astrocytes.

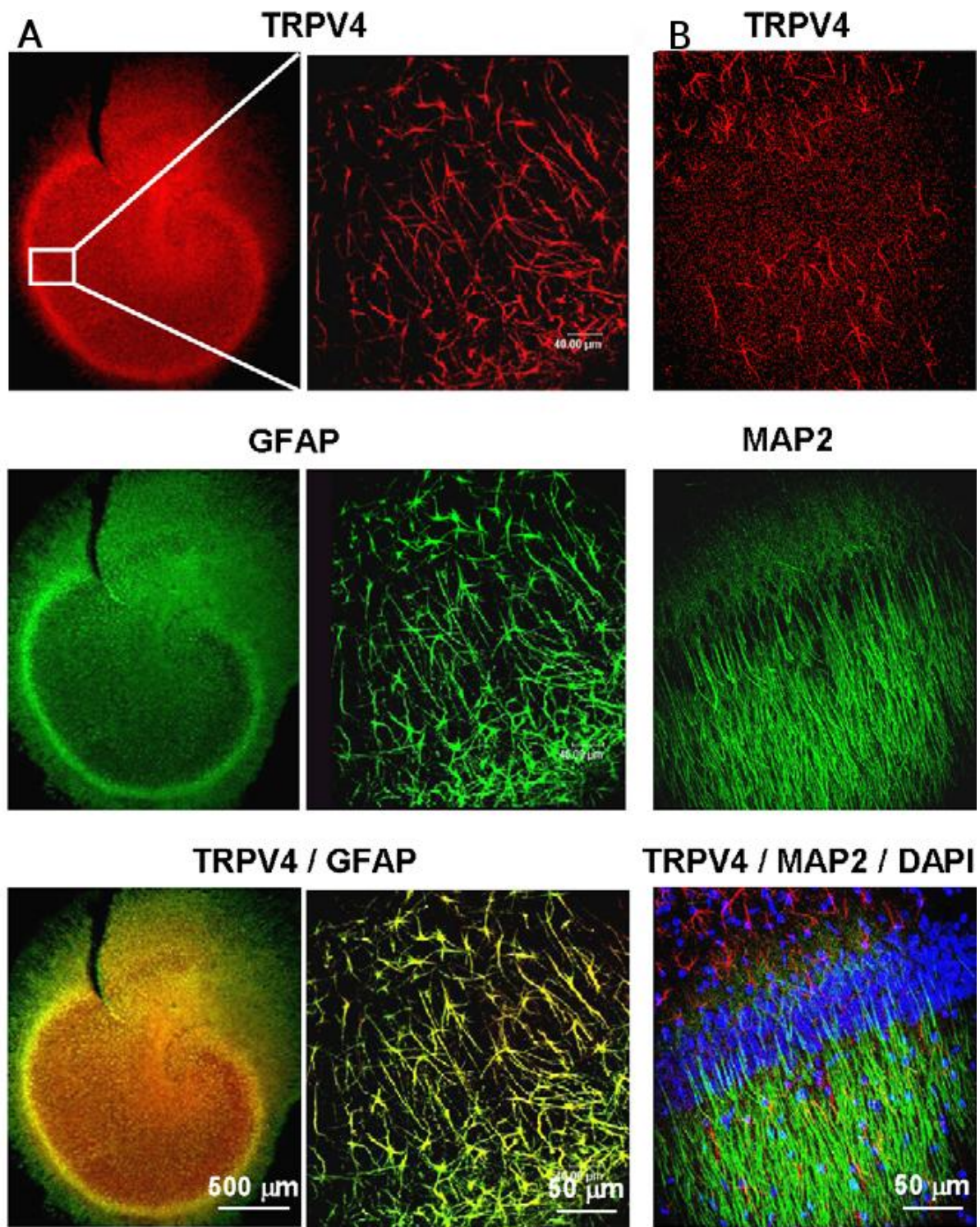


Figure 22. TRPV4 immunoreactivity in rat cultured organotypic hippocampal slices. (A) Double labeling with antibodies against transient receptor potential vanilloid 4 (TRPV4) and glial fibrillary acidic protein (GFAP) revealed co-localization, demonstrating that TRPV4 immunoreactive cells were astrocytes. (B) Confocal images of an organotypic slices labeled for TRPV4 and neuronal microtubule-associated proteins (MAP2). Merged image shows the absence of TRPV4 signals in MAP2-positive cells. (Bai and Lipski, 2010).

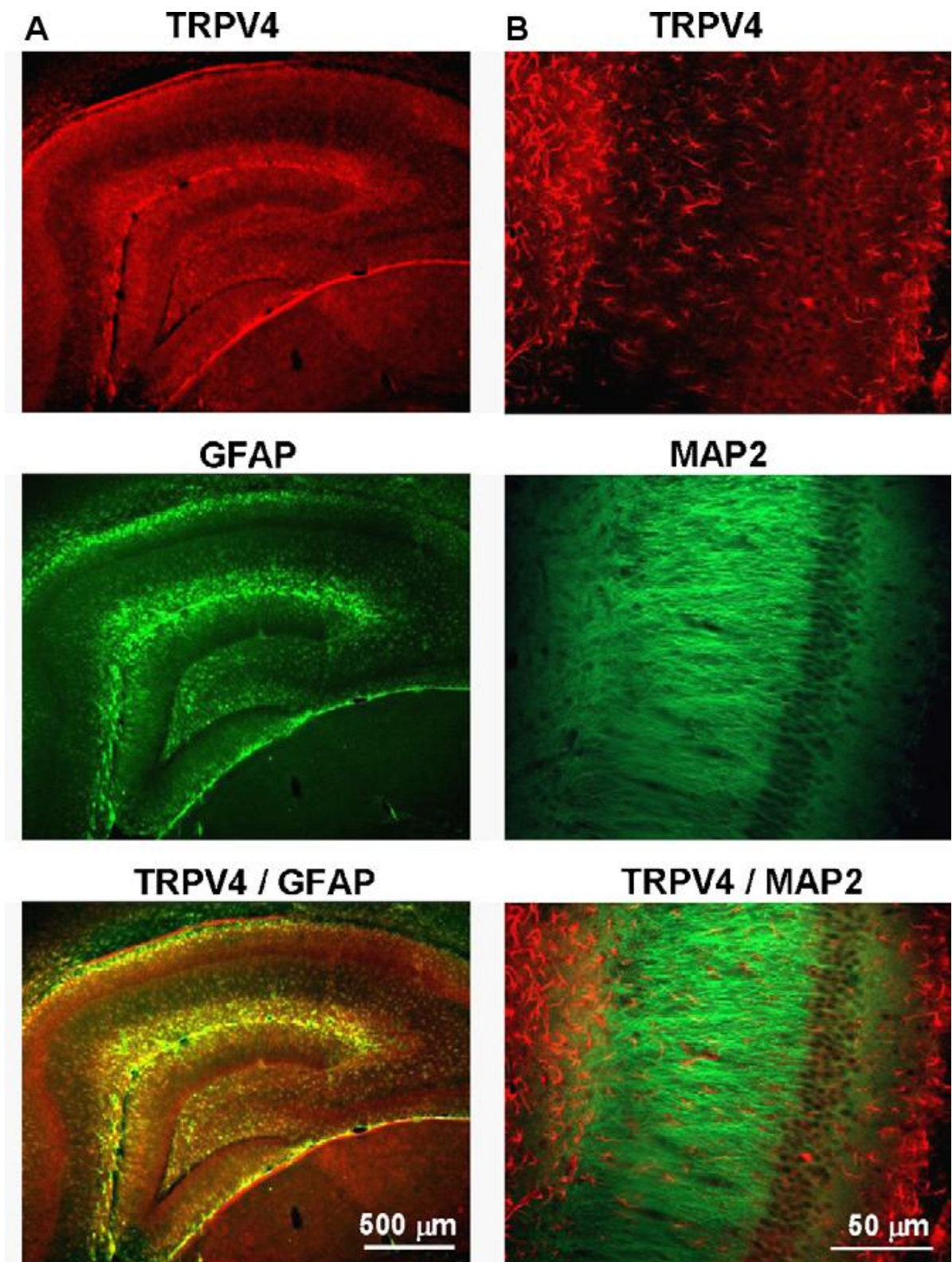


Figure 23. TRPV4 immunoreactivity in hippocampal sections obtained from juvenile rats. (A) Hippocampal section labeled for transient receptor potential vanilloid 4 (TRPV4) and glial fibrillary acidic protein (GFAP). TRPV4 positive cells are strongly detected outside the pyramidal and dentate granule cell layers. Double labeling with antibodies against TRPV4 and GFAP shows co-localization, demonstrating that TRPV4 immunoreactive cells are astrocytes. **(B)** Confocal images of a culture labeled for TRPV4 and neuronal microtubule-associated proteins (MAP2). Merged image shows the absence of TRPV4 signals in MAP2-positive cells (Bai and Lipski, 2010).

2. The aims of my PhD thesis experiments:

1. To characterize the pathological changes in the CA1 region of adult rat hippocampus during reperfusion after cerebral hypoxia/ischemia (H/I) employing a bilateral occlusion of the carotids combined with hypoxic conditions as a model of ischemic injury.
2. To elucidate the changes in TRPV4 expression at mRNA- and protein levels in the hippocampal CA1 region from sham-operated rats and those after H/I, and to correlate these changes with the development of astrogliosis.
3. To characterize astrocyte membrane properties *in situ* in the hippocampal CA1 region of sham-operated rats and those after H/I employing immunohistochemistry and patch-clamp technique in the whole-cell configuration.
4. To isolate astrocytes from the hippocampal CA1 region of post-ischemic and sham-operated rats and to characterize their electrophysiological properties and morphology using patch-clamp technique and immunocytochemistry.
5. To clarify the impact of H/I on TRPV4 channel activity in astrocytes *in situ* in the hippocampal CA1 region as well as *in vitro* in astrocytes isolated from the CA1 region of the hippocampus employing microfluorimetric intracellular Ca²⁺ imaging and patch-clamp technique.

3. MATERIALS AND METHODS

3.1 Ethics Statement

All procedures involving the use of laboratory animals were performed in accordance with the European Communities Council Directive 24 November 1986 (86/609/EEC) and animal care guidelines approved by the Institute of Experimental Medicine, Academy of Sciences of the Czech Republic Animal Care Committee on April 17, 2009.

3.2 Induction of cerebral hypoxia/ischemia in rats

The global hemispheric ischemia was induced by a bilateral 15-minute occlusion of the common carotids combined with hypoxic ventilation (Dijkhuizen et al., 1998; Anderova et al., 2011). Adult male Wistar rats (200 to 250 g) were pre-medicated with atropine (100 µg/kg, s.c.; Biotika, Slovak Republic) and anesthetized with sodium pentobarbital (PTB, 65 mg/kg, i.p.; Sigma-Aldrich, St. Louis, MO, USA). Body temperature was controlled with a heating pad and maintained at $37 \pm 1^\circ\text{C}$ throughout the surgery. The rats were intubated by a cannula tube (Abbocath-T 16G, Abbott, Sligo, Ireland) and mechanically ventilated with 33.3% O₂ and 66.6% N₂ (rate 60 cycles/min, Linde Gas, Prague, Czech Rep.) using a CIV-101 animal ventilator (Columbus Instruments, Columbus, OH, USA) for 15 minutes prior to carotid artery occlusion and during the first 60 minutes of reperfusion. Both carotid arteries were exposed and occluded with aneurism clips for 15 minutes (**Fig. 24**). During the occlusion the rats were ventilated with 6% O₂ and 94% N₂ (Linde Gas, Prague, Czech Rep.). After 15 minutes of H/I the clamps were removed, breathing gas composition was normalized and the blood flow was renewed. In sham-operated rats, which were used as a control, the common carotid arteries were exposed but not occluded. The rats were left to survive for 1 hour (1H H/I), 6 hours (6H H/I), 1 day (1D H/I), 3 days (3D H/I) or 7 days after hypoxia/ischemia (7D H/I). The animals were housed individually and allowed food and water *ad libitum*.

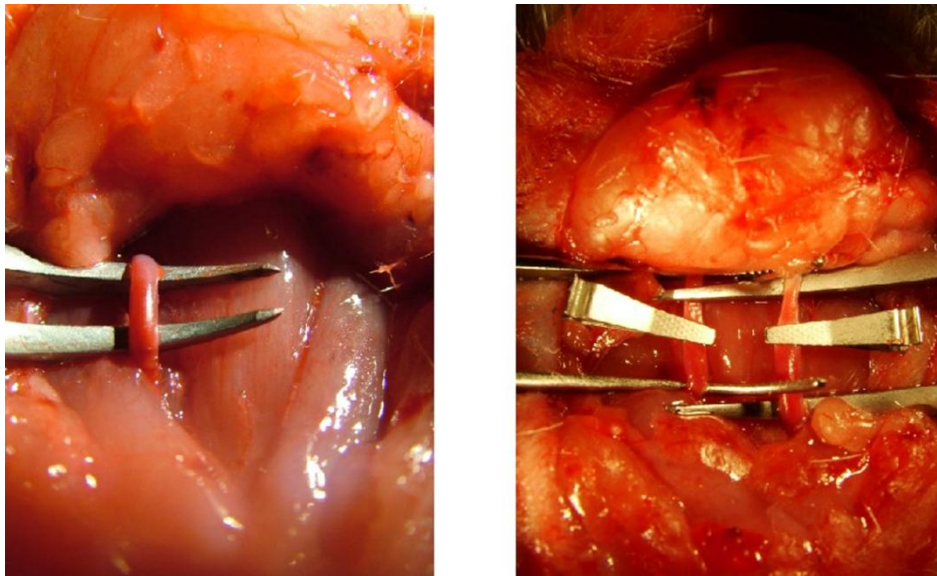


Figure 24. The model of global cerebral ischemia induced by a bilateral 15-minute occlusion of the common carotids combined with hypoxic ventilation. Common carotid arteries were exposed bilaterally then occluded with atraumatic microvascular clamps for 15 minutes. After 15 minutes of global cerebral ischemia the carotid artery clamps were removed and the blood was reinfused. Sham surgery included placement of arterial threads and exposure of common carotid arteries.

3.3 Acute brain slice preparation for electrophysiology

After the reperfusion period, the rats were deeply anesthetized with a sub-lethal dose of PTB (100 mg/kg, i.p.) and perfused transcardially with cold (4°C, 40 ml) isolation solution containing (in mM): 110 NMDG-Cl, 2.5 KCl, 24.5 NaHCO₃, 1.25 Na₂HPO₄, 0.5 CaCl₂, 7 MgCl₂, 20 glucose (pH 7.4, osmolality 290 mOsm/kg). After decapitation, the brains were quickly dissected out and fixed on a cutting disk using 3M Vetbond tissue adhesive (World Precision Instruments, Sarasota, FL, USA). Then the brains were transferred to a microtome chamber containing cold (4°C) isolation solution gassed with 95% O₂ and 5% CO₂. Transversal 220 µm thick slices were cut using an HM 650V vibration microtome (Thermo Scientific Microm, Walldorf, Germany). Subsequently, the slices were incubated in isolation solution (34°C) for 30 minutes and then kept in artificial cerebrospinal fluid, further termed aCSF (see **Table 3**), at room temperature for at least 1 hour.

3.4 Preparation of primary cultures of dissociated astrocytes from the CA1 region of the hippocampus

Primary cultured astrocytes were prepared from all experimental groups of rats: sham-operated rats and those 1 hour and 7 days after hypoxia/ischemia. Transcardial perfusion and

slice preparation were performed as described above, only the thickness of the coronal slices was 700 μm . The hippocampal CA1 region was dissected out from the slice (**Fig. 25**), cut into small pieces and transferred into a Falcon tube with 4 ml of Dubelcco's Modified Eagle Medium (DMEM, Gibco-Invitrogen, Carlsbad, CA, USA) containing 15% fetal bovine serum (FBS, PAA Laboratories GmbH, Pasching, Austria), then centrifuged for 3 minutes at 2000 rpm.

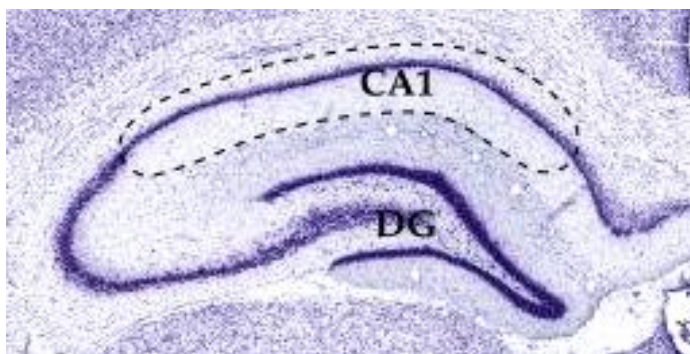


Figure 25. The hippocampal CA1 region was dissected for Western blot analyses and culture preparation. Dashed line indicates the dissected region.

The supernatant was discarded and the tissue was dissociated by a micropipette in 2 ml of solution containing 0.05% Trypsin and 2 g/l ethylene-diamine-tetraacetic acid (EDTA, Sigma-Aldrich, St. Louis, MO, USA). After 3 minutes, the dissociated cells were transferred into Falcon tubes containing 2 ml of FBS solution to block the trypsinization. After centrifugation (3 min at 2000 rpm), the supernatant was removed and fresh cultivation medium (DMEM containing 15% FBS) was added to the final volume of 6 ml. The cells were resuspended and plated in 0.5 ml volumes onto 12 poly-L-lysine (PLL, Sigma-Aldrich, St. Louis, MO, USA) -coated coverslips. Cells were cultured in DMEM containing 15% FBS in an incubator (100% humidity, 5% CO_2) at 37°C medium was changed on the fourth day. After 4-5 days the cells were used for immunocytochemistry, patch-clamp and $[\text{Ca}^{2+}]_i$ measurements.

3.5 Solutions and reagents

Solutions: Various extracellular and intracellular solutions were used in our experiments and they are listed in Table 3, 4, 5.

Table 3. Composition of the extracellular and intracellular solutions for Ca^{2+} imaging and patch-clamp measurements.

Extracellular solutions used for $[\text{Ca}^{2+}]_i$ measurements <i>in vitro</i> and <i>in situ</i>								
	NaCl	KCl	MgCl ₂	CaCl ₂	NaHCO ₃	Na ₂ HPO ₄	Glucose	mOsm/kg
aCSF	122	3	1.3	1.5	28	1.25	10	305 ± 5
aCSF_{∅Ca}	122	3	1.3	-	28	1.25	10	305 ± 5

Abbreviations: aCSF, artificial cerebrospinal fluid; aCSF_{∅Ca}, calcium free artificial cerebrospinal fluid. All concentrations are in mM.

Table 4. Composition of the extracellular solutions for patch-clamp measurements.

Extracellular solutions used for whole-cell patch-clamp recordings <i>in vitro</i> and <i>in situ</i>									
	NaCl	KCl	MgCl ₂	CaCl ₂	HEPES	CsCl	Glucose	mOsm/kg	pH
Ext1	140	4	2	2	10	-	5	315 ± 5	NaOH
Ext2	-	-	2	10	10	122	5	315 ± 5	CsOH
Ext2_{∅Ca}	-	-	2	-	10	122	5	315 ± 5	CsOH

Abbreviations: Ext, extracellular solution; Ext2_{∅Ca}, calcium free extracellular solution. All concentrations are in mM. The pH of the extracellular solutions was adjusted to 7.4 with NaOH in Ext1 or with CsOH in Ext2 and Ext2_{∅Ca}. Osmolality was adjusted with mannitol in Ext1, Ext2, Ext2_{∅Ca} solutions.

Table 5. Composition of the intracellular solutions for patch-clamp measurements.

Intracellular solutions used for whole-cell patch-clamp recordings <i>in vitro</i> and <i>in situ</i>									
	CsGluc	CsCl	KCl	CaCl ₂	MgCl ₂	EGTA	HEPES	mOsm/kg	pH
Int1	-	-	130	0.5	2	5	10	280 ± 5	KOH
Int2	100	26	-	-	2	1	10	300 ± 5	CsOH

Abbreviations: Int, intracellular solution. All concentrations are in mM. The pH of the intracellular solutions was adjusted to 7.2 with KOH in Int1 or CsOH in Int2. Osmolality was adjusted with mannitol in Int1 solutions.

For microfluorimetric analyses of $[\text{Ca}^{2+}]_i$ *in vitro* and *in situ*, extracellular aCSF and aCSF_{∅Ca} were used. For the electrophysiological characterization of astrocytes *in situ* and

in vitro, extracellular aCSF and the intracellular solution Int1 were used, whereas recordings for TRPV4 channel characterization were obtained using the extracellular solution Ext1 and the intracellular solution Int2 (Benfenati et al., 2007). In order to facilitate the isolation of TRPV4 currents, Na⁺ and K⁺ conductances were eliminated by replacing Na⁺ and K⁺ with Cs⁺ in the extracellular (Ext2) and intracellular solutions (Int2). In the intracellular solution, Cl⁻ was partially replaced by gluconate to diminish the activation of astroglial Cl⁻ conductance (Makara et al., 2003). All chemicals were purchased from Sigma-Aldrich, St. Louis, MO, USA.

Agonists and antagonists: The TRPV4 activator 4 α PDD (Sigma-Aldrich, St. Louis, MO, USA) was applied at 5 μ M for *in vitro* and 5-10 μ M for *in situ* studies (Fig. 26). Cells were exposed to 4 α PDD for 6-8 min. 4 α PDD was kept in aliquots in dimethyl sulfoxide (DMSO, Sigma-Aldrich, St. Louis, MO, USA) at -20°C. Aliquots of Ruthenium Red (RR, Sigma-Aldrich, St. Louis, MO, USA) and RN1734 (Tocris Bioscience, Bristol, UK) were also prepared in DMSO. Aliquots were stored at -20°C, and the solutions were prepared immediately before use (the final concentration of DMSO was less than 0.03%).

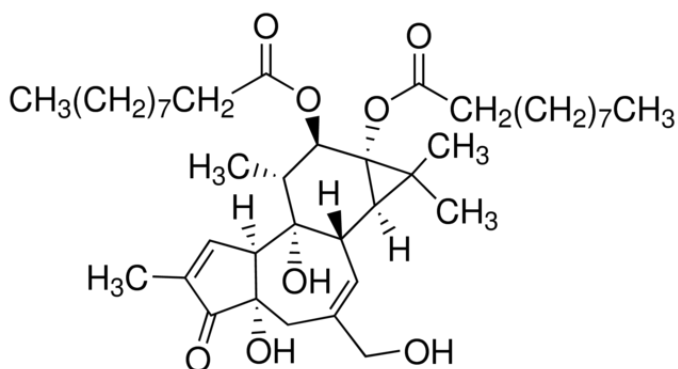


Figure 26. Structural formula of synthetic TRPV4 agonist 4- α -phorbol 12, 13-didecanoate (4 α PDD).

3.6 Patch-clamp recording

Acute brain slices or coverslips with primary astrocyte cultures were transferred to the recording chamber of an upright Axioscop microscope (Zeiss, Gottingen, Germany) equipped with electronic micromanipulators (Luigs & Neumann, Ratingen, Germany) and a high-resolution AxioCam HRc digital camera (Zeiss, Germany). Since TRPV4 is a moderately heat sensitive channel (Shibasaki et al., 2007), the electrophysiological experiments were performed at $28 \pm 2^\circ\text{C}$. To visualize the recorded cells, the intracellular solution contained either Lucifer Yellow (LY, Sigma-Aldrich, St. Louis, MO, USA) or Alexa-Fluor hydrazide

488/594 (Molecular Probes, Carlsbad, CA, USA). The fluorescently labelled cells were used for further post-recording immunocytochemical identification.

Membrane currents were recorded using the patch-clamp technique in the whole-cell configuration in slices as well as in primary cultured astrocytes. Recording pipettes with a tip resistance of 8-12 M Ω were made from borosilicate capillaries (0.86 ID, Sutter Instruments Company, Novato, CA, USA) using a P-97 Brown-Flaming micropipette puller (Sutter Instruments, Novato, CA, USA).

Electrophysiological data were measured with 10 kHz sample frequency using an EPC10 amplifier controlled by PatchMaster software (HEKA Elektronik, Lambrecht/Pfalz, Germany) and were filtered at 2.9 kHz using a Bessel filter.

Resting membrane potential (V_{rest}) was measured by switching of the EPC10 amplifier to the current clamp mode.

The membrane capacitance (C_m) was measured automatically from the Lock-in protocol by PATCHMASTER.

Input resistance (IR) was determined from the currents evoked by membrane depolarization from -70 mV to -60 mV, 40 ms after the onset of depolarization.

The current patterns of the cells were obtained in aCSF solution by hyperpolarizing and depolarizing the astrocytic membrane from -100 mV to +100 mV in 20 mV increments, from the holding potential (V_h) of -70 mV. The pulse duration was 50 ms. For measurement of TRPV4-specific cation current, astrocytes were measured in K⁺ and Na⁺ containing extracellular solution (Ext1). Membrane currents were evoked by hyperpolarizing and depolarizing voltage steps from -100 mV to +100 mV (at V_h of -70 mV) (**Fig. 27 A**). To block the dominant K⁺ conductance in hippocampal astrocytes and isolate more accurately the TRPV4-specific cation currents, additional recordings were performed in intra- and extracellular solutions in which K⁺ and Na⁺ were replaced with Cs⁺ (Ext2 and Int2) ([Benfenati et al., 2007](#)). Under these experimental conditions, membrane currents evoked by hyperpolarizing and depolarizing voltage steps from -100 mV to +100 mV (at V_h of -40 mV) were diminished (**Fig. 27 B**). To extract TRPV4-dependent whole-cell current, the cells were measured in Ext2 extracellular solution. They were held at 0 mV and stimulated with a voltage ramp from -100 mV to +100 mV (500 ms) after a 500 ms potential step to -100 mV (**Fig. 27 C**).

Electrophysiological data were analyzed using Fitmaster software (HEKA, Lambrecht, Germany). Recorded membrane potentials were corrected for the liquid junction potential using JPCALCW software ([Barry, 1994](#)).

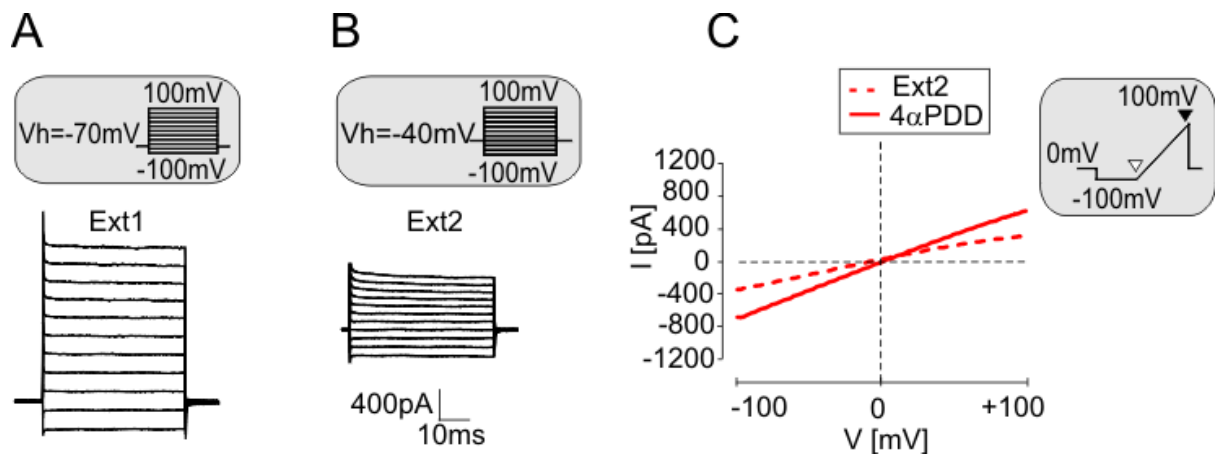


Figure 27. Patch-clamp recording of astrocytes *in situ*. (A) For TRPV4 channel characterization, astrocytes were measured in Na⁺-containing extracellular solution (Ext1) which was switched to Cs⁺-containing extracellular and intracellular solutions (Int2 and Ext2). (B) Note the marked reduction in membrane conductance. (C) The 4 α PDD-evoked current was recorded in Ext2 solution from a voltage stimulation ramp protocol from -100 mV (white arrowhead) to +100 mV (black arrowhead) (see the inset).

3.7 Microfluorimetric analysis of intracellular calcium levels

Coverslips with 4-5-day-old cell cultures were incubated for 1 hour in 1.5 ml DMEM + 15% FBS medium containing 3.3 μ M Fluo-4 AM and 0.07% Pluronic F-127 (Invitrogen, Carlsbad, CA, USA) at 37°C in an incubator (100% humidity, 5% CO₂). The coverslips were then transferred to a microscope superfusion chamber, and two measurements were made on each coverslip with a sufficient distance between the measurement regions. After the measurements, immunocytochemical staining for GFAP was performed to confirm the measured cells were astrocytes.

In situ measurements were performed in the *stratum radiatum* of the CA1 region of the hippocampus, 10-20 μ m below the surface of the slice. As described earlier, 220 μ m thick transversal brain slices were cut in 4°C isolation solution using a vibration microtome. They were then incubated for 20 min in isolation solution containing 1 μ M Sulforhodamine 101 (SR-101, Sigma-Aldrich, St. Louis, MO, USA) and gassed with 95% O₂ and 5% CO₂ at 34°C. The slices were then placed onto a nylon mesh in a dish (3 ml volume) and incubated for 60 min in aCSF containing 4 μ M Fluo-4 AM and 0.01% Pluronic F-127 at room temperature. During incubation, the dish was in a dark environment and gassed with 95% O₂ and 5% CO₂. The slices were then transferred to a microscope superfusion chamber, and two measurements were performed with a sufficient distance between them. To verify that the measured cells

were astrocytes, SR-101 staining was used since this fluorescent dye is preferentially taken up by astrocytes (Nimmerjahn et al., 2004).

During the measurements, the microscope superfusion chamber was continually perfused with aCSF at a flow rate of 2.5 ml/min. The temperature was held at $28 \pm 2^\circ\text{C}$ throughout the experiments by a ThermoClamp-1 (AutoMate Scientific, Inc. Berkeley, CA, USA). The solutions were applied through a capillary (i.d. 250 μm) located 0.5 – 1 mm from the recorded cell and connected to a Perfusion Pressure Kit pressurized application system (flow rate 600 $\mu\text{l}/\text{min}$) controlled by a ValveBank II controller (AutoMate Scientific, Inc. Berkeley, CA, USA). Since TRPV4 channels are stretch-sensitive (O'Neil and Heller, 2005), aCSF was applied before and after 4 α PDD application with the same flow rate to verify that the response was not influenced by the application itself. Fluo-4 AM fluorescence was detected with a TILL Photonics Imaging System installed on a Zeiss Axioskop 2 FS Plus microscope equipped with a long-distance 10x objective (Achromplan 0.3 W, Ph 1, Zeiss, Germany) for measurements *in vitro* or a long-distance 40x objective (IR Achromplan 0.8 W, Zeiss, Germany) for measurements *in situ*. A digital camera (PCO Sensicam, Kelheim, Germany) was controlled by TILLvisION software. The excitation light (488 nm) was generated by a Polychrome V (TILL Photonics GmbH, Gräfelfing, Germany), filtered by a BP 450-490 excitation band-pass filter, reflected by a FT 510 beam splitter and the emitted light was filtered by a LP 515 long-pass filter (Filter Set 09, Zeiss, Germany). Images were acquired at 0.83 Hz and were analyzed offline. Fluorescence intensity (F) was measured in the cell bodies and expressed as $(F-F_0)/F_0$ after background correction, where F_0 is the baseline fluorescence intensity before drug application. The threshold for a Ca^{2+} response *in vitro* was 120% of F_0 , and the threshold amplitude for a transient peak *in situ* was 200% of the amplitude of the noise signal. The excitation light for SR-101 (570 nm) was filtered by a 565/30 band-pass filter, reflected by a FT585 beam splitter and the emitted light was filtered by a 620/60 band-pass filter (Filter Set 31, Zeiss, Germany).

3.8 Immunocytochemistry/Immunohistochemistry

Primary cultured astrocytes attached to PLL-coated coverslips were fixed on the 4-5th day of culture in 4% paraformaldehyde solution in 0.2 M phosphate buffer (PB, pH 7.4) for 8 minutes and kept in 10 mM phosphate buffered saline (PBS) at 4°C for further processing. Coverslips were incubated in a blocking solution containing 5% Chemiblocker (Millipore, Billerica, MA, USA) and 0.5% Triton X-100 (Sigma-Aldrich, St. Louis, MO, USA) in 10 mM PBS at 4°C for two hours. They were then incubated overnight at 4°C with primary antibodies

in PBS containing 0.2% Triton X-100. The next day three 10-min washes with PBS were performed, followed by incubation with the appropriate species/subclass-specific secondary antibody for two hours at 4°C. For double labelling, antibody was subsequently applied and incubated overnight at 4°C. Afterwards, the coverslips were washed in PBS three times for 10 minutes each. To visualize the cell nuclei, the coverslips were incubated with 300 nM 4', 6-diamidino-2-phenylindole (DAPI) in PBS for 5 minutes at room temperature. Finally, the coverslips were mounted using Aqua Poly/Mount (Polysciences Inc., Eppelheim, Germany).

Brain slices were prepared from control rats and those 1H, 6H, 1D, 3D and 7D after H/I. Animals were anesthetized with a sub-lethal dose of PTB (100 mg/kg, i.p.) and perfused transcardially with 70 ml of 0.9% saline with heparin (2500 IU /100 ml), (Zentiva, Prague, Czech Republic), followed by 70 ml of 4% paraformaldehyde solution in PBS (PFA/PBS). Dissected brains were post-fixed overnight in 4% PFA/PBS, cryoprotected by 10%, 20% and 30% sucrose gradient in 0.2 M PB, then sectioned in the coronal plane (30 µm thickness). To enhance the efficiency of immunostaining, the sections were incubated for 20 minutes in citrate buffer (10 mM Citric Acid, 0.05% Tween 20 in PB, pH 6.0) at 80°C. After washout in PB, the sections were further incubated in a blocking solution containing 2% normal goat serum (NGS, Millipore, Billerica, MA, USA), 5% Chemiblocker, 1% bovine serum albumin (BSA, Sigma-Aldrich, St. Louis, MO, USA) and 0.5% Triton X-100 in PB for 2 hours at 4°C. The sections were incubated with the primary antibodies overnight at 4°C. After the incubation, three 10-min washes with PBS removed the unbound antibodies. The appropriate species/subclass-specific secondary antibodies were applied and the slices were incubated for two hours at 4°C. Slices were then washed in PBS and mounted with Vectashield containing DAPI (Vector Laboratories, Burlingame, CA) for visualization of the nuclei. The specificity of the TRPV4 staining was confirmed by strong TRPV4 immunostaining in the choroid plexus (**Fig. 28**).

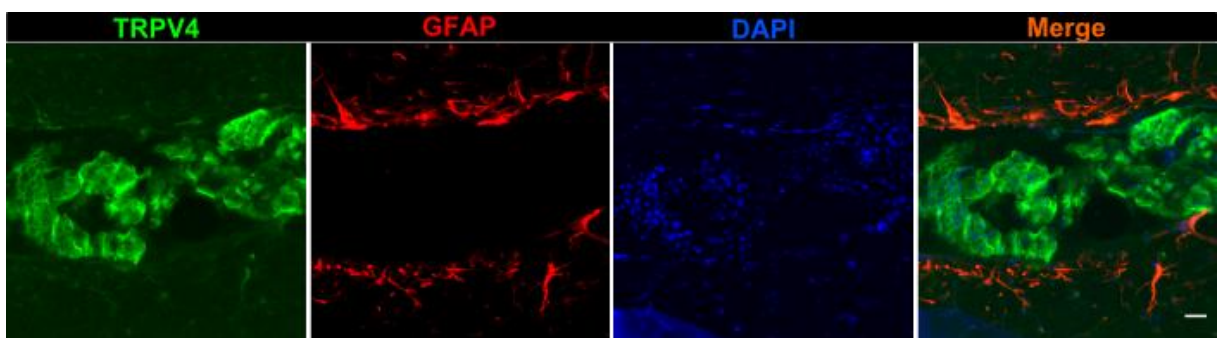


Figure 28. The ependymal cells of choroid plexus highly express TRPV4 protein. This staining was used as a positive control for TRPV4 antibodies. The scale bar indicates 10 µm.

For cell identification after patch-clamp recording, the measured cells were filled either with Alexa Fluor 488 hydrazide or LY by dialyzing the cytoplasm with the patch pipette solution. Post-recording, the coverslips and slices were fixed with 4% PFA in 100 mM PB for 8 min or 1 hour, respectively. The cells were incubated in blocking solution followed by the overnight incubation with primary antibody and then with specific secondary antibodies for two hours. The slices/coverslips were then examined using an LSM 5 DUO spectral confocal microscope (Zeiss, Germany). All primary and secondary antibodies, their dilutions and manufacturers are listed in **Table 6**. In order to detect degenerating neurons, the hippocampal slices were stained by polyanionic fluorescein Fluoro-Jade B.

Table 6. Primary and secondary antibodies used for immunohistochemistry and immunocytochemistry

Antigen	Dilution	Isotope	Manufacture	Secondary antibody
NeuN	1:100	Mouse IgG	Millipore	GAM-488
GFAP	1:800	Mouse IgG	Sigma-Aldrich	Cy3-conjugated
GLAST	1:4000	Guinea Pig IgG	Chemicon	GAGP-Cy3
TRPV4	1:500	Rabbit IgG	Novus Biologicals	GAR-488
Nestin	1:1000	Mouse IgG	Chemicon	GAM-488
PCNA	1:1000	Mouse IgG	Sigma-Aldrich	GAM-594
Cleaved Casp 3	1:50	Rabbit IgG	Cell Signalling	GAR488/594
Iba1	1:300	Mouse IgG	Millipore	GAM-594
NG2	1:400	Rabbit IgG	Chemicon	GAR488

Abbreviations: **GAR 488** - goat anti-rabbit IgG conjugated with Alexa Fluor 488; **GAM 488/594** - goat anti-mouse IgG conjugated with Alexa Fluor 488 or 594; **GFAP** - glial fibrillary acidic protein; **GFAP Cy3** - mouse glial fibrillary acidic protein conjugated with Cy3; **GLAST** - Glutamate-aspartate transporter; **GAGP-Cy3** - goat anti-guinea pig IG conjugated with Cy3; **PCNA** - Proliferating cell nuclear antigen; **Cleaved Casp3** - cleaved caspase 3; **NG2** - NG2 chondroitin sulfate proteoglycan; **Iba1** - ionized calcium binding adaptor molecule 1.

3.9 Western Blotting

Hippocampal samples for Western blot analysis were isolated from rats after H/I (1H, 6H, 1D, 3D, 7D, 5 weeks (5W)), sham-operated animals or intact animals. Rats were deeply anesthetized with PTB (100 mg/kg, i.p.), perfused transcardially with chilled isolation

solution and decapitated. The brains were dissected out and cut into 500 μm thick slices. The CA1 region of the hippocampus was excised from each slice and homogenized using an ultrasound homogenizator in Tris buffer (pH 6.8) containing 10% glycerol and 1% sodium dodecyl sulphate (SDS). Total protein content in the homogenates was determined by the Micro BCATM protein assay kit (ThermoFisherScientific, Rockford, IL, USA). Tissue homogenates were heated at 100°C for 5 minutes with 0.5% dithiothreitol. Equal amounts of proteins were separated on a 6% SDS-polyacrylamide gel (for TRPV4 protein) or 10% SDS-polyacrylamide gel (for GFAP and β -actin) and subsequently electrotransferred to a nitrocellulose membrane using a TE 70XP Semi-Dry Transfer unit (Hoefer, Holliston, MA, USA). Membranes were blocked with 5% non-fat dry milk in PBS-Tween buffer (0.05% Tween) for 1 hour at room temperature. The incubation with the primary antibodies diluted in PBS containing 1% non-fat dry milk, 0.05% Tween and 0.1% NaN_3 was performed at 4°C overnight, followed by a 2 hour incubation with goat anti-rabbit IgG conjugated with peroxidase (Sigma-Aldrich, St. Louis, MO, USA) at room temperature. The following primary antibodies were used: rabbit anti-GFAP (1:600, Sigma-Aldrich, St. Louis, MO, USA), rabbit anti-TRPV4 (1:300; Alomone Labs, Jerusalem, Israel) and rabbit anti- β -actin (Abcam, Cambridge, UK). SuperSignal West Pico Chemiluminiscent Substrate (Thermo Fisher Scientific, Rockford, IL, USA) was used to develop the Western blots. To quantify the changes in TRPV4 protein content, Quantity One software (Bio-Rad Laboratories, Hercules, CA, USA) was employed for imaging and analyzing 1D electrophoresis gels. Quantification was carried out using 3 independent Western blot analyses.

3.10 Quantitative PCR analyses

The hippocampal CA1 regions from 3 sham-operated and 3 ischemic rats were immediately after dissection placed into RNeasy Lysis buffer (RLT) (Qiagen, Germany). Total RNA was extracted using an RNeasy Mini Kit, including DNase treatment (Qiagen, Germany). RNA concentrations were measured with a NanoDrop ND-1000 spectrophotometer (Nanodrop Technologies). In order to isolate cDNA, reverse transcription reaction was performed using SuperScript III (Life Technologies). Lysed single cells in 5 μl water containing 0.5 mM dNTP (Promega, Germany), 1.0 mM oligo (dT15) (Invitrogen) and 1.0 mM random hexamers (Invitrogen) were incubated at 70°C for 5 min. 50 mM Tris-HCl, 75 mM KCl, 3 mM MgCl_2 , 5 mM dithiothreitol, 20 U RNaseOut and 100 U SuperScript III (all Invitrogen; final concentrations) were added to a final volume of 10 μl . Reverse

transcription was performed at 25°C for 5 min, 50°C for 60 min, 55°C for 10 min and terminated by heating to 70°C for 15 min. All samples were diluted to 40 µl with water before qPCR. Real-time PCR measurements were performed using a Biorad CFX (Bio-Rad Laboratories, Hercules, CA, USA) and a temperature profile of 95°C for 3 minutes, followed by 40 cycles at 95°C for 15 s, 60°C for 15 s, and 72°C for 20 s. The ten-microliter reactions contained iQ SYBR Green Supermix (Bio-Rad Laboratories, Hercules, CA, USA) and 400 nM of each primer (Metabion, Germany). Primers were designed using BeaconDesigner software (version 7.91, Premier Biosoft International). All primers were designed to span an intron to avoid amplification of genomic DNA. BLAST (Basic Local Alignment Search Tool) searches revealed no pseudogenes. The employed primer sequences were: *Trpv4*_forward: TTTGCTCTTATTTCTACTCCTCCC and *Trpv4*_reverse: GCTGGCTTAGGTGACTCC. The assay was optimized so as not to generate primer dimers before cycle 45. Calibration curves with purified PCR products (QIAquick PCR Purification Kit; Qiagen, Germany) were used to establish the linearity of the assays. The formation of the correct PCR products was confirmed by electrophoresis on 20 g/L agarose gels for all assays and by melting-curve analysis of all samples. Reference genes were evaluated using the Mouse Endogenous Control Gene Panel (TATAA Biocenter, Sweden) and NormFinder. All data were normalized against β 2-microtubulin (*B2M*). Relative changes in expression were calculated using the $\Delta\Delta Cq$ Method.

3.11 Data Analysis and Statistics

Data are presented as means \pm S.E.M. (standard error of the mean) for *n* cells. Student's unpaired *t*-test or one-way ANOVA for multiple comparisons were used to determine significant differences between the experimental groups. Values of **p* < 0.05 were considered significant, ***p* < 0.01 very significant and ****p* < 0.001 extremely significant.

4. RESULTS

4.1 Cerebral hypoxia-ischemia induces hippocampal cell damage and development of astrogliosis

The cerebral hypoxia ischemia (H/I) triggers the irreversible neuronal damage of the CA1 region of the hippocampus and marked glial cell alterations, which considerably progress during the period of reperfusion (Dijkhuizen et al., 1998). In our study the cerebral hypoxia/ischemia was induced by 15-minute bilateral cerebral occlusion of common carotid arteries in adult male Wistar rats. Immunohistochemical analyses were carried out to assess ischemic damage of rat hippocampus in control and ischemic rats at different time points after reperfusion. In addition, we assessed the changes in GFAP content at different time points of reperfusion using Western blot technique (Fig. 29). We have detected the decrease of GFAP protein in the hippocampus 6 hours and 1 day after H/I; however, starting 3 days after H/I the amount of GFAP was markedly up-regulated and reached the maximum 7D after H/I; a phenomenon associated with development of astrogliosis (Pivonkova et al., 2010). Based on these results the period of reperfusion was separated into two stages: an acute stage comprising ischemic rats 1H and 6H after H/I and the late stage including rats 1D, 3D and 7D after H/I.

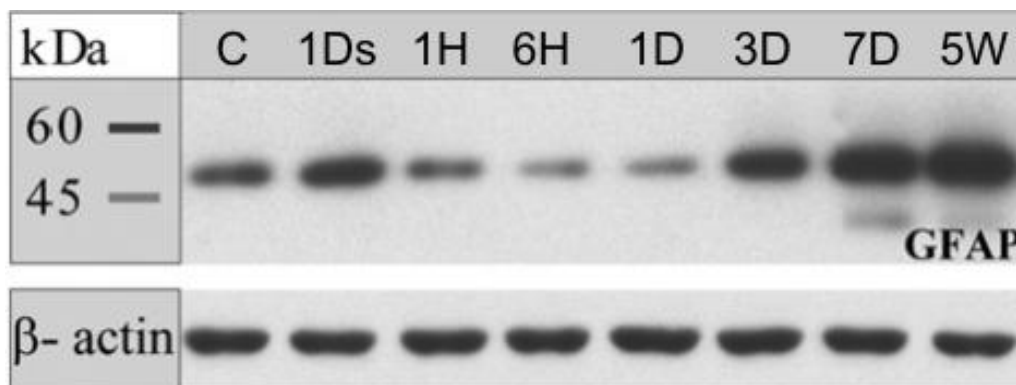


Figure 29. Changes in the expression of glial fibrillary acidic protein (GFAP) in the hippocampal CA1 region after hypoxia/ischemia (H/I). The GFAP content is reduced 1H, 6H and 1D after H/I and increased starting 3D after H/I when compared to non-operated (C) or sham-operated animals (1Ds) (Pivonkova et al., 2010).

To follow the dynamic of neuronal death and development of astrogliosis the neuronal nuclear antigen marker, NeuN and marker of mature astrocytes, GFAP were used. In sham-operated (control) rats NeuN staining was clearly observed in neurons in *stratum pyramidale*. One hour as well as 6H after H/I no obvious neuronal damage was detected in *stratum*

pyramidale of the CA1 region of the hippocampus. Also hippocampal astrocytes in control rats as well as those 1H and 6H after H/I were not altered, showing thin, long processes in both *stratum radiatum* and *stratum oriens* (**Fig. 30**). The reduction of NeuN immunoreactivity in hippocampal pyramidal layer started 3D after H/I, and 7D after H/I the number of NeuN-positive cells markedly decreased. GFAP immunoreactivity of hippocampal astrocytes was slightly increased 1D after H/I and displayed moderate hypertrophy. However, 3D after H/I GFAP immunoreactivity was greatly increased and reached maximal level 7D after H/I (**Fig. 31**). The reactive astrocytes within gliotic scar 7D after H/I were characterized by hypertrophic cell bodies and thick processes when compare to astrocytes in control rats.

Thus, 7D after hypoxic/ischemic injury the hippocampal CA1 was characterized by a marked decrease in NeuN immunoreactivity due to neuronal loss and by an increase in GFAP immunoreactivity owing to the development of astrogliosis.

Previously, it has been shown that the post-ischemic formation of astroglial scar in the CA1 region of the hippocampus is associated with significant cell proliferation, especially of astrocytes, microglia and NG2 glia ([Anderova et al., 2011](#); [Sizonenko et al., 2008](#)). Our study showed that in the CA1 hippocampal region of the controls and post-ischemic rats in acute phase of reperfusion nestin, a marker of intermediate filaments in proliferating cells, was expressed predominantly in endothelial cells of the brain vessels as it has been shown previously ([Hendrickson et al., 2011](#)) while no hippocampal astrocytes were stained for nestin (**Fig. 32**). Nevertheless, single nestin positive astrocytes started to appear 1D after H/I and their amount gradually increased 3D after ischemia, at the onset of astroglia scar formation. In rats 3D and 7D after H/I most of reactive astrocytes within *stratum pyramidale* in the CA1 region co-expressed nestin and GFAP (**Fig. 33**). Moreover, in rats 7D after H/I proliferating cell nuclear antigen (PCNA), the indicator of cell proliferation, was also expressed in GFAP-positive reactive astrocytes within the gliotic scar in the CA1 hippocampal region when compared to control rats (**Fig. 34**). This result indicates that reactive astrocytes are actively proliferating cells in the injured zone 7D after H/I.

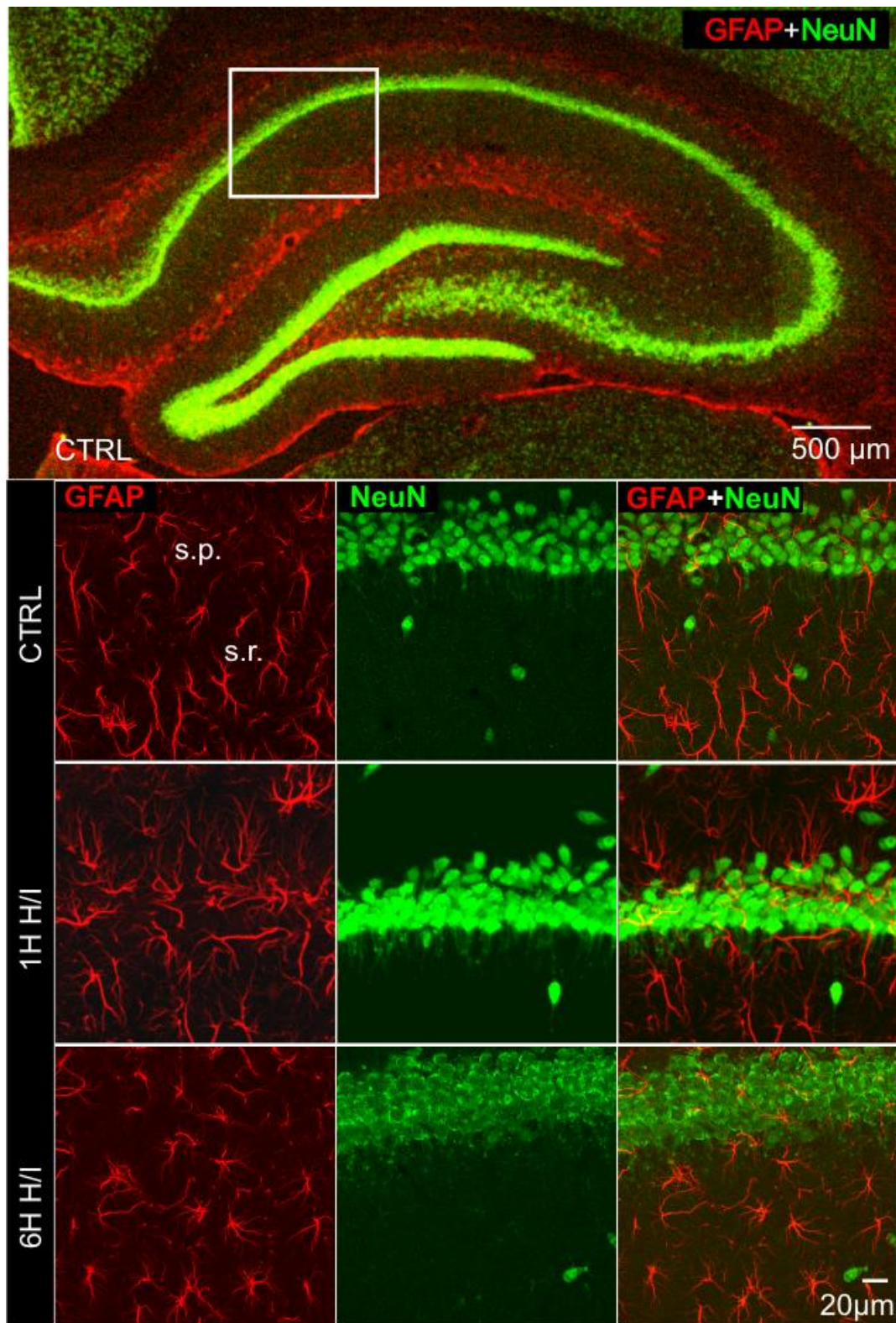


Figure 30. Immunohistochemical staining of the rat hippocampus for NeuN and GFAP after hypoxia/ischemia followed by acute phase of reperfusion. Coronal hippocampal section of control rat immunostained for a neuronal marker (NeuN) and the astrocytic marker glial fibrillary acidic protein (GFAP) (**top**). In enlargements of CA1 region sections of the rat hippocampus (**bottom**) in sham-operated rats (CTRL) and rats 1 hour, and 6 hours after hypoxia/ischemia neuronal loss and reactive astrocytes is not detected when compared to controls. Abbreviations: H/I - hypoxia/ischemia; 1H - 1 hour; 6H - 6 hours; s.p. - *stratum pyramidale*; s.r. - *stratum radiatum*.

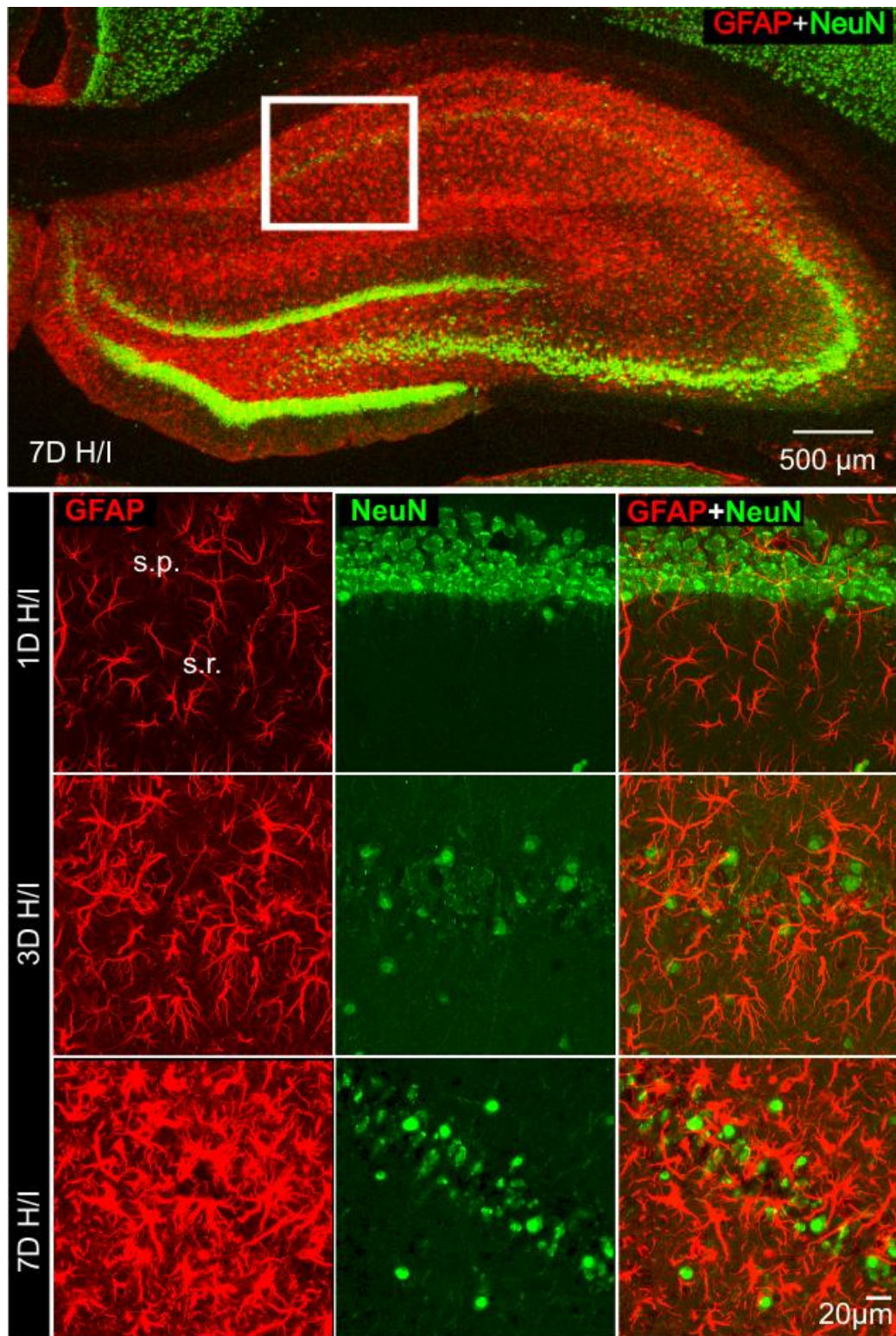


Figure 31. Immunohistochemical staining of the rat hippocampus for NeuN and GFAP after hypoxia/ischemia followed by late stage of reperfusion. Coronal hippocampal section of rat 7 days after hypoxia/ischemia (H/I) immunostained for a neuronal marker (NeuN) and the astrocytic marker glial fibrillary acidic protein (GFAP) (**top**). Enlargements of CA1 region sections of the rat hippocampus (**bottom**) after H/I demonstrate pyramidal cell loss and the formation of reactive gliosis in the hippocampal CA1 region in 3 days and 7 after H/I when compared to sham-operated rats (CTRL). Abbreviations: H/I - hypoxia/ischemia; 1D - 1 day; 3D - 3 days; 7D - 7 days; s.p - *stratum pyramidale*; s.r. - *stratum radiatum*.

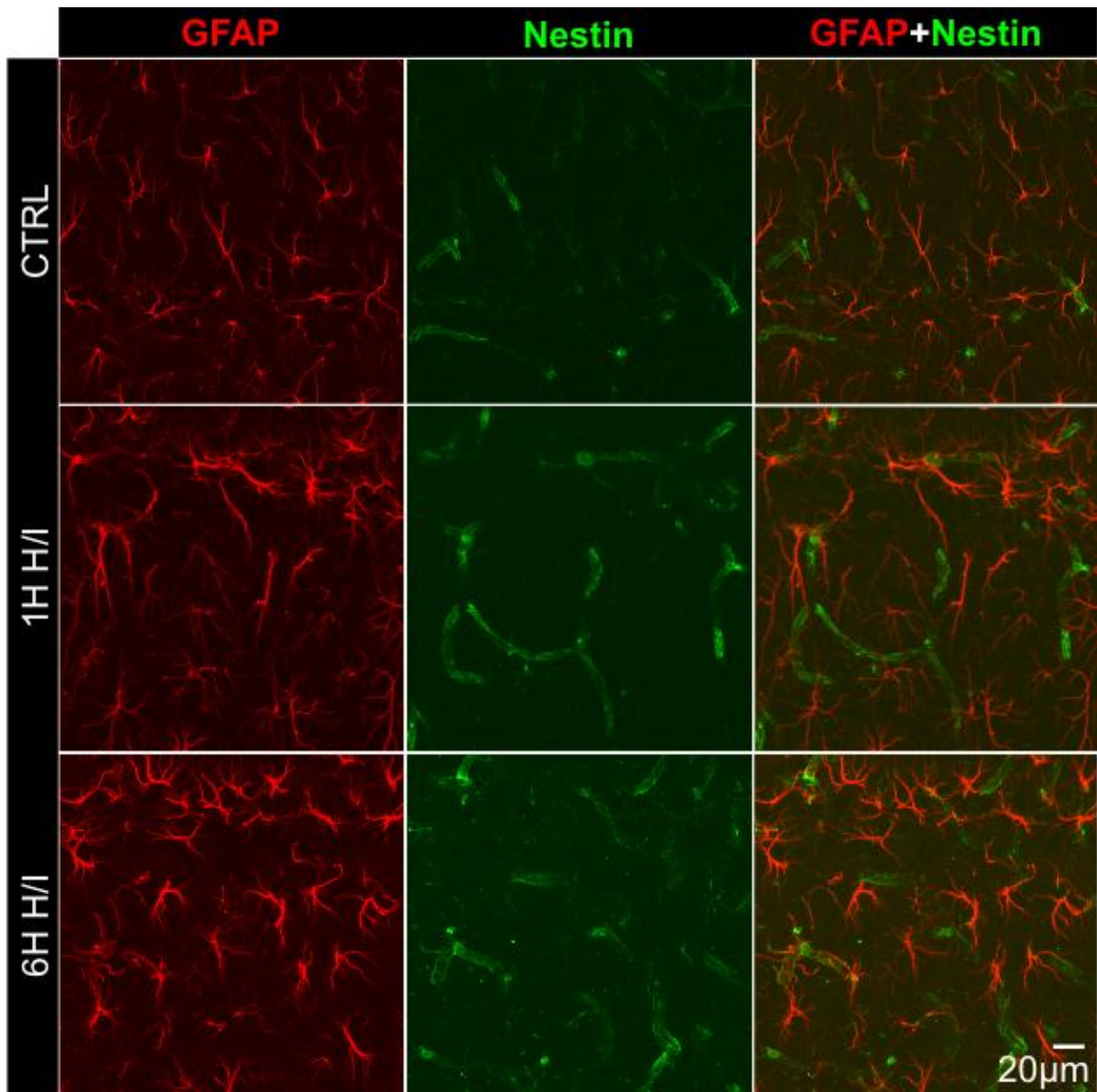


Figure 32. Immunohistochemical staining of the rat hippocampus for GFAP and nestin after hypoxia/ischemia followed by acute stage of reperfusion. Coronal hippocampal sections were immunostained for glial fibrillary acidic protein (GFAP) and for a marker of intermediate filaments in proliferating cells nestin. In sham-operated rats (CTRL) and those 1 hour and 6 hours after hypoxia/ischemia nestin immunoreactivity was detected in hippocampal slices solely in endothelial cells, but not in astrocytes. Abbreviations: H/I - hypoxia/ischemia; 1H - 1 hour; 6H - 6 hours.

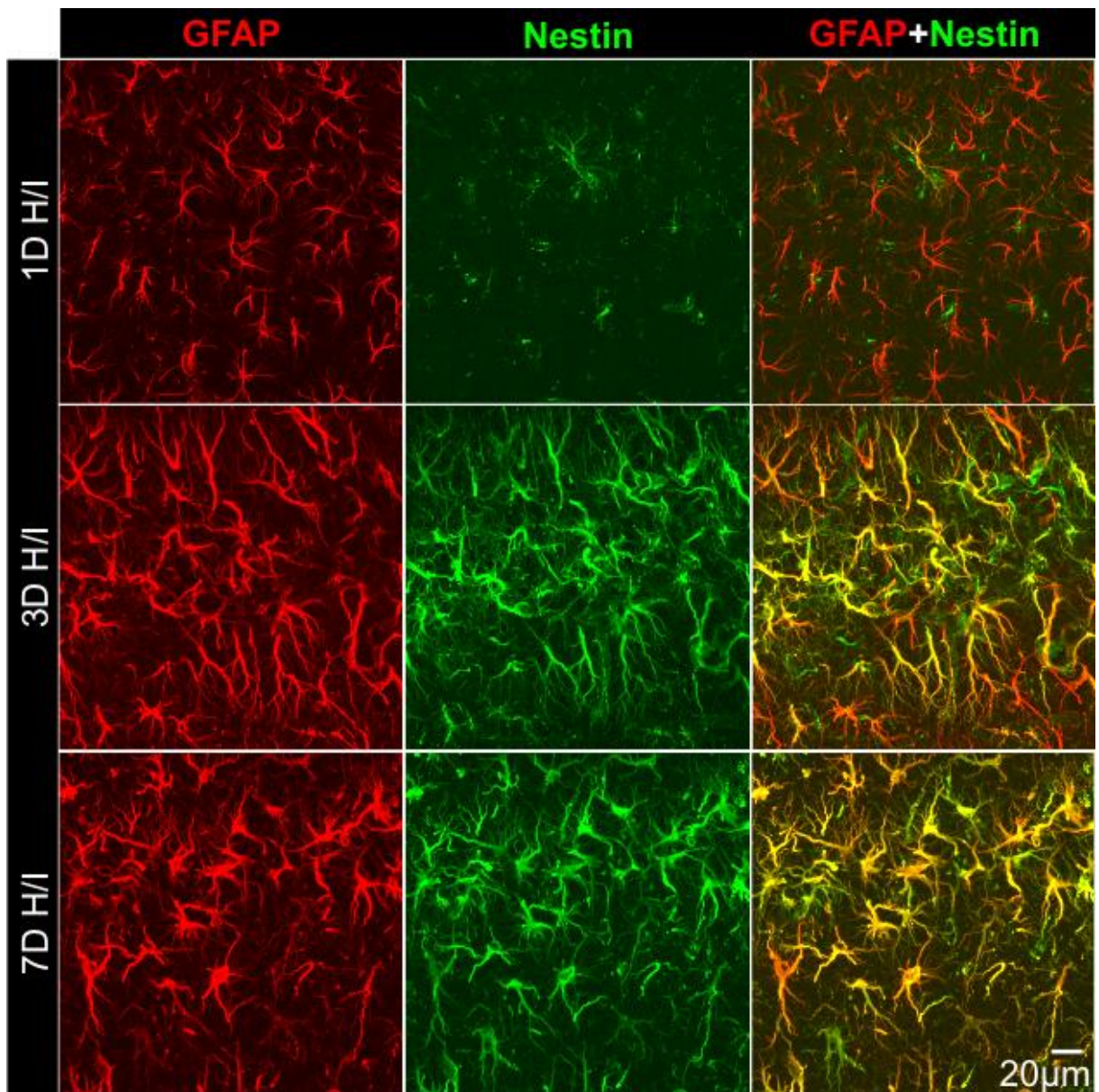


Figure 33. Immunohistochemical staining of the rat hippocampus for glial fibrillary acidic protein (GFAP) and a marker of intermediate filaments in proliferating cells nestin followed by late stage of reperfusion. In the CA1 hippocampal region astrocytes 1 day after hypoxia/ischemia started to express nestin, while astrocytes 3 and 7 days after H/I displayed strong immunoreactivity for GFAP-and nestin. Abbreviations: H/I - hypoxia/ischemia; 1D - 1 day; 3D - 3 days; 7D - 7 days.

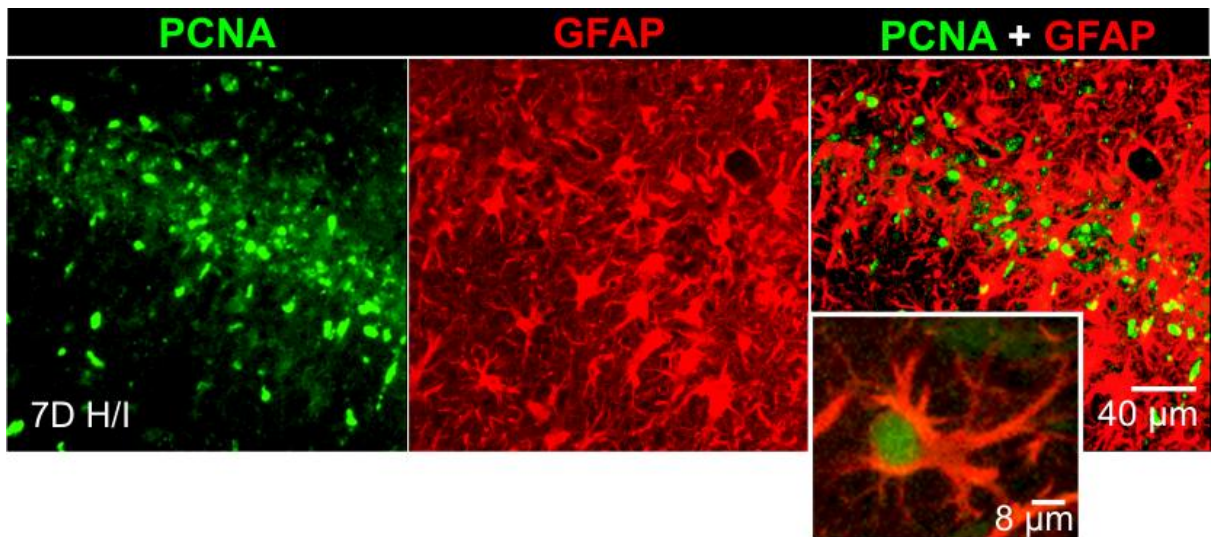


Figure 34. Immunohistochemical staining of the rat CA1 area of the hippocampus for proliferating cell nuclear antigen (PCNA) and glial fibrillary acidic protein (GFAP) in rats 7 days after hypoxia/ischemia. The PCNA immunoreactivity was increased in reactive hippocampal astrocytes in the CA1 region in rats 7D after H/I. Enlargement of slice section depicts nuclear localization of PCNA in reactive astrocyte. Abbreviation: 7D - 7 days after H/I.

To detect microglia activation in the hippocampal CA1 region after H/I Iba1, a marker of microglia, was employed (Ito et al., 2001). The increased Iba1-immunoreactivity was detected in acute stages of reperfusion with a further increased towards late stages of reperfusion reaching the maximum 7 days after H/I (Fig. 35, 36). Interestingly, the double immunostaining revealed Iba1⁺/NG2⁺ cell population in rats 3D and 7D after H/I (Fig. 36). Furthermore, the immunohistochemical staining revealed increased expression of microglial surface constitutive marker CD11b in the hippocampal CA1 region of rats 7D after H/I when compared with controls. The large number of activated microglial cells were accumulated mainly in *subiculum*, pyramidal layer of the CA1 hippocampal region and hilus of gyrus dentatus; specifically in those areas, where marked degeneration of neurons occurred (Fig. 37).

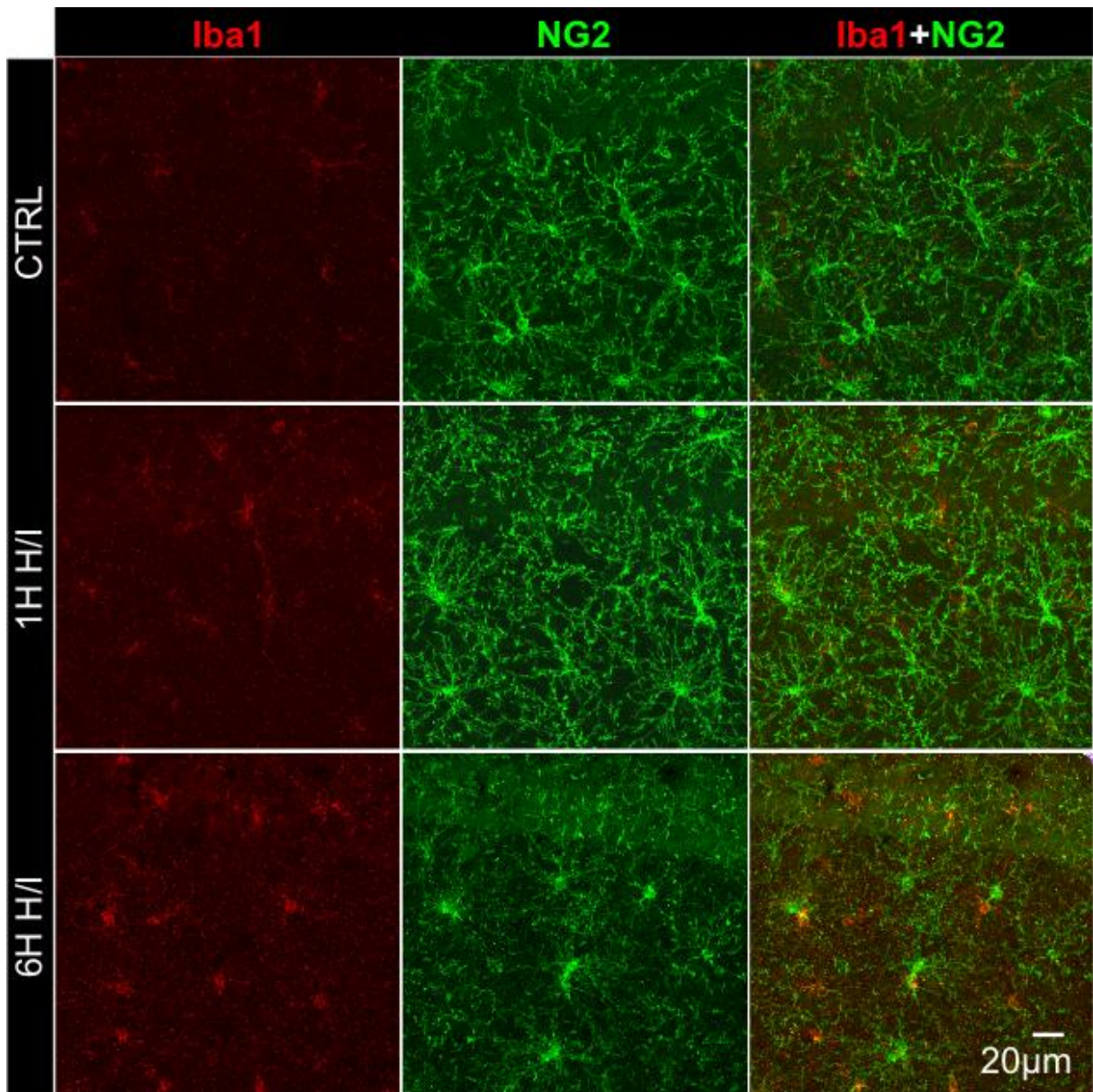


Figure 35. Immunohistochemical staining of the hippocampal CA1 region for Iba1 and NG2 after hypoxia/ischemia (H/I) - during acute stage of reperfusion. Coronal sections of the rat hippocampus were double immunostained for Iba1, a marker of microglia, and NG2 chondroitin sulphate proteoglycan (NG2). The Iba1 immunoreactivity was slightly increased 1 hour and 6 hours after H/I when compared with sham-operated rats (CTRL). NG2 immunoreactivity in the CA1 hippocampal region did not change during acute phase of reperfusion. Abbreviations: H/I - hypoxia/ischemia; 1H - 1 hour; 6H - 6 hours.

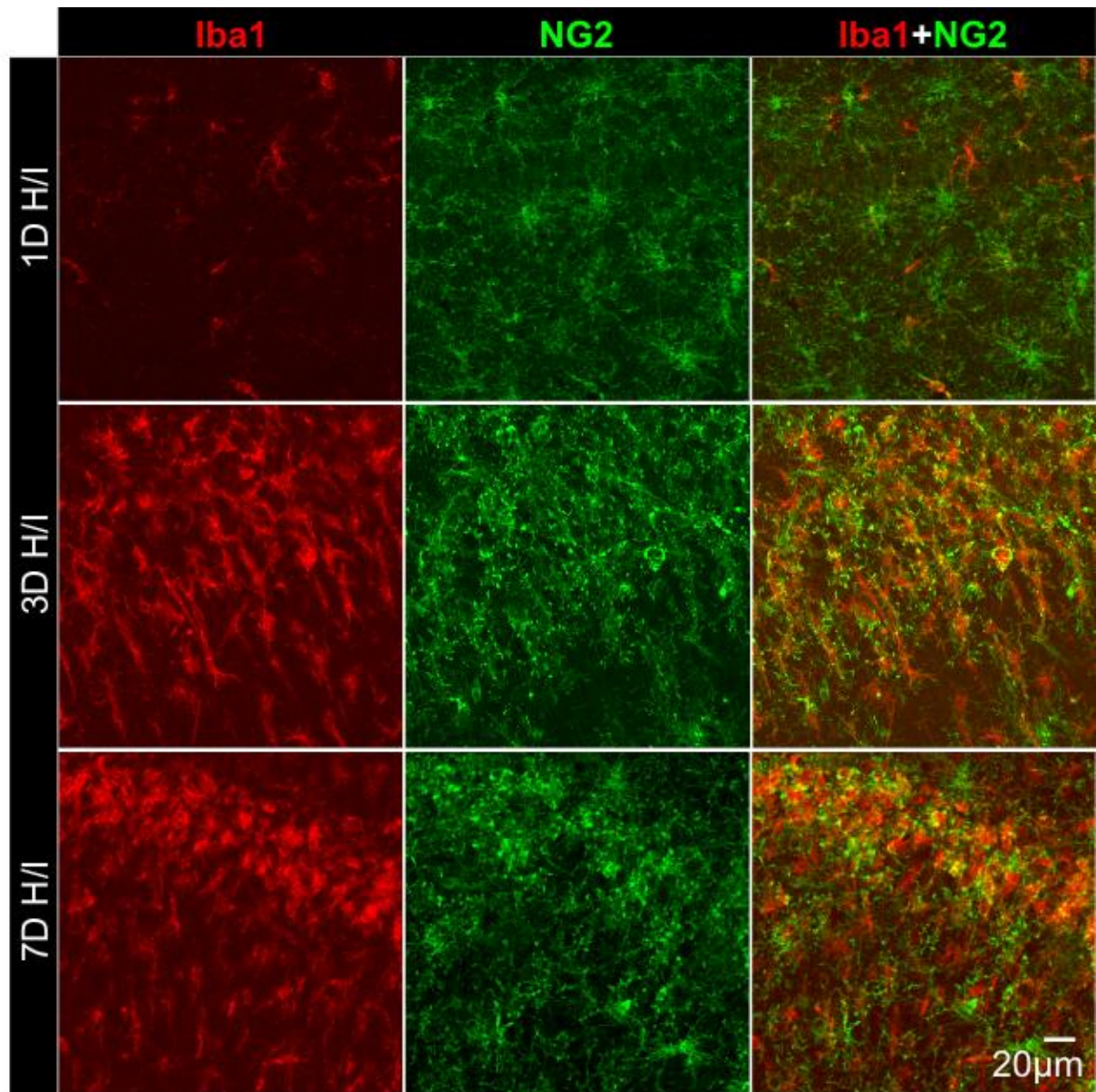


Figure 36. Immunohistochemical staining of the CA1 hippocampal region for Iba1 and NG2 after hypoxia/ischemia - during late stages of reperfusion. Coronal sections of the rat hippocampus were double immunostained for Iba1 and NG2. The Iba1 immunoreactivity was clearly detected 1, 3 and 7 days after hypoxia/ischemia. In CA1 hippocampal slices 3 days and 7 days after hypoxia/ischemia Iba1- and NG2-immunoreactivity was markedly increased when compared with CTRL or acute phase of reperfusion (see Fig.23). Abbreviations: H/I- hypoxia/ischemia; 1D - 1 day; 3D - 3 days; 7D - 7 days.

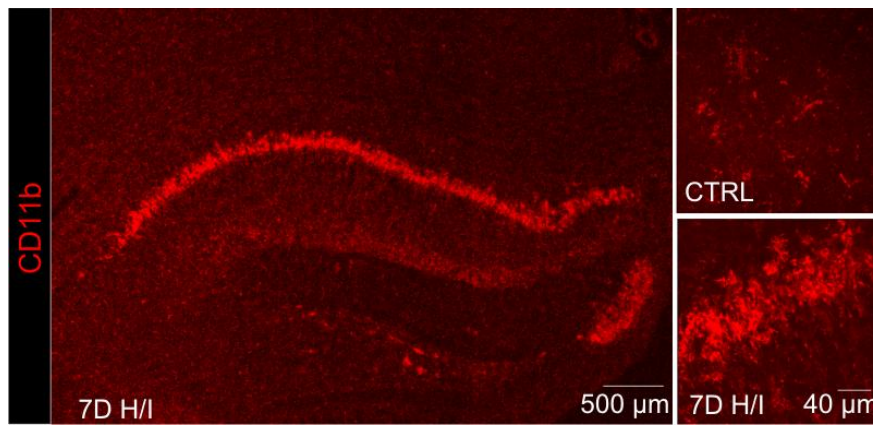


Figure 37. Immunohistochemical staining of the hippocampal CA1 region for CD11b. Coronal sections of the rat hippocampus were immunostained for CD11b, a marker of activated microglia. The CD11b immunoreactivity was markedly increased in *subiculum*, *stratum pyramidale* of the CA1 hippocampal region and *hilus* of the *gyrus dentatus*. Enlargements of tissue section shown on the right depict increased CD11b expression in rats 7 days after hypoxia/ischemia (7D H/I) when compared with control rats.

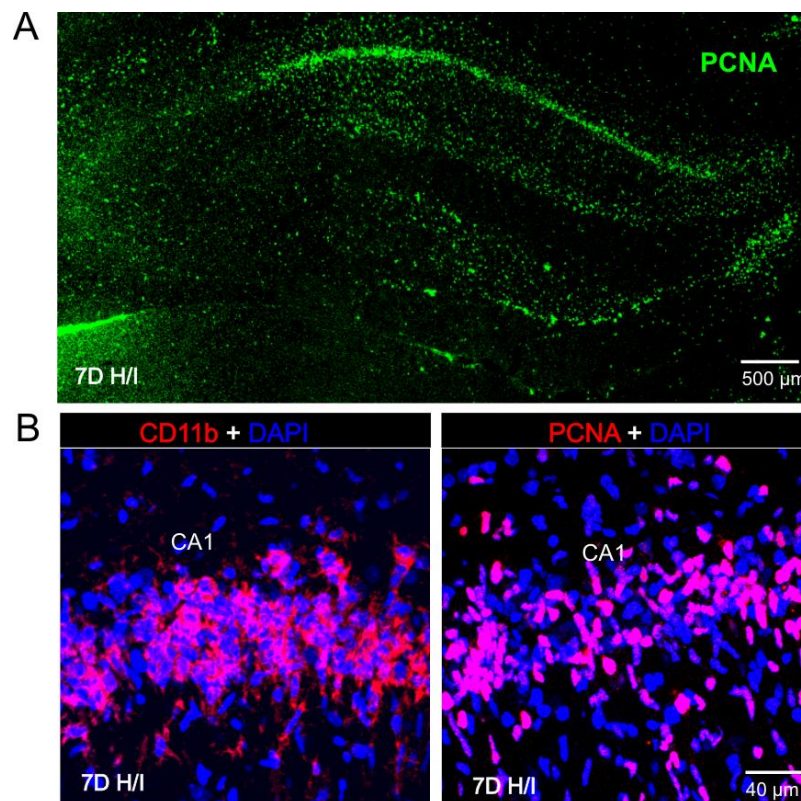


Figure 38. Immunohistochemical staining of the rat hippocampus for CD11b and PCNA in control rats and 7 days after hypoxia/ischemia (7D H/I) rats. (A) Coronal sections were immunostained for proliferating cells nuclear antigen antibodies (PCNA). PCNA-immunoreactivity was increased in rats 7D after H/I, namely in *subiculum*, *stratum pyramidale* of the CA1 region and *hilus* of the *gyrus dentatus* when compared with controls. (B) PCNA immunostaining depict highly proliferated area in the CA1 region of the hippocampus in rats 7D after H/I.

Seven days after H/I the antibody against PCNA indicated that activated microglia were located in actively proliferating zone in the CA1 region of the hippocampus and majority of proliferating cells belong to CD11b positive cells (**Fig. 38**).

The immunohistochemical staining with antibodies against NG2 chondroitin sulfate proteoglycan revealed NG2-expressing glial cells in all experimental groups (**Fig. 35, 36**). However, in the rat hippocampus 3 and 7 days after H/I the NG2 immunoreactivity was markedly increased in the CA1 region and accumulated within the zone of astrogliosis (**Fig. 36**). Furthermore, immunohistochemistry revealed that the hippocampal NG2 glia are highly proliferative cells and they express nestin and PCNA following H/I (**Fig. 39**). The double staining of sections 7D after H/I showed that some NG2-positive cells express GFAP (**Fig. 40**).

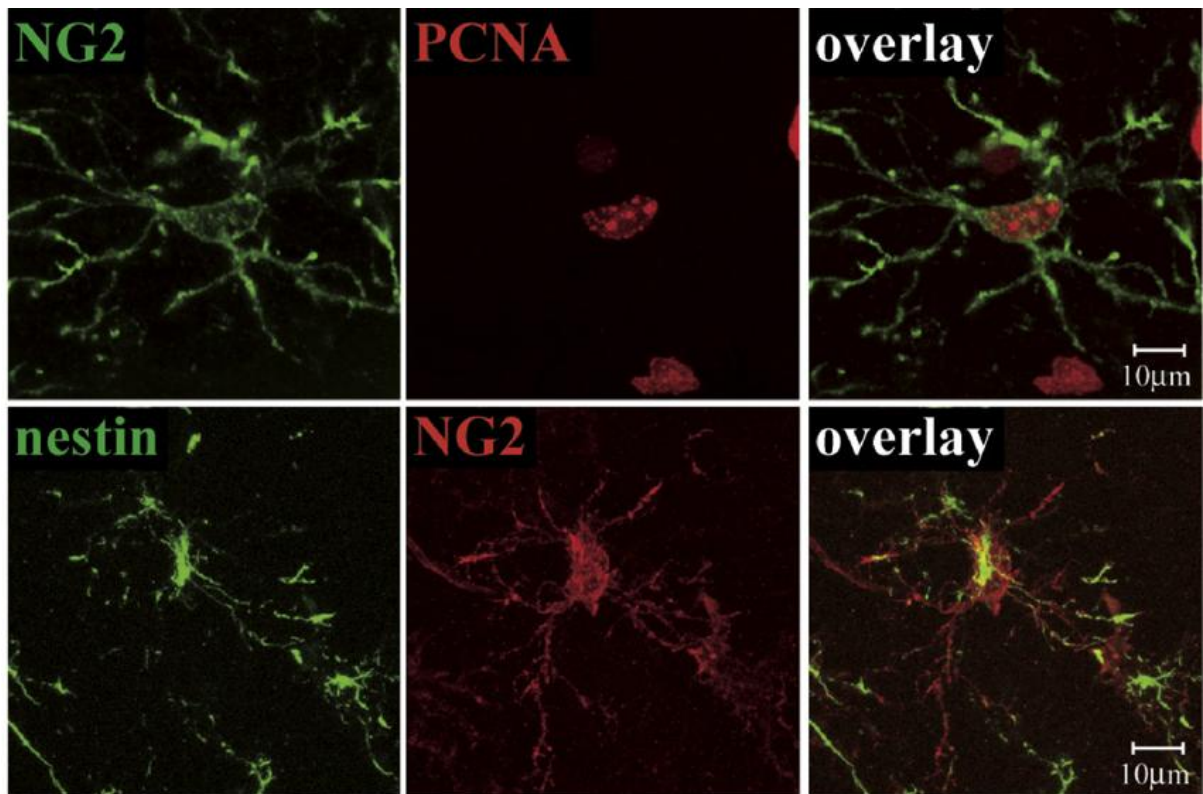


Figure 39. Proliferation of NG2 glia following ischemic injury. A detailed image of NG2 glia in the CA1 region of the hippocampus 3 days after hypoxia/ischemia stained for proliferating cell nuclear antigen (PCNA) and nestin (Pivonkova et al., 2010).

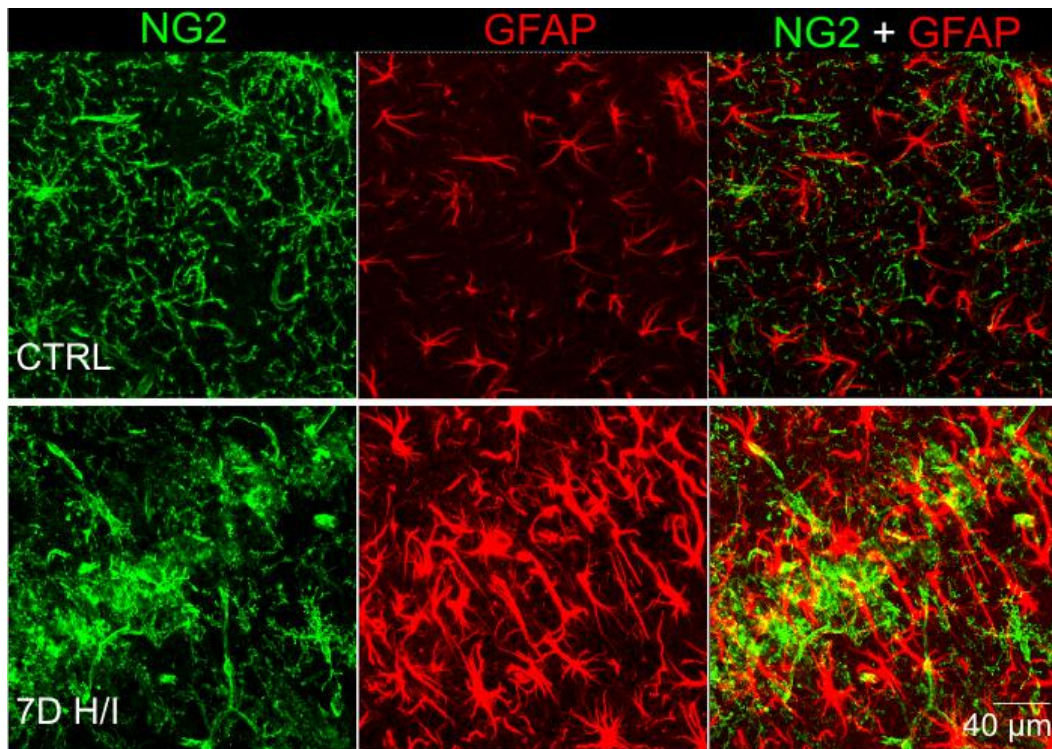


Figure 40. Immunohistochemical staining of the hippocampal CA1 region for NG2 and glial fibrillary acidic protein (GFAP) in control rats and those 7 days after hypoxia/ischemia (7D H/I). Coronal sections of the rat hippocampus were double immunostained for NG2 and GFAP. NG2 immunoreactivity in the CA1 hippocampal region was increased 7D after H/I when compared with sham-operated rats (CTRL).

To detect neurodegeneration the Fluoro-Jade B (FJB) histofluorescence staining was performed in hippocampal slices. The FJB-positive neurons were revealed in hippocampal *stratum pyramidale* 3D and 7D after H/I while no FJB-positive staining was detected in control animals and rats 1D after H/I (**Fig. 41**).

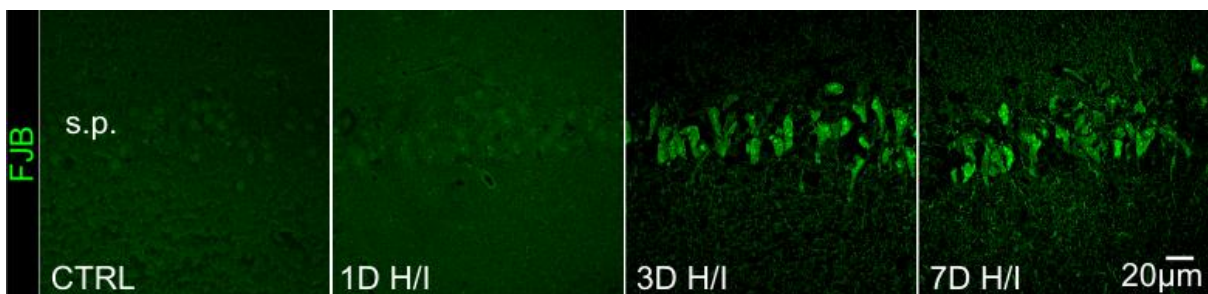


Figure 41. Fluoro-Jade B (FJB) histofluorescence staining of the CA1 region of the hippocampus. In sham-operated rats (CTRL) FJB-positive cells were not detected. FJB-labelled neurodegeneration was observed in *stratum pyramidale* in rats 3 days and 7 days after hypoxia/ischemia (7D H/I). Abbreviations: H/I - hypoxia/ischemia; 1D - 1 day; 3D - 3 days; 7D - 7 days; s.p. - *stratum pyramidale*.

To characterize apoptotic cellular events in ischemic hippocampus the terminal deoxynucleotidyl transferase-mediated 2'-deoxyuridine 5'-triphosphate-biotin nick end labeling (TUNEL) assay detecting DNA fragmentation and immunohistochemical staining for cleaved caspase-3 (Casp3), an apoptotic marker, were performed. The TUNEL assay revealed mainly neuronal cell death in *stratum pyramidale* of the hippocampal CA1 region in rats 7D after H/I, while astrocytes with fragmented nuclei were not detected at this time point (**Fig. 42 A**). Nevertheless, double staining for GFAP and cleaved caspase-3 revealed specific nuclear caspase-3 immunoreactivity in astrocytes of *stratum radiatum* in rats 7D after H/I (**Fig. 42 B**).

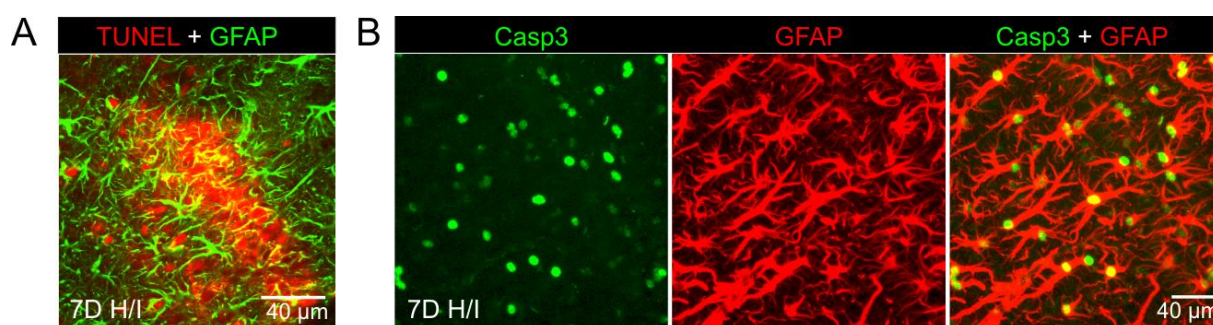


Figure 42. Double immunostaining for glial fibrillary acidic protein (GFAP) with the terminal deoxynucleotidyl transferase-mediated 2'-deoxyuridine 5'-triphosphate-biotin nick end labelling (TUNEL) and with cleaved caspase-3 of the CA1 region. (A) TUNEL-positive nuclei were indicated only in pyramidal neurons in rats 7days after hypoxia/ischemia (7D H/I), while the astroglial nuclei were not labelled. **(B)** The reactive GFAP-positive astrocytes show immunoreactivity for cleaved caspase-3 (Casp3), an apoptotic marker, which was expressed in nuclei of reactive astrocytes.

In summary, the immunohistochemical analysis showed that after 1 hour of reperfusion the cerebral H/I did not caused any neuronal degeneration or morphological changes in glial cells. However, after 7 days of reperfusion the H/I injury is characterized by selective CA1 neuronal death and gliotic scar formation comprising intensively proliferating reactive astrocytes and activated microglia.

Based on our immunohistochemical analyses we have selected two time points of reperfusion for further investigation: 1 hour after H/I (1H H/I) as acute post-ischemic stage that precedes the onset of microglia activation/proliferation, astrocyte activation and vast neuronal death, and a period of massive neuronal death and permanent glia scar formation 7 days after H/I (7D H/I).

4.2 Increased TRPV4 immunoreactivity in hippocampal astrocytes coincides with the development of astrogliosis

To investigate the expression of TRPV4 channels in astrocytes and their possible contribution to hypoxia/ischemia-induced astroglial reactivity, we performed immunohistochemical analyses of the rat hippocampus in control and ischemic rats. In control hippocampal sections double immunostaining with antibodies against TRPV4 and GFAP revealed neuronal TRPV4 immunoreactivity in the *stratum pyramidale* of the CA1 region and only a few TRPV4-positive astrocytes in the *stratum radiatum* of controls (**Fig. 43**). Interestingly, TRPV4 immunoreactivity gradually increased in astrocytes with the progression of reactive gliosis in response to H/I, and it declined in CA1 pyramidal neurons in conjunction with ongoing neuronal cell death. Within 7 days of reperfusion we have observed a shift in TRPV4 immunoreactivity from neurons to reactive astrocytes, ultimately leading to TRPV4 expression only in reactive astrocytes. No pyramidal cells positive for TRPV4 were found in the CA1 hippocampal region after 7 days of reperfusion (**Fig. 44**).

To verify the molecular expression of TRPV4 after H/I and coincidence of TRPV4 protein expression with development of astrogliosis, we performed Western blot analyses of protein lysates extracted from the CA1 region of the hippocampus in control rats and those 1H, 6H, 1D, 3D and 7D after H/I. Previously, Anderova and co-authors demonstrated that neuronal cell death and reactive astrogliosis are observed starting 3D after H/I ([Anderova et al., 2011](#)). Similarly, we observed increased GFAP protein level 3D and 7D after H/I. TRPV4-positive bands were detected with an increase in TRPV4 protein levels 1H after H/I, while 1D and 7D after H/I the overall expression of TRPV4 was down-regulated (**Fig. 45**). According to these findings, we suggest that in 1H after H/I rats the level of TRPV4 protein could be increased in astrocytes as well as in neurons, however 3D and 7D after H/I the detected amount of TRPV4 protein belongs mainly to reactive astrocytes.

Since there was a marked increase in TRPV4 protein level after 1 hour of reperfusion following H/I, we performed quantitative real-time PCR analyses of cell lysates obtained from the CA1 region of the hippocampus, which revealed that there was a 2.4-fold increase in TRPV4 mRNA 1H after H/I when compared to the mRNA content of the hippocampal CA1 region in sham-operated rats (**Fig. 46**).

The apparent discrepancy in TRPV4 expression between immunocytochemistry and Western blotting could be due to the fact that following H/I, neuronal viability decreases, and

this could account for the overall decrease in TRPV4 protein levels observed in total cell lysates of the hippocampal CA1 region.

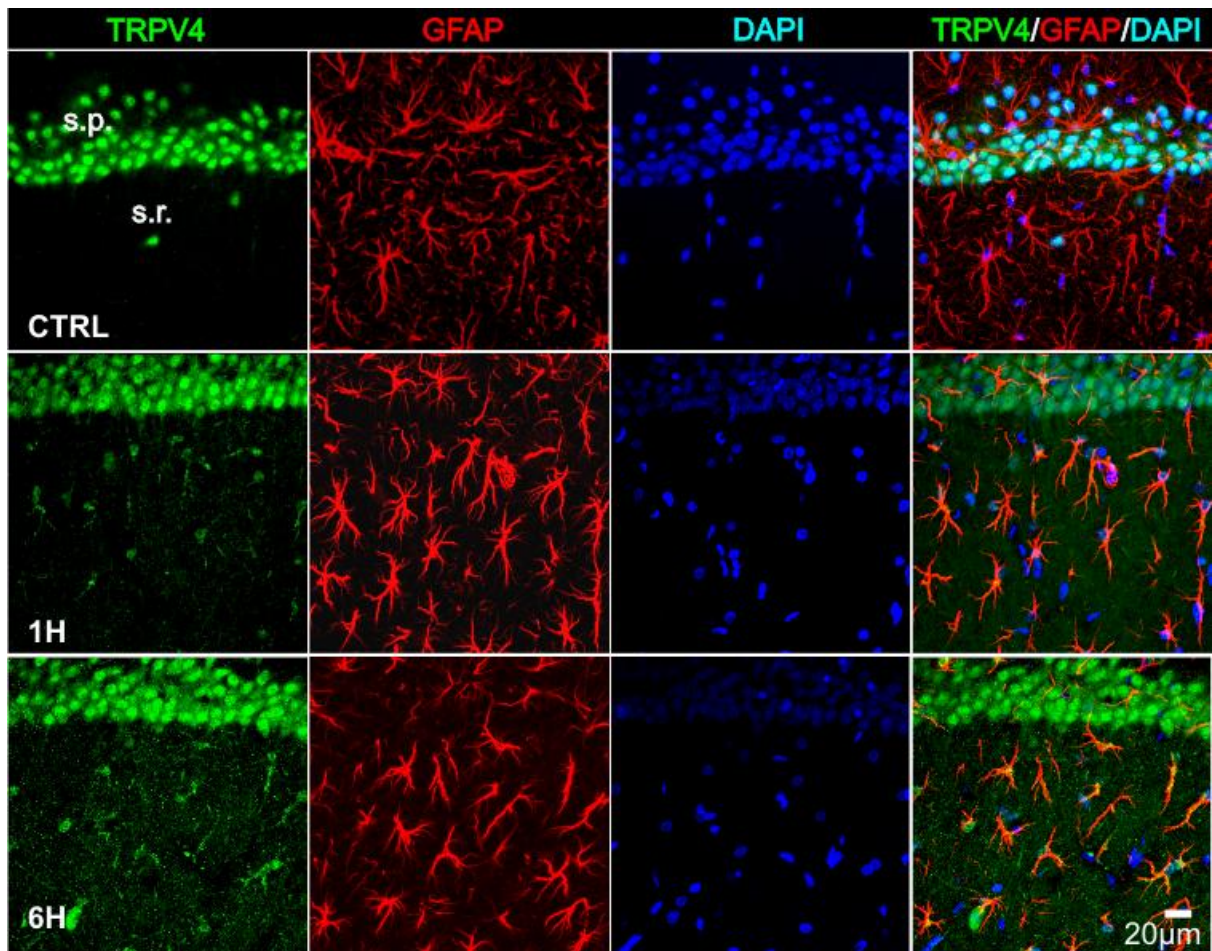


Figure 43. TRPV4 immunostaining in the CA1 region of the hippocampus in control rats and rats after hypoxia/ischemia (H/I) - acute stage of reperfusion. Coronal slices from sham-operated (CTRL) and ischemic rats were labeled for transient receptor potential vanilloid 4 (TRPV4) and glial fibrillary acidic protein (GFAP). Note that in controls, the TRPV4 immunoreactivity was detected in pyramidal cells and rarely in astrocytes. Abbreviations: H/I - hypoxia/ischemia; CTRL - sham-operated rats; 1H - 1 hour; 6H - 6 hours; s.p. - *stratum pyramidale*; s.r. - *stratum radiatum*.

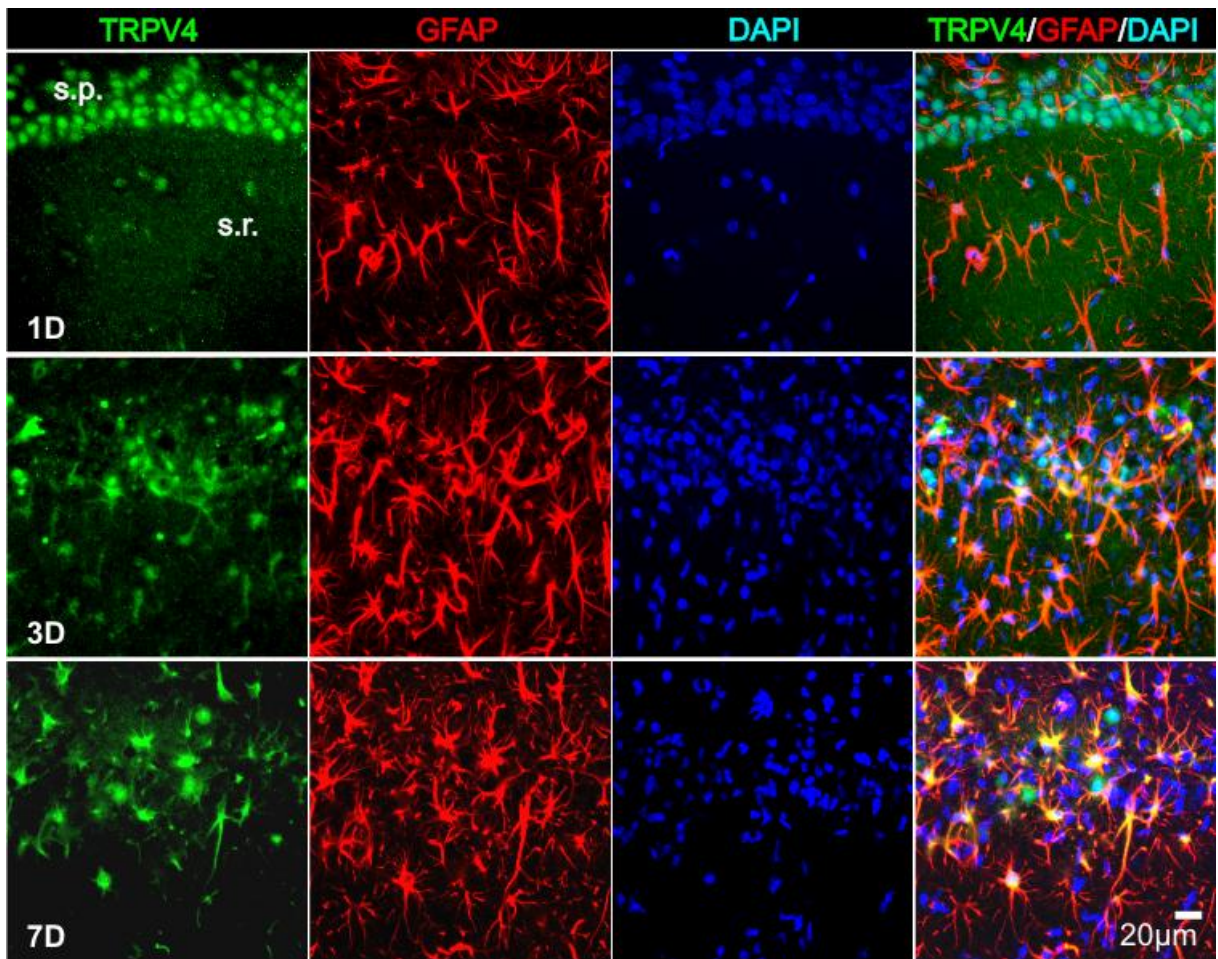


Figure 44. TRPV4 immunostaining in the CA1 region of the hippocampus in rats after hypoxia/ischemia (H/I) - late stages of reperfusion. Coronal slices from sham-operated (CTRL) and ischemic rats were labeled for transient receptor potential vanilloid 4 (TRPV4) and glial fibrillary acidic protein (GFAP). With developing astrogliosis TRPV4 immunoreactivity increased in astrocytes. Seven days after hypoxia/ischemia no TRPV4 expression was detected in pyramidal cells, whereas it was markedly increased in astrocytes. Abbreviations: H/I - hypoxia/ischemia; 1D - 1 day; 3D - 3 days; 7D - 7 days; s.p. - *stratum pyramidale*; s.r. - *stratum radiatum*.

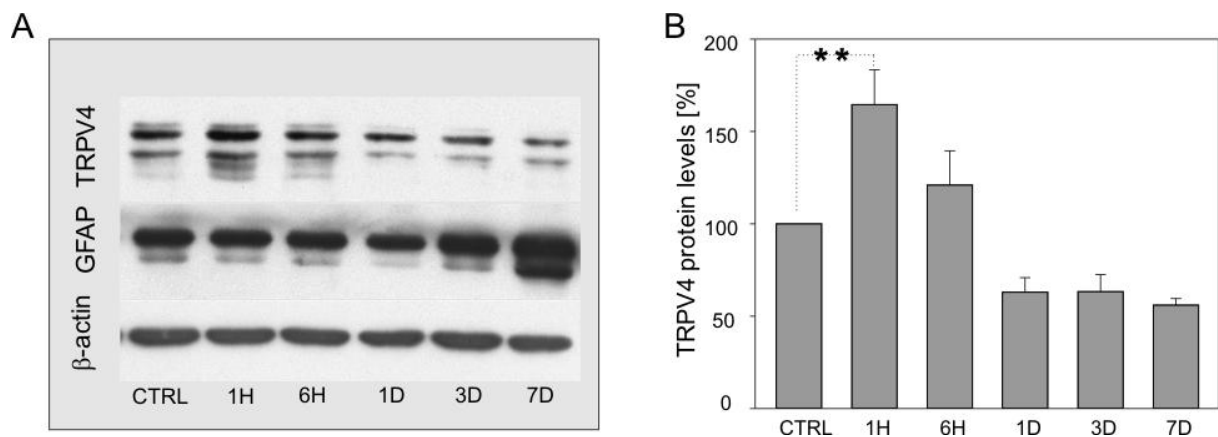


Figure 45. Western blot analyses of TRPV4 protein in the CA1 region of the hippocampus after hypoxia/ischemia. (A) Time-dependent changes in the expression of transient receptor potential vanilloid 4 (TRPV4), glial fibrillary acidic protein (GFAP) and β -actin proteins in the CA1 region of the hippocampus of sham-operated rats (CTRL), 1 hour (1H), 6 hours (6H), 1 day (1D), 3 days (3D) and 7 days (7D) after hypoxia/ischemia (H/I). Note that the expression of GFAP gradually increased 3 and 7 days after H/I. β -actin was used as a loading control. (B) Time-dependent changes in TRPV4 protein levels showing the significant increase in TRPV4 protein 1H after H/I. Data were obtained from 3 independent Western blot analyses. Statistical significance was calculated using one-way ANOVA test; ** $p < 0.01$ very significant.

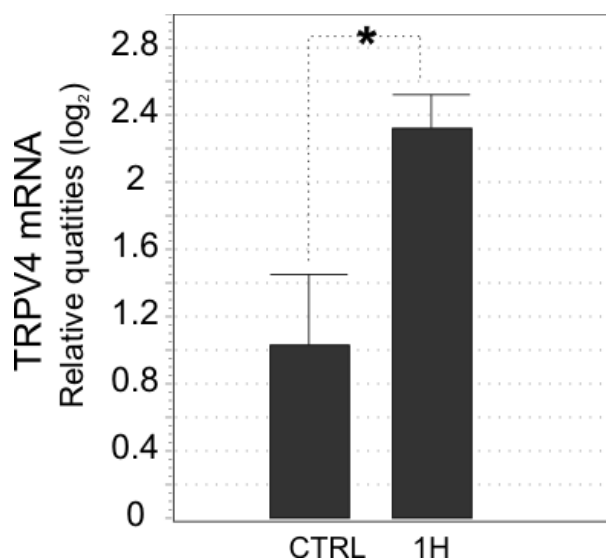


Figure 46. Quantitative RT-PCR revealing significantly increased TRPV4 mRNA levels 1 hour after H/I compared (1H) to sham-operated rats (CTRL). Data were obtained from 3 independent isolations of total mRNA from the hippocampal CA1 region. Statistical significance was calculated using one-way ANOVA; test * $p < 0.05$ significant.

4.3 TRPV4-mediated intracellular Ca^{2+} oscillations in reactive astrocytes are augmented *in situ* after hypoxia/ischemia

Having demonstrated that TRPV4 expression in astrocytes increases in response to H/I, we next sought to elucidate the impact of ischemic injury on TRPV4 channel activity in astrocytes in the CA1 region of the hippocampus by analysing the changes in $[\text{Ca}^{2+}]_i$ signals. During the microfluorimetric $[\text{Ca}^{2+}]_i$ measurements of astrocytes *in situ* we observed spontaneous transient $[\text{Ca}^{2+}]_i$ oscillations measured in aCSF in astrocytes from control animals ($n = 35$) as well as rats 1H ($n = 27$) and 7D ($n = 30$) after H/I (**Fig. 49 A**). The oscillation frequency and amplitude of these spontaneous transient Ca^{2+} spikes significantly increased with the time of reperfusion and were a ~20-fold increase in astrocytes 7D after H/I when compared to controls. Interestingly, we found that 7D after H/I the spontaneous Ca^{2+} transients are partly mediated by TRPV4 channels as the application of RN1734 blocked ~45% of such spontaneous Ca^{2+} transients (**Fig. 47**).

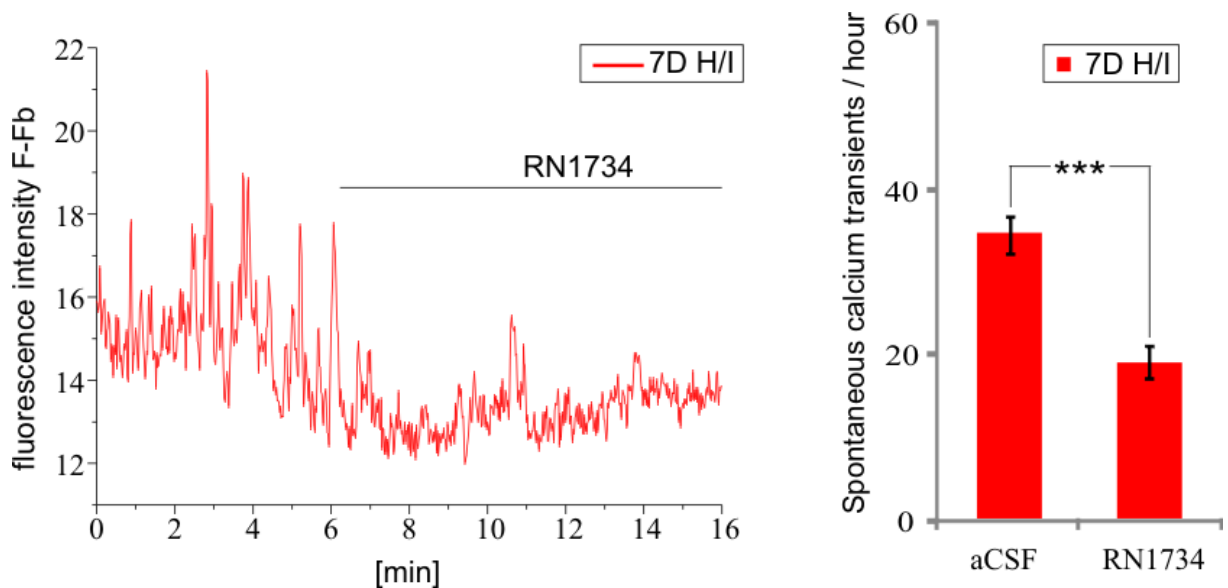


Figure 47. The TRPV4 antagonist RN1734 decreases spontaneous Ca^{2+} oscillations in astrocytes of the hippocampal CA1 region 7 days after ischemia. (Right) The representative traces measured in astrocytes from acute hippocampal slices 7 days after hypoxia/ischemia (7D H/I) showed reduction of spontaneous Ca^{2+} oscillation after RN1734 application. **(Left)** Histogram of the mean spontaneous intracellular calcium transients per hour before RN1734 application (aCSF) and during the application of 10 μM RN1734 (RN1734), measured in astrocytes from acute hippocampal slices 7 days after hypoxia/ischemia (7D H/I, $n=10$). The values are presented as mean \pm S.E.M. Statistical significance was calculated using paired t-test; *** $p < 0.001$ extremely significant.

Nonetheless, the subsequent application of 5 μM 4 α PDD, a selective TRPV4 agonist (Watanabe et al., 2003) resulted in fluorescence intensity increase in Fluo-4 AM loaded

astrocytes and an additional increase in spike frequency (**Fig. 48, 49 A**). In a few astrocytes 1H after H/I and in most of the astrocytes 7D after H/I, 4 α PDD evoked a sustained increase in the amplitude of the $[Ca^{2+}]_i$ signals (**Fig. 48 F**). Although initially 4 α PDD application evoked $[Ca^{2+}]_i$ oscillations similar to those observed in astrocytes of controls or those 1H after H/I, in astrocytes 7D after H/I prolonged exposure to 4 α PDD resulted in the generation of sustained Ca^{2+} entry (**Fig. 48 F, 49 A**). Moreover, the incidence of 4 α PDD-specific responses increased in post-ischemic astrocytes; only 56% of astrocytes from controls exhibited a 4 α PDD-evoked increase in $[Ca^{2+}]_i$, oscillations, while 78% and 84% of astrocytes responded to 4 α PDD application 1 hour and 7 days after H/I, respectively (**Fig. 49 B**).

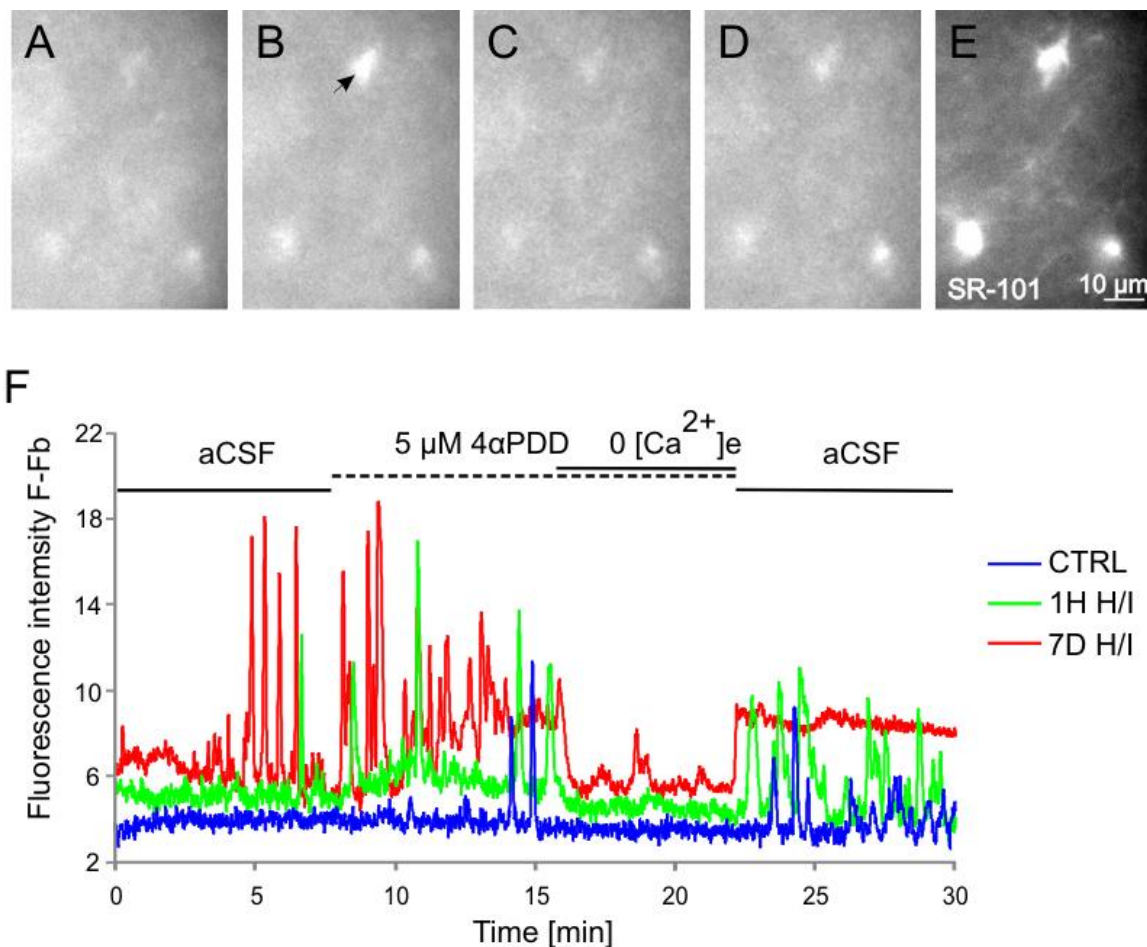


Figure 48. The TRPV4 agonist 4 α PDD triggers Ca^{2+} oscillations in astrocytes of the hippocampal CA1 region. (A-D) Astrocytes in acute rat hippocampal slices loaded with the calcium fluorescent probe Fluo-4 AM respond with an increase in fluorescence to the application of the TRPV4 channel agonist 4 α PDD (5 μ M). (A) Cells before 4 α PDD application in aCSF, (B) during 4 α PDD application, (C) during 4 α PDD application in aCSF without Ca^{2+} (aCSF $_{\emptyset Ca}$) and (D) during washout with aCSF. Note the increased fluorescence indicated by the arrow in B. (E) Cells were loaded with Sulforhodamine 101 (SR-101) to verify that the measured cells are astrocytes. (F) Representative fluorescence traces with background correction of astrocytes in acute slices prepared from sham-operated rats (CTRL) and rats 1 hour (1H H/I) and 7 days (7D H/I) after hypoxia/ischemia.

The application of 4 α PDD in the absence of extracellular Ca²⁺ (aCSF_{∅Ca}) immediately and almost completely abolished the Ca²⁺ spike activity, which was restored upon re-addition of Ca²⁺. During washout, in some of the astrocytes 7D after H/I, the elevated signal amplitude was restored, but distinct spikes were no longer detectable (**Fig. 49 A**).

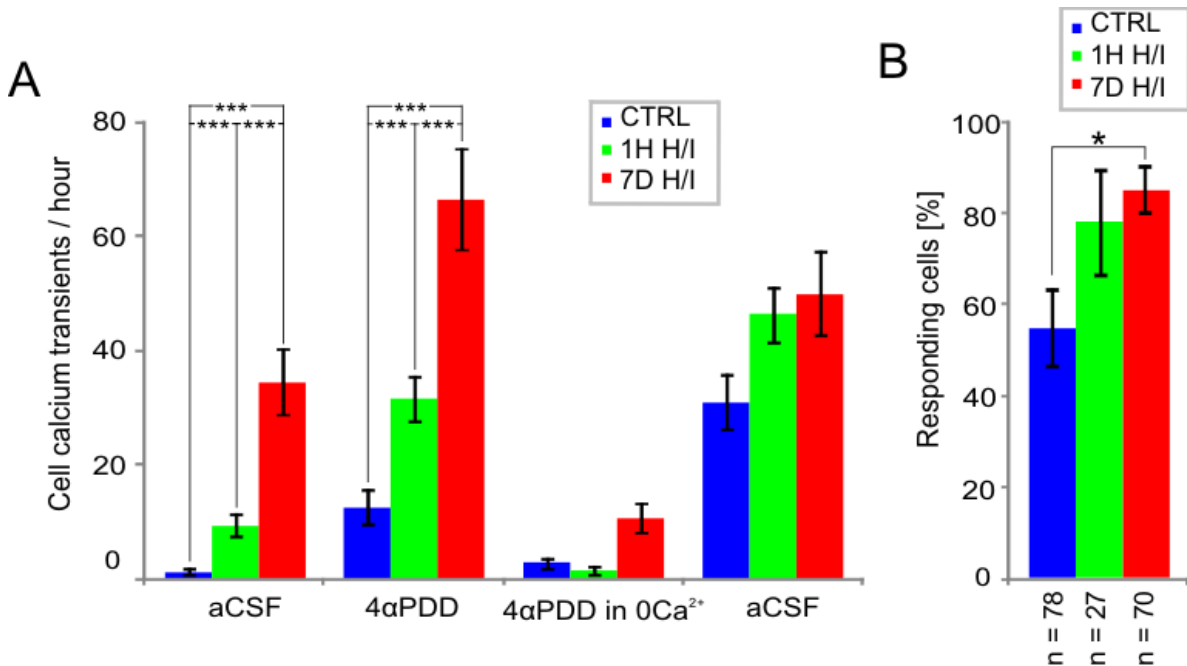


Figure 49. Changes in 4 α PDD-evoked transient Ca²⁺ oscillations in response to hypoxia/ischemia. (A) Histogram of the mean intracellular calcium transients per hour before 4 α PDD application (aCSF), during 4 α PDD application (4 α PDD), during 4 α PDD application in aCSF_{∅Ca} (4 α PDD in aCSF_{∅Ca}) and following washout (aCSF), measured in astrocytes from acute hippocampal slices prepared from the brains of sham-operated rats (CTRL) and those 1 hour (1H H/I) and 7 days (7D H/I) after hypoxia/ischemia. (B) Histogram of the number of responding cells (n = number of all analyzed cells). The values are presented as mean \pm S.E.M. Statistical significance was calculated using one-way ANOVA. *p < 0.05, significant; ***p < 0.001, extremely significant.

The application of 5 μ M 4 α PDD in the presence of 10 μ M RN1734, a novel selective TRPV4 inhibitor (Vincent et al., 2009), abolished ~70% of the Ca²⁺ spike activity in astrocytes 7D after H/I, which was not restored after washout in aCSF (**Fig. 50**).

Seven days after H/I 4 α PDD not only increased Ca²⁺ transients, but also resulted in sustained Ca²⁺ entry as demonstrated in **Fig.48 F** (red line), represented by an increase in the baseline fluorescence intensity. Such sustained Ca²⁺ entry, which was always completely blocked in the absence of extracellular Ca²⁺, was rare in controls (1 cell out of 35); however, it increased with the time of reperfusion: it was detected in 4 cells out of 27 1H after H/I and in 17 cells out of 30 7D after H/I. Surprisingly, RN1734 blocked only Ca²⁺ transients; we never observed a decline of sustained Ca²⁺ entry in response to this inhibitor (**Fig. 50 A**, red line).

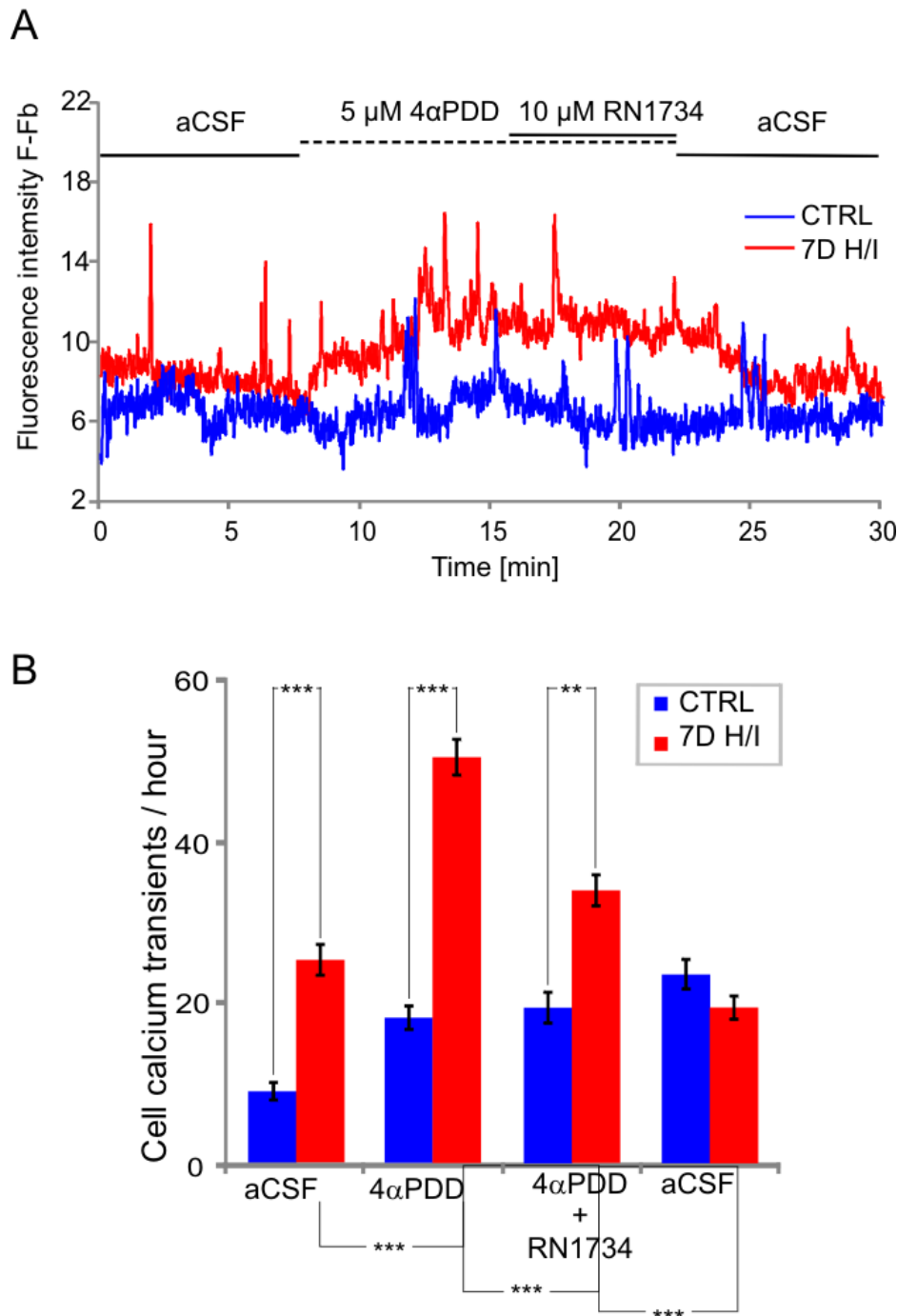


Figure 50. The TRPV4 antagonist RN1734 decreases 4αPDD-induced Ca^{2+} transients in astrocytes of the hippocampal CA1 region 7 days after ischemia. (A) Representative fluorescence traces of hippocampal astrocytes in slices prepared from sham-operated rats (CTRL) and rats 7 days after hypoxia/ischemia (7D H/I) before 4αPDD application (aCSF), during 5 μM 4αPDD application, during the application of 5 μM 4αPDD with 10 μM RN1734 and following washout (aCSF). (B) Histogram of the mean intracellular calcium transients per hour before 4αPDD application (aCSF), during the application of 5 μM 4αPDD, during the application of 5 μM 4αPDD + 10 μM RN1734 and following washout in aCSF, in astrocytes in hippocampal slices prepared from the brains of sham-operated rats (CTRL, n = 43) and those 7 days after hypoxia/ischemia (7D H/I, n = 40). The values are presented as mean ± S.E.M. Statistical significance was calculated using one-way ANOVA; ***p < 0.001 extremely significant, **p < 0.01 very significant.

These results indicate that the increased expression/immunoreactivity of TRPV4 in ischemic astrocytes is accompanied by enhanced TRPV4-mediated Ca^{2+} oscillations.

4.4 TRPV4-specific cation currents are up-regulated in reactive astrocytes *in situ* after hypoxia/ischemia

Next, we examined the effect of H/I on TRPV4-mediated currents in astrocytes *in situ*. The typical membrane current patterns of hippocampal astrocytes in control and ischemic tissue were identified in Ext1 solution by hyper- and depolarizing the astrocytic membrane from -100 mV to +100 mV in 20 mV increments, with the holding potential (V_h) at -70 mV (Fig. 51).

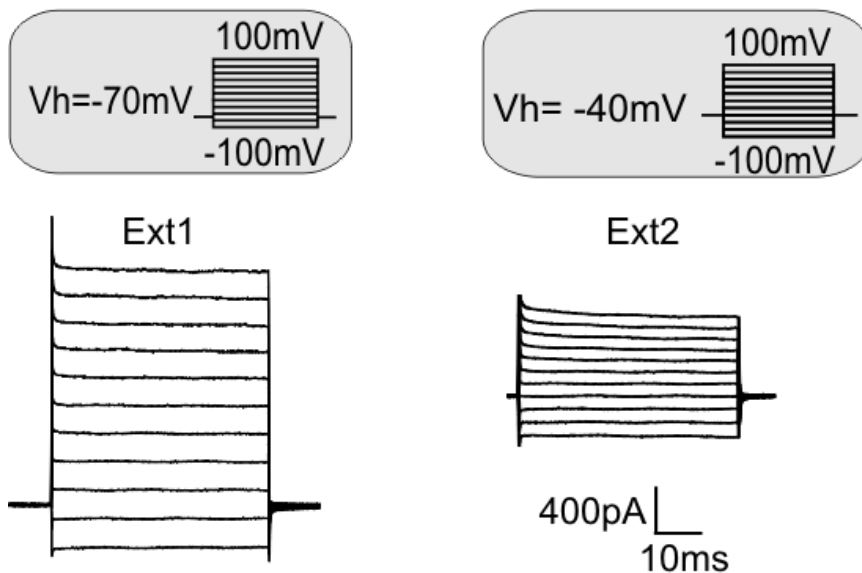


Figure 51. Typical current pattern of astrocytes *in situ* recorded in the CA1 region of the hippocampus 7 days after hypoxia/ischemia. Astrocytes were held at a holding potential of -70 mV (left, the extracellular solution Ext1 contained K^+ and Na^+) and at -40 mV (right, K^+ and Na^+ were replaced by Cs^+ in the extracellular solution Ext2).

Generally, the mature hippocampal astrocytes of sham-operated- as well as post-ischemic rats displayed a passive current pattern, characterized by time- and voltage-independent currents, mainly carried by K^+ channels, and their passive membrane properties are listed in **Table 7**.

Table 7. Membrane properties of hippocampal astrocytes recorded in slices from sham-operated (CTRL) rats and 1H and 7D after H/I.

	V_{rest} (mV)	IR (M Ω)	C_m (pF)	n
CTRL	-75.3 \pm 1.2	65.1 \pm 9.7	25.8 \pm 3.7	16
1H H/I	-72.3 \pm 1.4	66.8 \pm 6.7	24.9 \pm 3.6	16
7D H/I	-69.1 \pm 1.5**	89.4 \pm 9.6	20.4 \pm 2.6	14

The values are presented as mean \pm S.E.M. Asterisks (**p < 0.01) indicate very significant differences between astrocytes from control and ischemic rats. Abbreviations: V_{rest} - resting membrane potential, IR - input resistance, C_m - membrane capacitance, n - number of cells.

The CA1 hippocampal astrocytes 1H after H/I displayed passive membrane properties comparable with those obtained in controls, while reactive hypertrophied astrocytes were significantly depolarized 7 days after H/I. Our Western blot analyses revealed that progression of astrogliosis correlates with astrocyte depolarization and moreover, with marked down-regulation of Kir4.1 protein expression (**Fig. 52**).

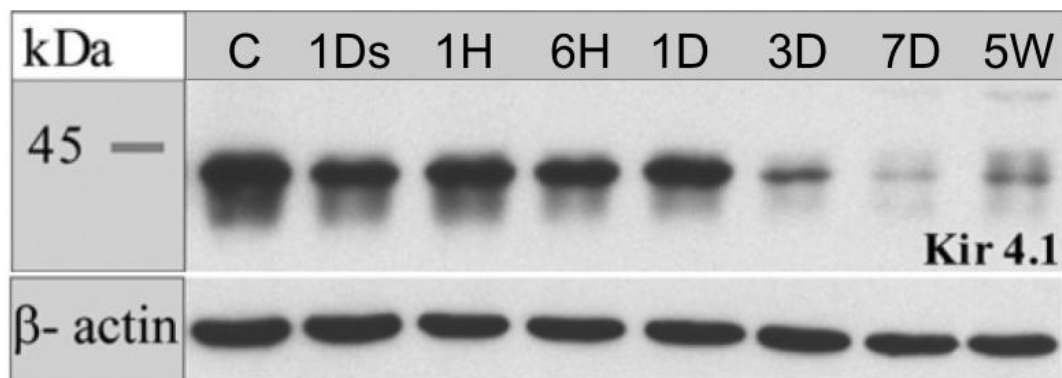


Figure 52. Changes in the expression of Kir4.1 K⁺ channels in the CA1 region of the hippocampus after hypoxia/ischemia. The Western blot technique showed marked down-regulation of Kir4.1 channel expression starting 3 days after hypoxia/ischemia compared to controls. Abbreviations: C - control, 1Ds – 1 day sham-operated, 1H – 1 hour after hypoxia/ischemia, 6H – 6 hour after hypoxia/ischemia, 1D – 1 day after hypoxia/ischemia, 3D – 3 days after hypoxia/ischemia, 7D – 7 days after hypoxia/ischemia, 5W – 5 weeks after hypoxia/ischemia.

To isolate more accurately the TRPV4-specific cationic currents, further recordings were performed in intra- and extracellular solutions, in which K^+ and Na^+ were replaced with Cs^+ (Benfenati et al., 2007). Under these experimental conditions, passive K^+ conductance evoked by hyperpolarizing and depolarizing voltage steps from -100 mV to +100 mV (at V_h of -40mV) were diminished (Fig. 51). To elicit TRPV4-mediated currents, astrocytes *in situ* were recorded in Ext2 solution and 10 μ M 4 α PDD was applied for 6 – 8 minutes. The cells were clamped at V_h of 0 mV and stimulated with a voltage ramp from -100 mV to +100 mV (500 ms) after a 500 ms potential step to -100 mV. Only 25% of astrocytes from controls exhibited 4 α PDD-evoked currents, whereas the incidence of responding astrocytes increased 1H (52%) and 7D (59%) after H/I (Fig. 53).

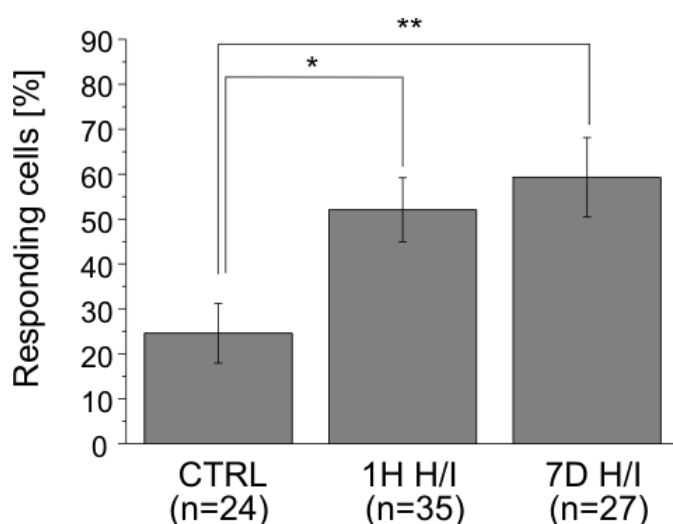


Figure 53. Percentage of hippocampal astrocytes from sham-operated rats (CTRL), and rats 1 hour (1H H/I) and 7 days after hypoxia/ischemia (7D H/I) that responded to 10 μ M 4 α PDD (n = number of cells). The threshold for a 4 α PDD current response was 120% of the control ramp current (prior to agonist application), at a voltage of +/-100 mV. The values are presented as mean \pm S.E.M. Statistical significance was calculated using one-way ANOVA. * $p < 0.05$, significant; ** $p < 0.01$, very significant.

The threshold for a 4 α PDD current response was 120% of the control ramp current (prior to agonist application), at a voltage of +/-100 mV. In response to 4 α PDD application, astrocytes exhibited an increase in outward and inward currents (Fig. 54 A). 4 α PDD-evoked current was delayed 1-3 minutes after the onset of agonist application, with a rather linear current-voltage relationship (Fig. 54 B).

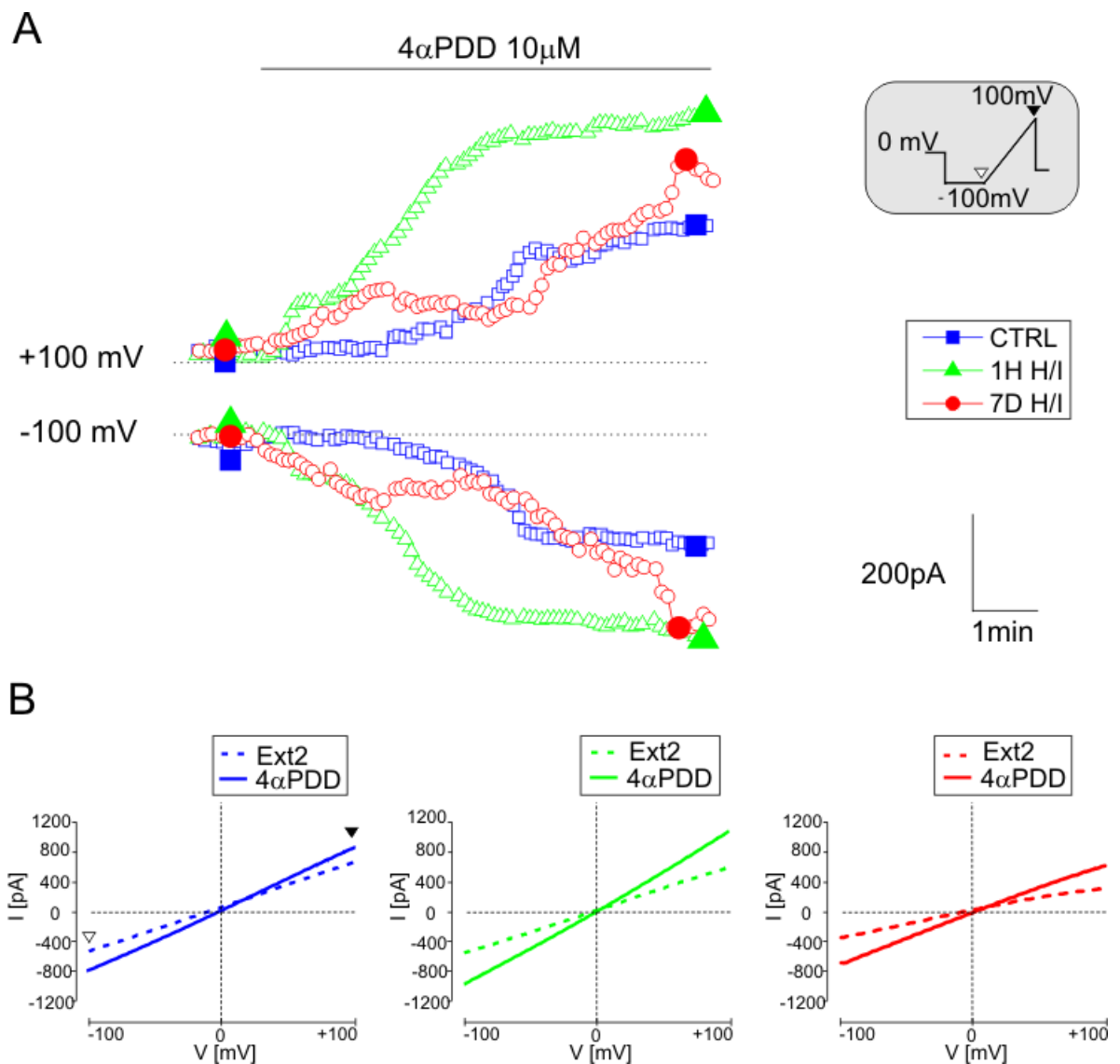


Figure 54. $4\alpha\text{PDD}$ -evokes an increase in membrane conductance in astrocytes *in situ*. (A) Time course of $4\alpha\text{PDD}$ -evoked currents measured from the ramp protocol in astrocytes of controls (blue squares) and astrocytes 1H (green triangles) and 7D after H/I (red circles). Currents were measured at -100 mV (white arrowhead) and +100 mV (black arrowhead) in response to a voltage ramp stimulation protocol (see the inset). (B) Representative traces of steady state currents (same cells as in A) recorded before (in Ext2 solution, dashed line) and during $4\alpha\text{PDD}$ application (full line) in hippocampal astrocytes of controls (left) and those 1H (middle) and 7D after H/I (right). Representative traces of steady state currents were obtained at the times indicated by the filled blue squares, green triangles and red circles in A. White and black arrowheads indicate the applied voltage ramp and the corresponding current traces (see the inset in A).

Nevertheless, the $4\alpha\text{PDD}$ -evoked current amplitudes were not significantly different when compared to those in control astrocytes or those recorded after H/I (Fig. 55).

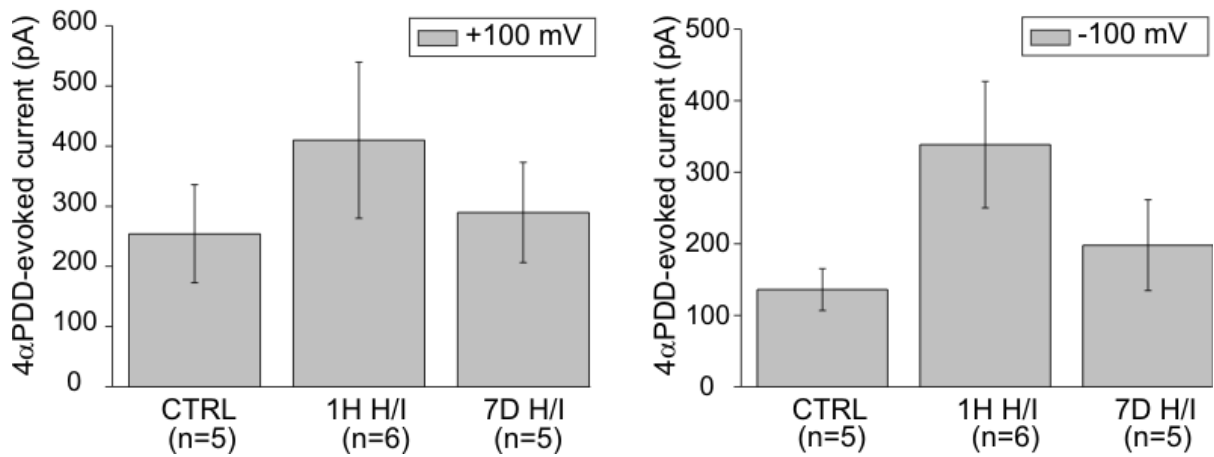


Figure 55. Changes in TRPV4-mediated currents in astrocytes *in situ* following hypoxia/ischemia. Histograms of 4αPDD-evoked changes in current amplitudes at +100 mV (**left**) and -100 mV (**right**) in control astrocytes (CTRL) and astrocytes in slices prepared from rats 1H and 7D after H/I.

Besides the increase of current amplitude in astrocytes after H/I, the exposure to 4αPDD shifted the reversal potential from -15.1 ± 2.2 mV to -5.9 ± 1.7 mV ($\Delta E_{rev} = 9.1 \pm 1.7$ mV, $n = 13$), which is consistent with the development of a cationic current. In the absence of extracellular Ca^{2+} ($Ext2_{\emptyset Ca}$), the amplitude of the 4αPDD-evoked currents was reduced by $68.7 \pm 18.3\%$ ($n = 4$, **Fig. 56 A**). Finally, the extracellular application of the non-specific inhibitor of TRP channels Ruthenium Red (RR, 10 μM) (Jia et al., 2004) or selective antagonist of TRPV4 channels RN1734 (10 μM) reduced the 4αPDD-evoked currents by $73.3 \pm 15.7\%$ ($n = 4$) and $56.9 \pm 15.0\%$ ($n = 4$), respectively (**Fig. 56 B, C**).

This finding is a further strong indication of the involvement of TRPV4 in the current response to 4αPDD. This pharmacological profile was qualitatively identical in all three experimental groups. These results overlap those described for the functional expression of TRPV4 in cultured astrocytes (Benfenati et al., 2007), and they strongly indicate that TRPV4 channels are also functionally expressed *in situ* in hippocampal astrocytes of the CA1 region and moreover, they are up-regulated after H/I.

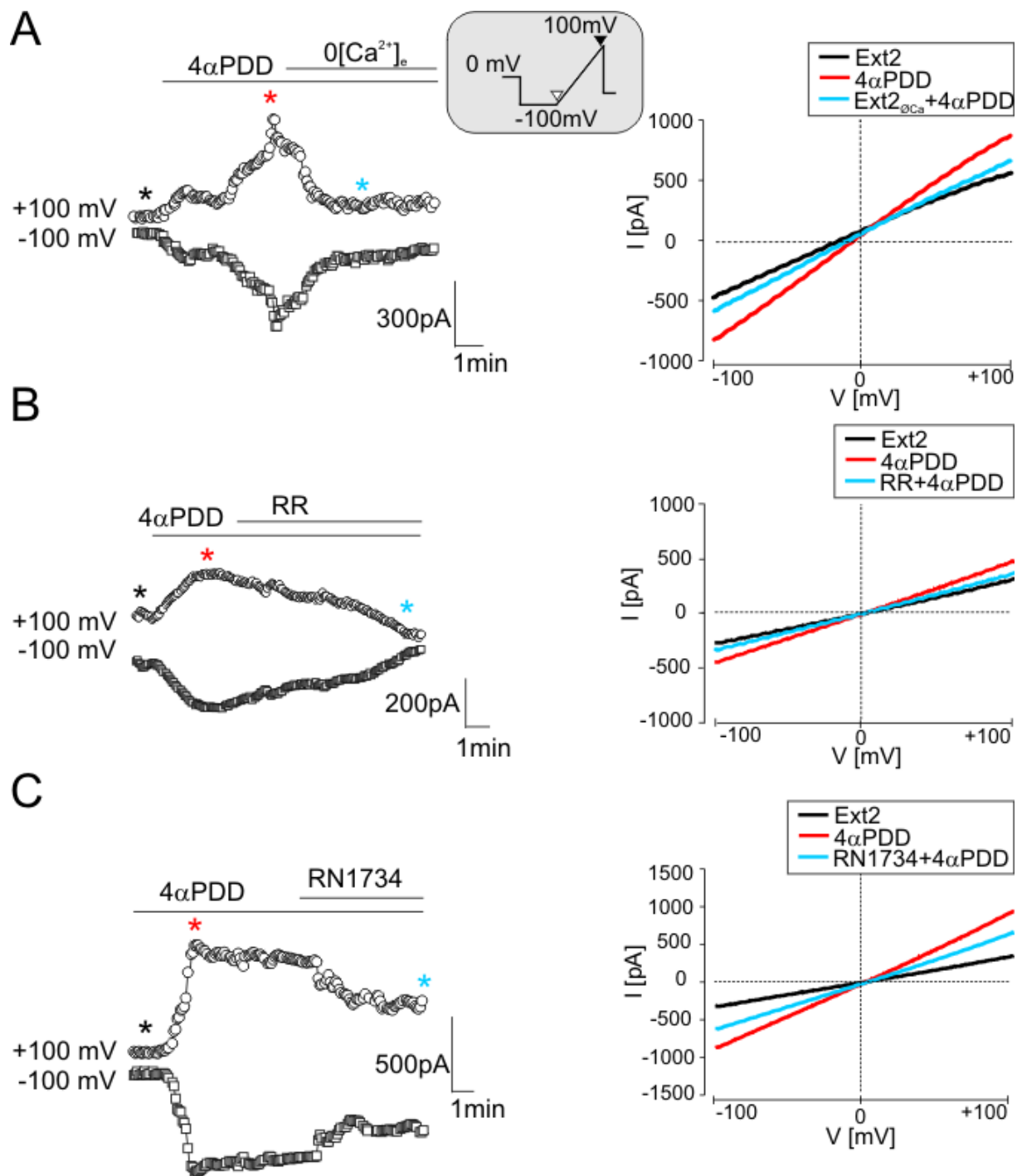


Figure 56. Currents evoked by 4αPDD in hippocampal astrocytes *in situ* are reduced by calcium-free extracellular solution, Ruthenium Red or RN1734. (A-C, left) Time course of 4αPDD-evoked currents measured from the ramp protocol in astrocytes 7D after H/I (for the voltage protocol see the inset) prior to and during 4αPDD (10 μM) application and after removing extracellular Ca²⁺ (Ext2_{0Ca}, A) or after the application of TRPV4 inhibitors, such as Ruthenium Red (RR, 10 μM, B) or RN1734 (10 μM, C). (A-C, right) The traces of the steady state currents (same cells as in left) obtained in Ext2 solution (black lines), during 4αPDD application (red lines) and after removing extracellular Ca²⁺ (Ext2_{0Ca}, A) or after the application of TRPV4 inhibitors, such as Ruthenium Red (RR, 10 μM, B) or RN1734 (10 μM, C), are indicated by blue lines. Representative traces of steady state currents were obtained at the times indicated by asterisks of the corresponding colors.

4.5 Immunohistochemical and electrophysiological analysis of primary cultured astrocytes isolated from hippocampal CA1 region revealed two distinct types of astrocytes

It is well known that recordings in astrocytes *in situ* are affected by their large passive K^+ conductance and by their functional coupling to other astrocytes. Moreover, from our *in situ* experiments we could not rule out that the TRPV4-mediated currents were evoked primarily in neurons and, as a result, could then trigger Ca^{2+} entry into astrocytes. To address this issue, we performed next experiments in individual primary astrocytes isolated from the CA1 region of the hippocampus from sham-operated rats and those 1H and 7D after H/I and cultured for 4-5 days.

In all experimental groups, immunocytochemical staining of primary cultured astrocytes with antibodies against GFAP and GLAST demonstrated two morphologically distinct types of astrocytes: i.e. astrocytes with a flat polygonal or elongated soma and astrocytes with a non-flat small oval soma and multiple long processes (Fig. 57).

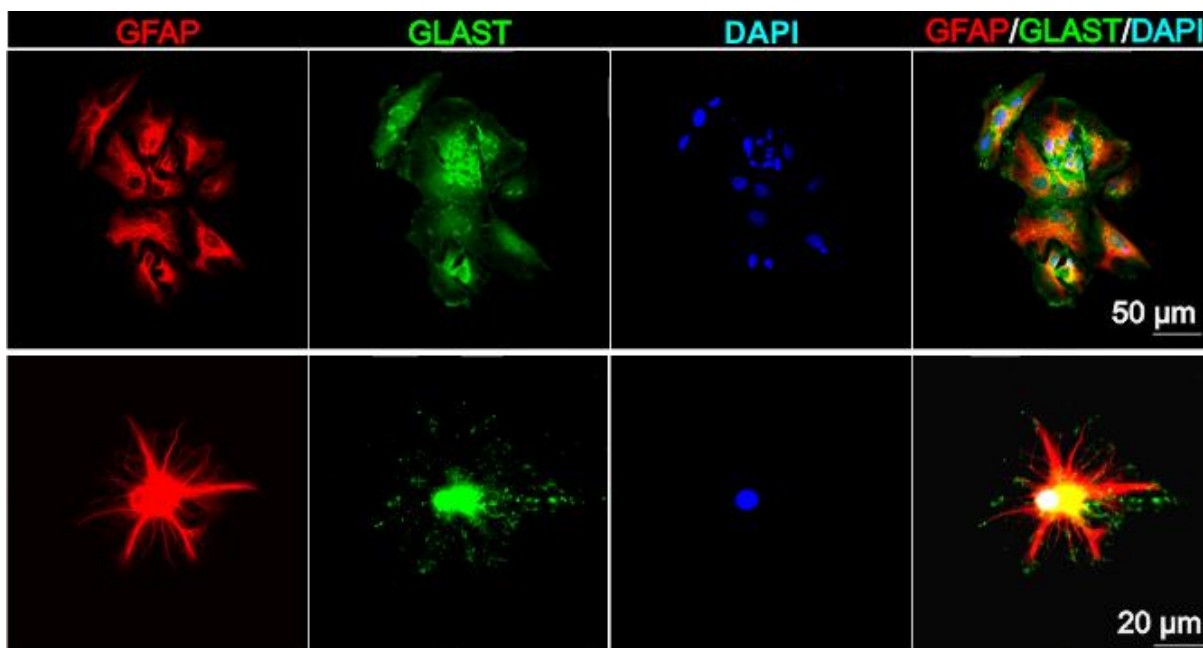


Figure 57. Immunocytochemical identification of cultured astrocytes dissociated from the CA1 region of the hippocampus. The distinct morphology of astrocytes isolated from sham-operated rats or from the ischemic hippocampal CA1 region: flat astrocytes (**top**) and non-flat astrocytes (**bottom**) cultured for 4-5 days. Both types of astroglial cells expressed glial fibrillary acidic protein (GFAP) and GLAST.

The numbers of GFAP-positive flat and non-flat astrocytes were determined in controls, 1H and 7D after H/I and expressed as the percentage of the total number of GFAP-positive cells. Interestingly, the proportions of the two morphologically distinct types of astrocytes changed in response to H/I (**Fig. 58**). Astrocyte cultures obtained from control rats comprised $56 \pm 3.6\%$ of flat astrocytes (number of coverslips, $n = 17$), while in cultures obtained from ischemic animals their number significantly declined to $31 \pm 3.9\%$ in cultures isolated 1H after H/I ($n = 17$) and to $17 \pm 4.3\%$ in cultures isolated 7D after H/I ($n = 21$). In contrast, the percentage of non-flat astrocytes increased in response to ischemic injury.

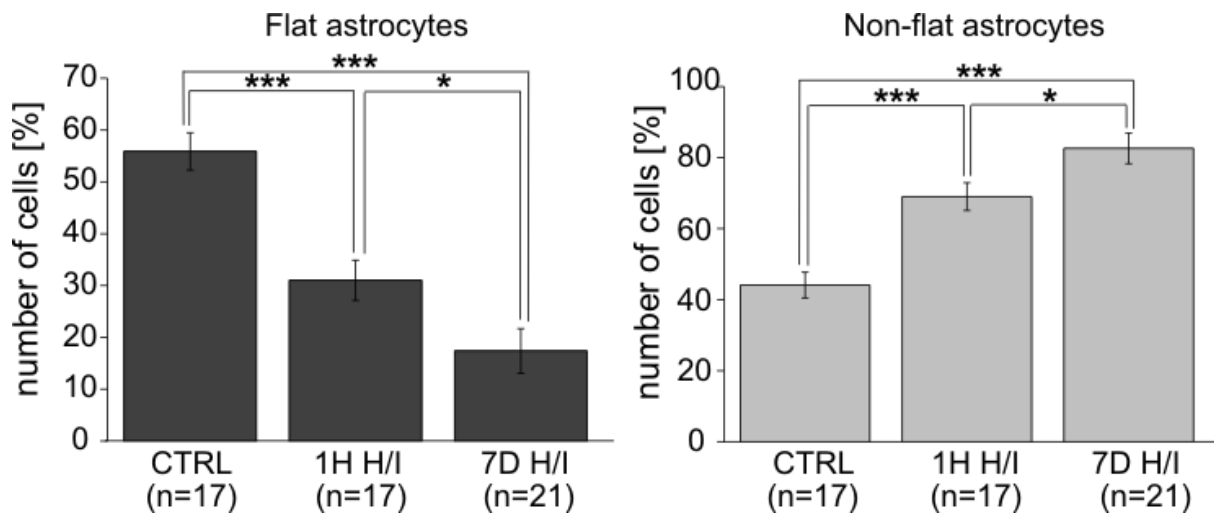


Figure 58. The incidence of flat and non-flat astrocytes in controls (CTRL) and those isolated from the CA1 hippocampal region 1H and 7D after H/I ($n =$ number of coverslips). The values are presented as mean \pm S.E.M. Statistical significance was calculated using one-way ANOVA. * $p < 0.05$, significant; *** $p < 0.001$, extremely significant.

The double immunostaining of cultured astrocytes dissociated from the CA1 region of the hippocampus with antibodies against TRPV4 and GFAP revealed TRPV4 immunoreactivity in flat astrocytes as well as in non-flat astrocytes in all experimental groups (**Fig. 59**).

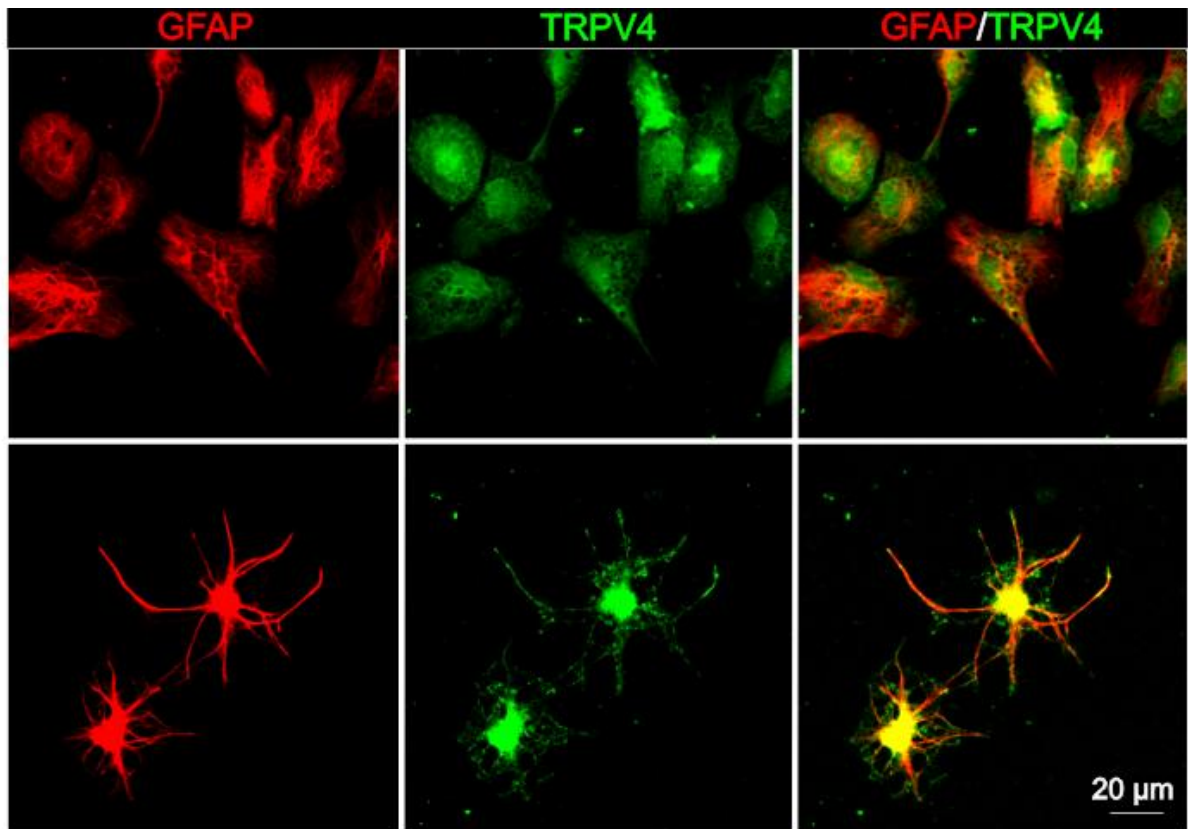


Figure 59. TRPV4 immunocytochemical staining of cultured astrocytes dissociated from the CA1 region of the hippocampus. Flat astrocytes (**top**) as well as non-flat astrocytes (**bottom**) were positive for TRPV4.

In order to identify the current pattern of the two types of astrocytes *in vitro*, physiological Na⁺- and K⁺-containing solutions were used (**Table 4, 5**). The cells labeled with Alexa-Fluor hydrazide during patch clamp recording were identified as astrocytes using an antibody against GFAP (**Fig. 60 A, B**). The membrane currents of astrocytes were recorded in response to hyperpolarizing and depolarizing voltage steps, ranging from -160 mV to +20 mV at V_h of -70 mV. Isolated astrocytes cultured for 4-5 days showed two distinct current profiles as described on freshly isolated astrocytes by Zhou and Kimelberg (Zhou and Kimelberg, 2000). The flat astrocytes were mainly characterized by passive K⁺ currents (**Fig. 60 C right**) whereas non-flat astrocytes showed a “complex” current profile (**Fig. 60 C left**).

Since the passive membrane properties of flat and non-flat astrocytes in each experimental group were not significantly different, they were pooled together (see **Table 8**).

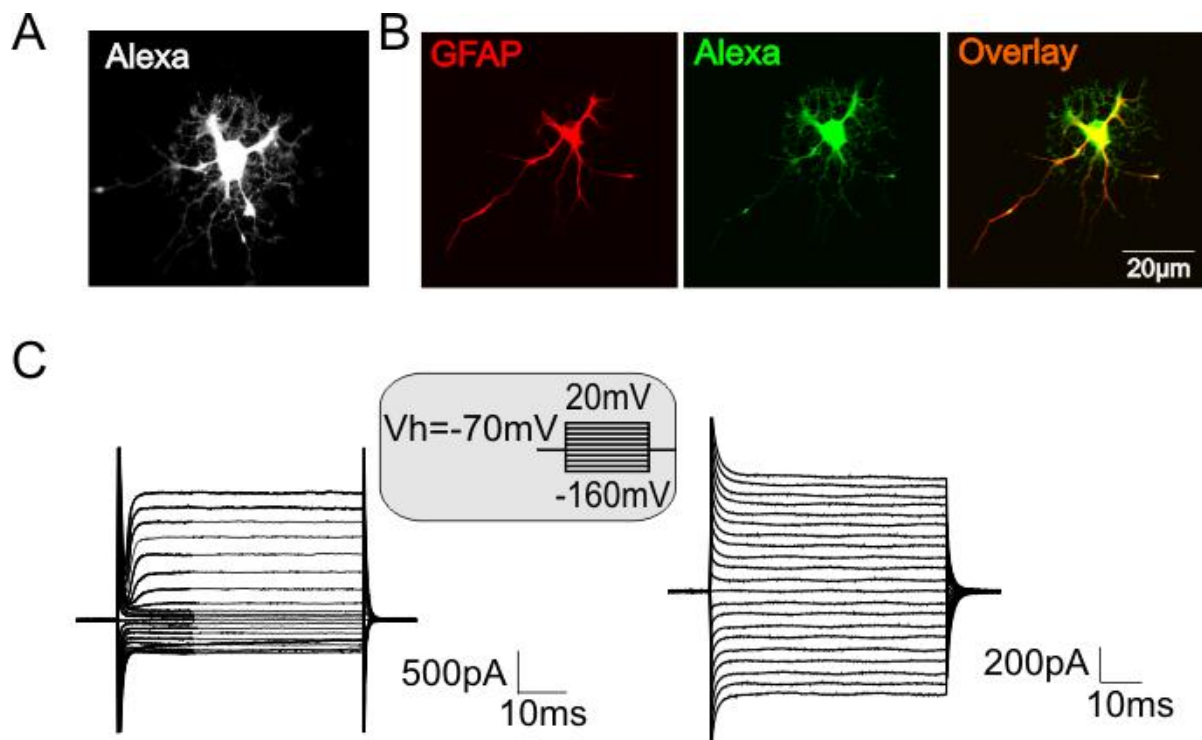


Figure 60. Patch-clamp recording of astrocytes *in vitro*. (A) An image of Alexa-Fluor hydrazide-loaded astrocyte taken by a digital camera immediately after patch-clamp recording and (B) the same astrocyte identified by immunostaining with glial fibrillary acidic protein (GFAP). The overlay image shows the co-localization of GFAP with Alexa. (C) “Complex” and “passive” current patterns in astrocytes *in vitro* evoked by membrane depolarization and hyperpolarization from the holding potential of -70 mV. The currents were recorded using K⁺- and Na⁺-containing intra- and extracellular solutions (Int1 and Ext1). The voltage step protocol is shown in the inset.

Table 8. Membrane properties of isolated astrocytes from CA1 region of hippocampus from sham-operated (CTRL) rats and 1H and 7D after H/I.

	V_{rest} (mV)	IR (M Ω)	C _m (pF)	n
CTRL	-71.3 ± 1.9	296.3 ± 78.1	18.5 ± 2.4	9
1H H/I	-77.2 ± 1.4	211.7 ± 64.4	26.6 ± 1.3**	25
7D H/I	-71.3 ± 2.7	265.3 ± 55.5	19.7 ± 2.7	8

The values are represented as mean ± S.E.M. Asterisks (**) indicate very significant differences between astrocytes from control and ischemic rats 1 hour after hypoxia/ischemia. Abbreviations: CTRL - controls, 7D H/I - 7 days after hypoxia/ischemia, 1H H/I - 1 hour after hypoxia/ischemia, V_{rest} - resting membrane potential, IR - input resistance, C_m - membrane capacitance, n - number of cells.

4.6 TRPV4-mediated intracellular Ca^{2+} oscillations are enhanced in primary cultured astrocytes isolated from the ischemic hippocampal CA1 region

The microfluorimetric measurements did not reveal any differences in 4 α PDD-evoked $[\text{Ca}^{2+}]_i$ signals between flat and non-flat astrocytes in each experimental group, therefore both types of astrocytes were used for the electrophysiological analyses.

The microfluorimetric experiments *in vitro* revealed an increase in $[\text{Ca}^{2+}]_i$ after the application of 5 μM 4 α PDD in astrocytes isolated from control animals (n = 92) as well as those 1H (n = 72) and 7D (n = 38) after H/I (**Fig. 61**). The $[\text{Ca}^{2+}]_i$ increase was significantly higher in astrocytes isolated from animals 7D after H/I when compared to the other two groups (**Fig. 62**). The Ca^{2+} signal was strongly diminished when 4 α PDD was applied in aCSF _{\emptyset Ca} (**Fig. 61, 62**).

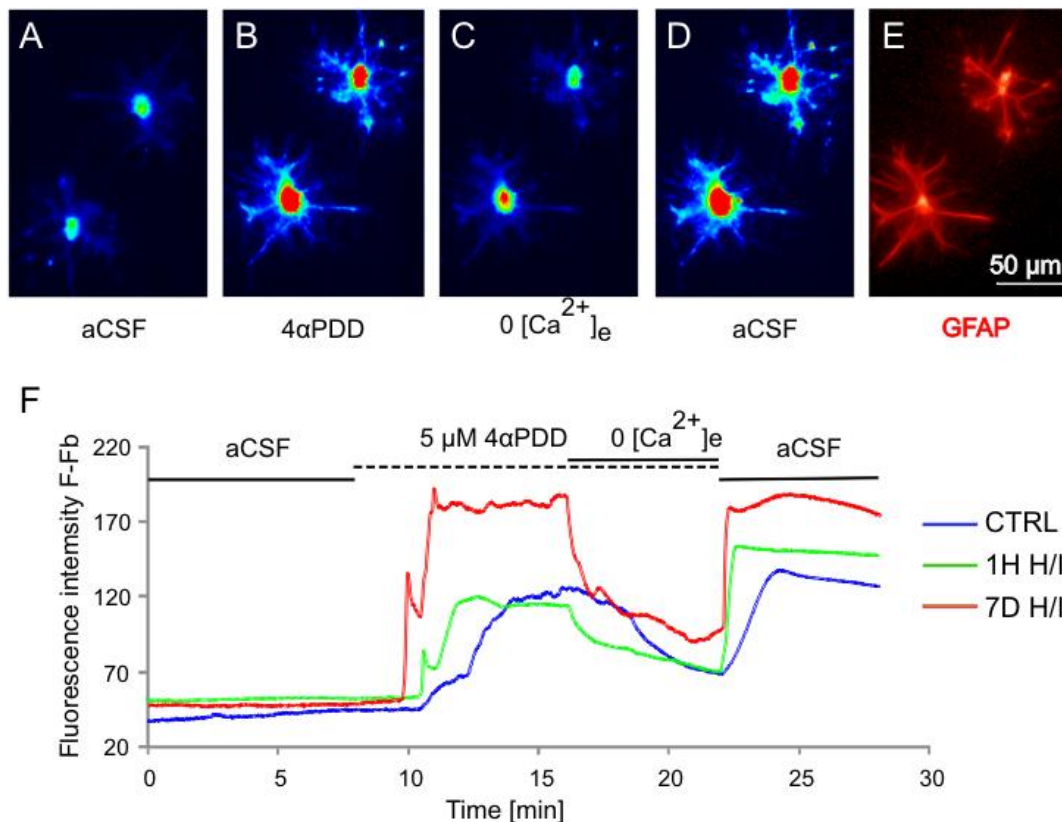


Figure 61. Intracellular Ca^{2+} measurements in cultured astrocytes dissociated from the hippocampal CA1 region. (A-D) Typical fluorescence response elicited by 5 μM 4 α PDD in cultured hippocampal astrocytes. (A) Two astrocytes in aCSF before 4 α PDD application, (B) during 4 α PDD application in aCSF, (C) during 4 α PDD application in aCSF _{\emptyset Ca} and (D) during washout with aCSF. (E) Immunocytochemical staining for glial fibrillary acidic protein (GFAP) to verify astrocyte identity. (F) Representative fluorescence traces of cultured astrocytes isolated from sham-operated animals (CTRL) and animals 1 hour (1H H/I) and 7 days (7D H/I) after H/I in response to stimulation as in A-D. Note the delay between the 4 α PDD challenge and the onset of the fluorescence increase under the 3 conditions.

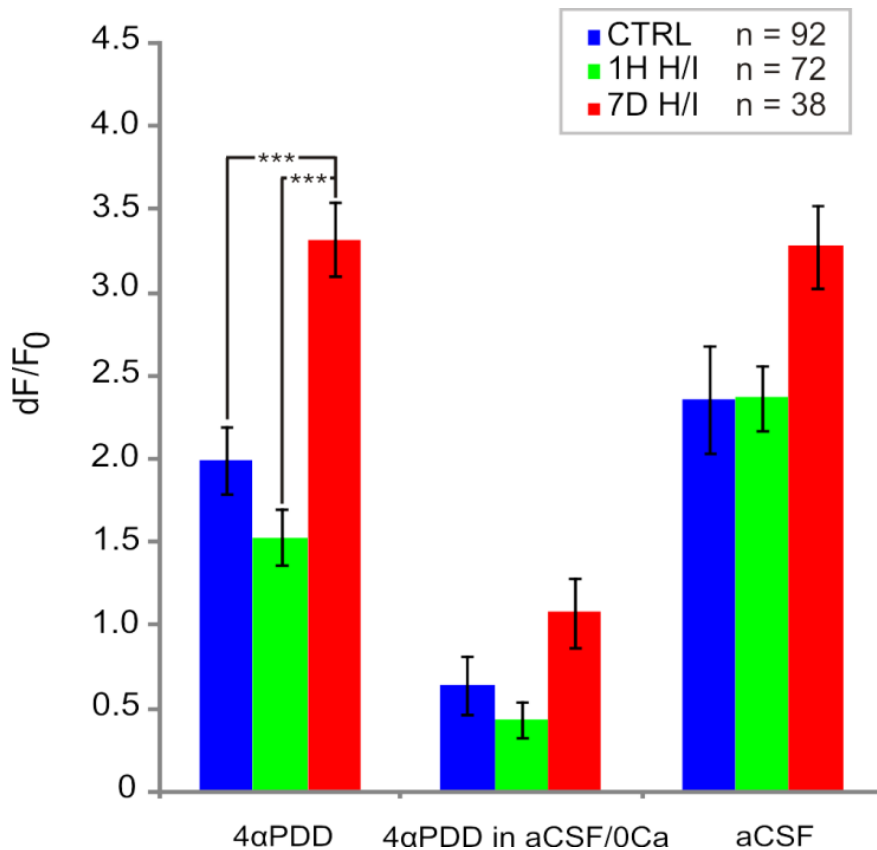


Figure 62. *In vitro* fluorescence intensity during 4αPDD application. Histogram of the variation in the fluorescence intensities dF/F_0 depicting the maximum intensity upon 4αPDD application in aCSF (4αPDD), the average intensity during the last minute of 4αPDD application in aCSF_{0Ca} (4αPDD in aCSF_{0Ca}) and the maximum intensity during washout (aCSF). The values are presented as mean ± S.E.M. Statistical significance was calculated using one-way ANOVA. ***p < 0.001, extremely significant.

The different 4αPDD-mediated Ca^{2+} responses of astrocytes isolated from animals 7D after H/I were also evidenced by the increased number of responding cells (**Fig. 63 left**) and by the faster onset of response to 4αPDD application (**Fig. 63 right**). Furthermore, the steepness of the onset of response to 4αPDD was also higher in this group. The differences in these $[Ca^{2+}]_i$ signal parameters observed in astrocytes were identical in the two morphologically distinct subpopulations.

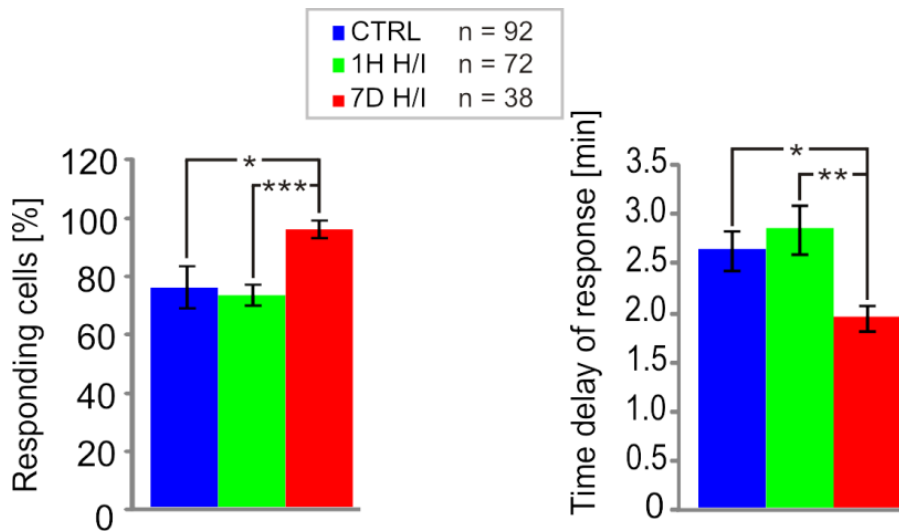


Figure 63. Histogram of the number of responding cells (left) and histogram of the 4 α PDD response time delay (right) during intracellular Ca²⁺ measurements in cultured astrocytes. Note that in cultured astrocytes 7 days (7D) after H/I, TRPV4-mediated Ca²⁺ entry is enhanced and the number of responding cells is higher when compared to control. The values are presented as mean \pm S.E.M. Statistical significance was calculated using one-way ANOVA. *p < 0.05, significant; **p < 0.01, very significant; ***p < 0.001, extremely significant.

4.7 TRPV4 current activity is significantly increased in cultured astrocytes isolated from the rat hippocampal CA1 region after hypoxia/ischemia

Similarly to the *in situ* experiments, TRPV4-specific cationic current recordings were performed using intra- and extracellular solutions in which K⁺ and Na⁺ were replaced with cesium. Under these experimental conditions, the membrane currents evoked by hyperpolarizing and depolarizing voltage steps from -100 mV to 100 mV were strongly diminished (**Fig. 64**).

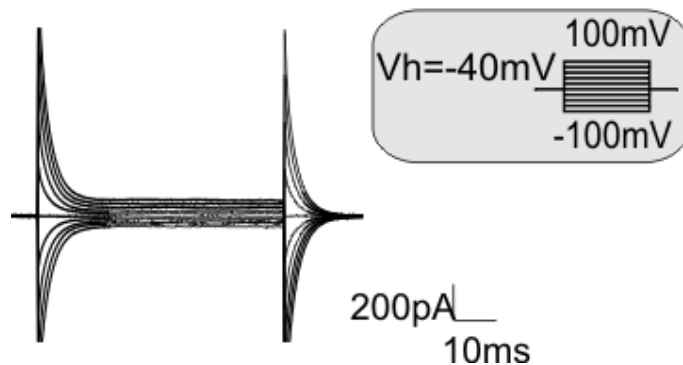


Figure 64. Current pattern evoked with a voltage step protocol (see the inset) in cultured astrocytes recorded in intra- and extracellular solutions in which K⁺ and Na⁺ were replaced by Cs⁺ (Int2 and Ext2). Note the marked reduction in membrane conductance.

The application of 4 α PDD (5 μ M) produced an increase in membrane conductance in the astrocytes of controls as well as in those 1H and 7D after H/I when stimulated with a voltage ramp from -100 mV to +100 mV from V_h of 0 mV (**Fig. 65**). Exposure to 4 α PDD caused a positive shift of E_{rev} from -5.8 ± 1.1 mV to -1.1 ± 0.9 mV ($\Delta E_{rev} = 4.7 \pm 0.9$ mV, $n = 19$). The increase in ramp current upon 4 α PDD application was diminished by 74.0 ± 11.9 % ($n = 6$) by omitting $[Ca^{2+}]_e$ and was depressed by RR (10 μ M) or RN1734 (10 μ M) by 79.7 ± 10.5 % ($n = 8$) and by 69.8 ± 18.7 % ($n = 8$), respectively (**Fig. 66**).

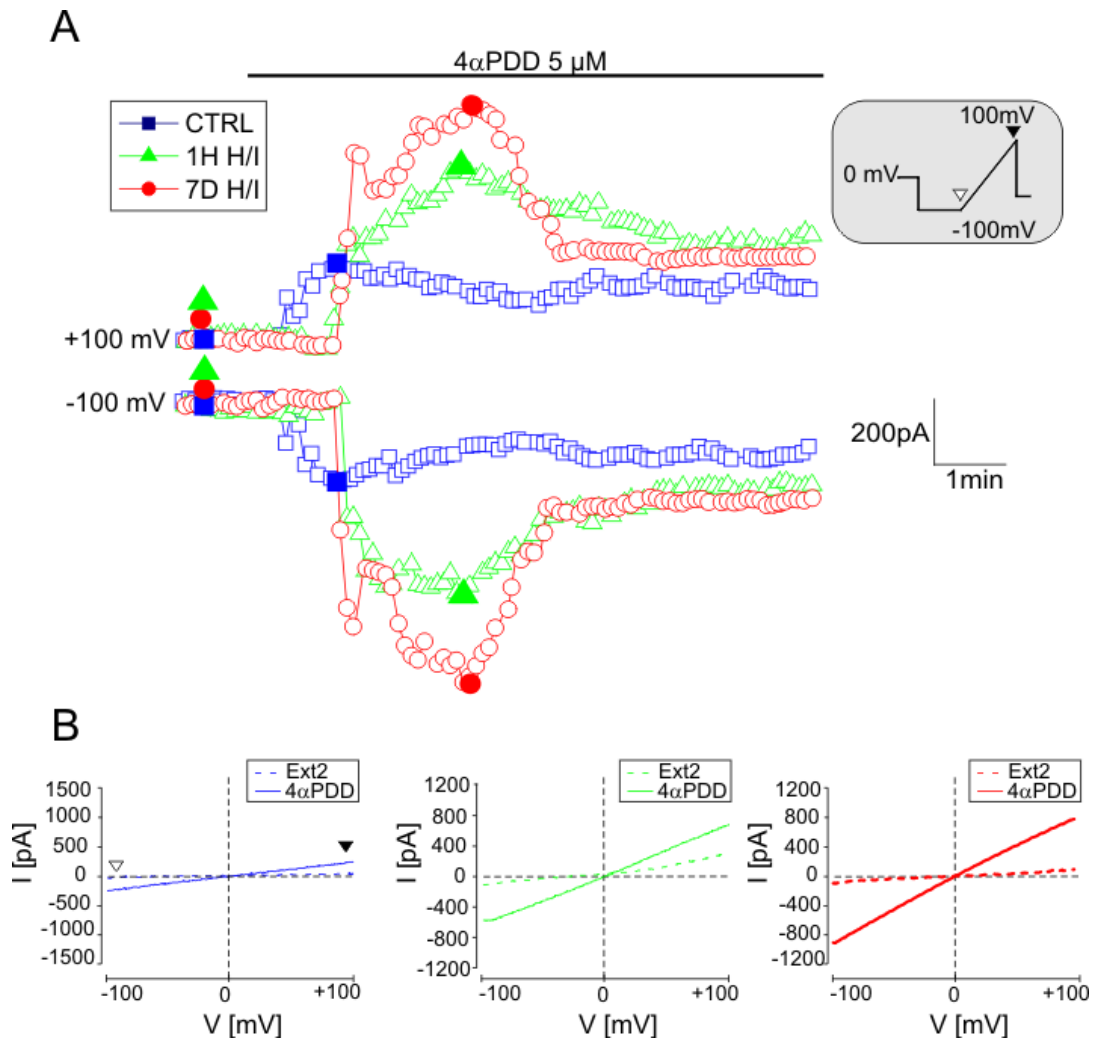


Figure 65. 4 α PDD-induced currents in cultured astrocytes dissociated from the hippocampal CA1 region. (A) Time course of 4 α PDD-evoked currents measured from the ramp protocol in astrocytes of controls (blue squares) and astrocytes 1 hour (1H H/I) (green triangles) and 7 days after hypoxia/ischemia (7D H/I) (red circles). Currents were measured at -100 mV (white arrowhead) and +100 mV (black arrowhead) in response to a voltage ramp stimulation protocol (see the inset). (B) Representative traces of steady state currents (same cells as in A) recorded prior to (in Ext2 solution, dashed line) and during 4 α PDD application (full line) in cultured astrocytes of controls (**left**) and those 1H (**middle**) and 7D after H/I (**right**). Representative traces of steady state currents were obtained at the times indicated by the filled blue squares, green triangles and red circles in A. White and black arrowheads indicate the applied voltage ramp and the corresponding current traces (see the inset in A).

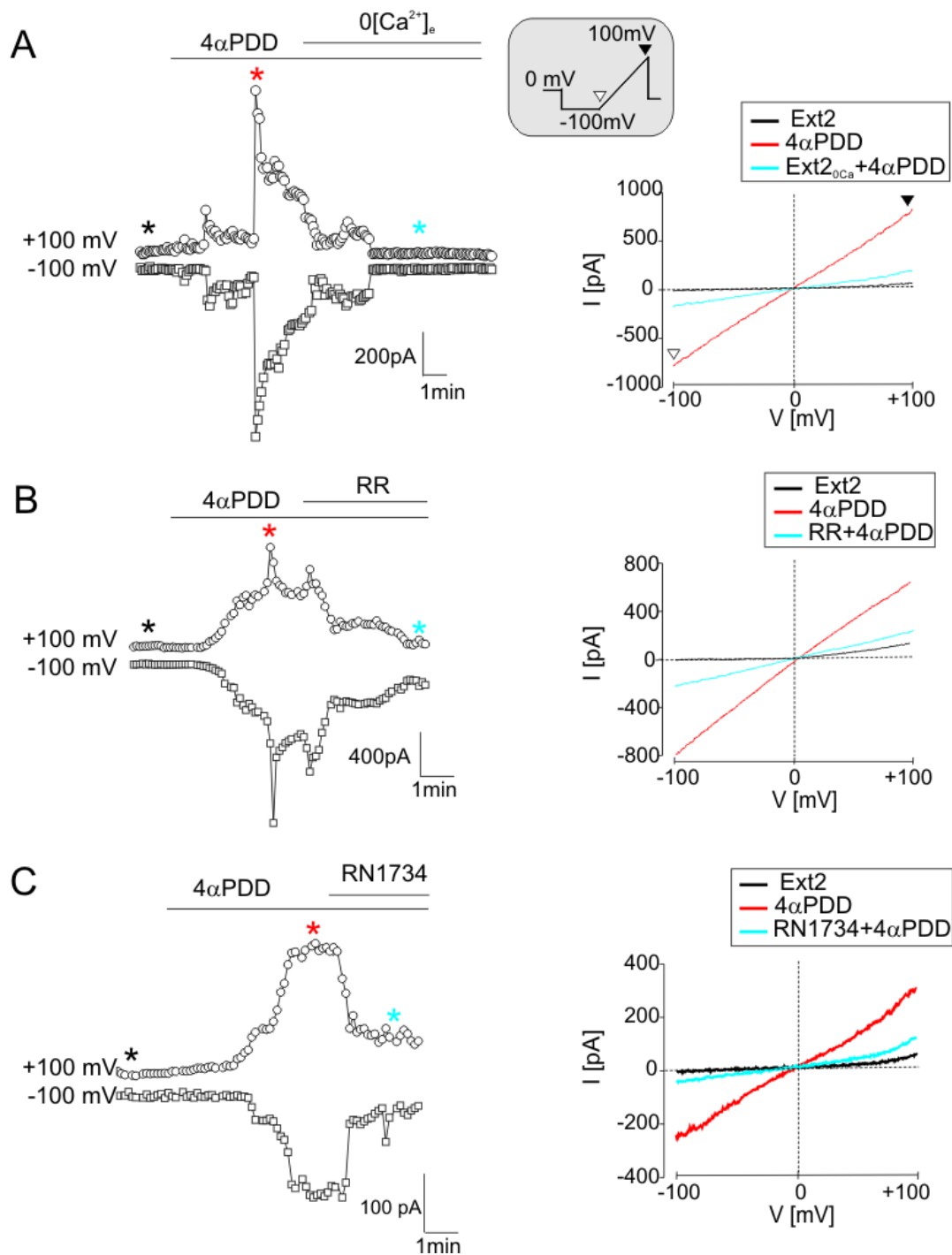


Figure 66. Currents evoked by 4αPDD in astrocytes *in vitro* are reduced by calcium-free extracellular solution, Ruthenium Red or RN1734. (A-C, left) Time course of 4αPDD-evoked currents measured from the ramp protocol in astrocytes isolated from the hippocampus 7D after H/I (for the voltage protocol see the inset) prior to and during 4αPDD (5μM) application and after removing extracellular Ca^{2+} (Ext2_{0Ca}, A) or after the application of TRPV4 inhibitors, such as Ruthenium Red (RR, 10 μM, B) or RN1734 (10 μM, C). (A-C, right) The traces of steady state currents (same cells as in left) obtained in Ext2 solution (black lines), during 4αPDD application (red lines) and after removing extracellular Ca^{2+} (Ext2_{0Ca}, A) or after the application of TRPV4 inhibitors, such as Ruthenium Red (RR, 10 μM, B) or RN1734 (10 μM, C), are indicated by blue lines. Representative traces of steady state currents were obtained at the times indicated by asterisks of the corresponding colors.

Of note, the 4 α PDD-evoked outward and inward current amplitudes and densities were significantly augmented in astrocytes isolated from the rat hippocampus 7D after H/I (Fig. 67).

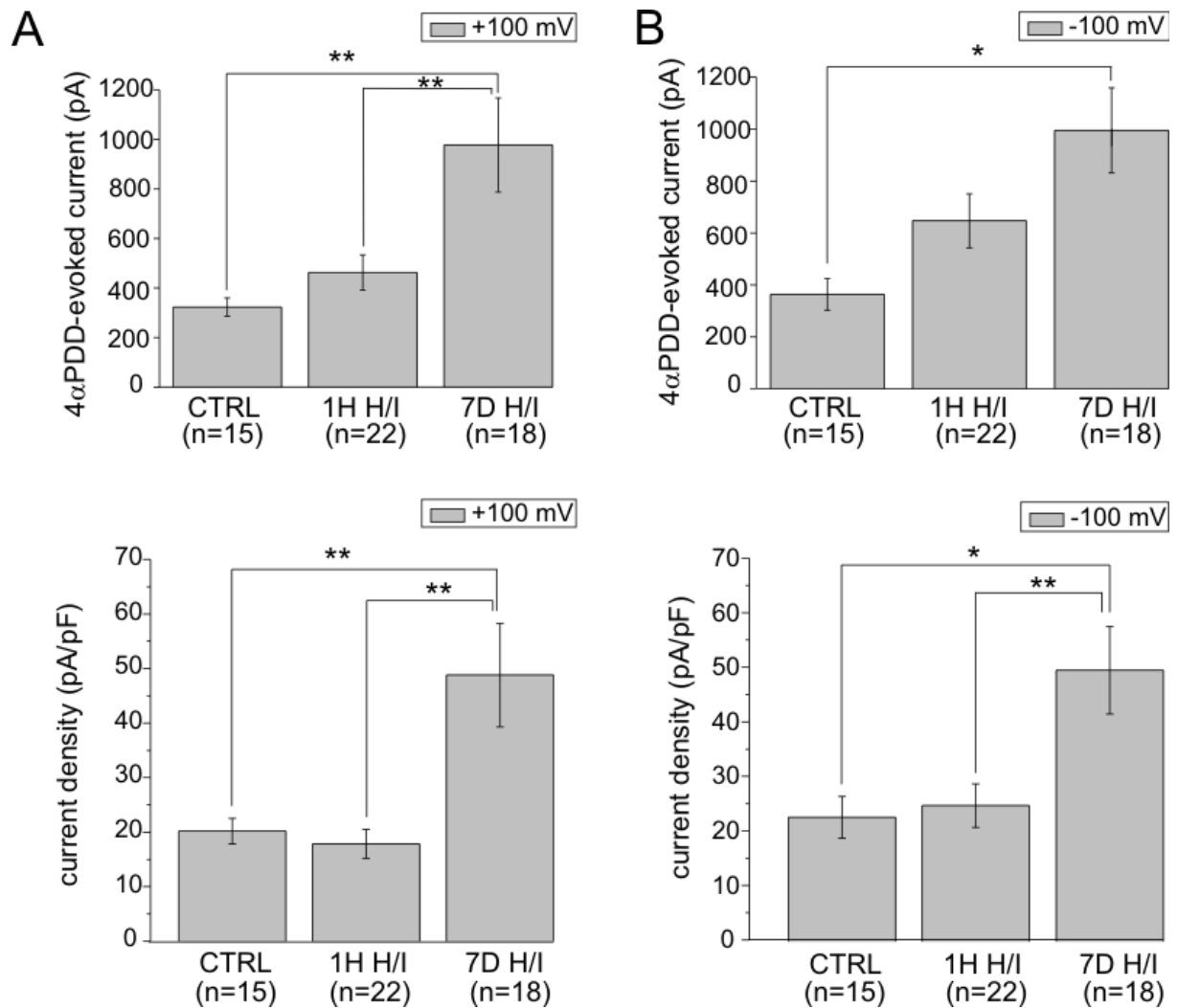


Figure 67. Changes in TRPV4-mediated currents in response to hypoxia/ischemia. Histograms of 4 α PDD-evoked changes in current amplitudes (A top) and current densities (A bottom) at +100 mV and current amplitudes (B top) and current densities (B bottom) at -100 mV in control astrocytes (CTRL), and those isolated from rats 1H and 7D after H/I. The values are presented as mean \pm S.E.M. Statistical significance was calculated using one-way ANOVA. *p < 0.05, significant; **p < 0.01, very significant.

Collectively, these results support the tenet that TRPV4 channels are expressed by CA1 primary astrocytes in culture and that their activity is significantly up-regulated in astrocytes isolated from the ischemic CA1 region seven days after H/I.

5. DISCUSSION

5.1 Histopathological changes after global cerebral hypoxia/ischemia

In our study, we used a model of cerebral hypoxia/ischemia, which was previously described by Dijkhuizen; however, we modified this model by reduction of O₂ fraction from 10 to 6% and period of occlusion from 20 to 15 minutes, therefore, we presented a large set of data to characterize histopathological changes in acute stages of reperfusion and stages of astrogliosis formation. Our immunohistochemical analyses showed that our model of hypoxic/ischemic injury possesses typical features of selective hippocampal injury, such as the delayed cell death of pyramidal neurons in the CA1 region occurring within 3-7 days, the formation of astrogliosis within 7 days and microglia activation within 1 – 3 days, as described by Ordy et al. (Ordy et al., 1993) and Sas et al. (Sas et al., 2008) after global cerebral ischemia (4-vessel occlusion model-rat) or by Kuan et al. (Kuan et al., 2004) after hypoxia-ischemia (2-vessel occlusion combined with hypoxia - rat, mouse).

Under ischemic conditions, cells lose their ability to maintain ion gradients, which ultimately leads to massive Ca²⁺ influx and activation of Ca²⁺-dependent proteolytic enzymes (Chvatal et al., 2008). There is also the over-expression of Ca²⁺-dependent caspase-3 proteases, which cleave specific proteins and trigger programmed cell death in astrocytes and neurons (Nikonenko et al., 2009). It was previously shown that cleaved caspase-3 was detected in pyramidal neurons in CA1 area as early as 6H after H/I (Anderova et al., 2011). Despite the fact that we used different model of H/I, our finding is in accordance with what showed Wei and co-authors (Wei et al., 2004) who detected cleaved caspase-3 in degenerated pyramidal neurons starting 3 days after ischemia accompanied by DNA fragmentation, usually visualized by TUNEL staining. In agreement with Benjelloun and colleagues who demonstrated caspase-3 immunoreactivity also in astrocytes after H/I (Benjelloun et al., 2003), we observed intense staining for nuclear cleaved caspase-3 in reactive hippocampal astrocytes 7 days after H/I; however, there was no DNA fragmentation observed. Cleaved caspase-3 activity in reactive astrocytes without DNA damage was also shown by Acarin and colleagues (Acarin et al., 2007). The authors suggested that the presence of cleaved caspase-3 in TUNEL-negative reactive astrocytes did not associate with mediate apoptotic cell death, but rather reorganization of cytoskeletal network, mainly intermediate filament proteins GFAP and vimentin, which lead to the morphological changes of astrocytes after injury (Acarin et al., 2007).

Previous studies have shown that the global cerebral ischemia induces selective neuronal cell death of CA1 pyramidal neurons, neurons of the hilus and the dentate gyrus and activation of astrocytes, microglia and NG2 glia, which form glial scar (Schmidt-Kastner et al., 1993; Sugawara et al., 2002; Harukuni and Bhardwaj, 2006; Pforte et al., 2005; Nikonenko et al., 2009). Our data document that GFAP protein expression in CA1 area is down-regulated in the acute stages after H/I, i. e. 1H and 6H after H/I; however, also 1D after H/I (**Fig. 29**). Similarly to our findings, Lukaszevicz and colleagues showed loss of GFAP 1H after a middle cerebral artery occlusion (MCAO) (Lukaszevicz et al., 2002). The authors suggested that immediate loss of GFAP protein in astrocytes 1H after MCAO could be associated with loss of GFAP mRNA caused by ATP depletion after ischemia or by early swelling resulting in rupture of gliofilaments. Moreover, Acarin and colleagues observed GFAP down-regulation within the lesion core also 24H after excitotoxic damage suggesting caspase-mediated cleavage of GFAP (Acarin et al., 2007), which is in agreement with our Western blot analyses. In later stages, we observed that hypoxia/ischemia induced an increase in GFAP immunoreactivity in the CA1 area of the hippocampus starting 1D after H/I and reaching maximal level 7D after H/I, as described previously by our group (Anderova et al., 2011). Despite the fact that the glial scar formation after CNS injuries is well documented, the mechanism of increased GFAP expression and astrocyte hypertrophy is not well understood. It has been suggested that NO, which is implicated in ischemic injury, might stimulate GFAP production via guanylate cyclase – cGMP-activated protein kinase (PKG) signalling pathway (Brahmachari et al., 2006).

We also detected an activation of Iba1-positive microglia in the CA1 area of the hippocampus already 6H after H/I, reaching a peak 7D after H/I. In the brain, resident microglia are the major inflammatory cells, which primarily respond to cerebral injury (Jin et al., 2010). Previously, Ito and colleagues showed in an MCAO model the early appearance of Iba1 immunoreactivity already 3.5 hours after reperfusion, which became maximal also 7D after reperfusion (Ito et al., 2001). In addition, the Iba1 protein was highly expressed in monocytic lineage cells, which accumulated within ischemic core (Ito et al., 2001; Imai et al., 1996). Interestingly, in the late stage of reperfusion distinct population of cells double stained for NG2 and Iba1, which are polydendrocytic and microglial markers, respectively (**Fig. 36**). Previously, such cell population was detected in lesion after focal brain ischemia and was termed as brain Iba1⁺/NG2⁺ macrophage-like cells (BINCs) (Matsumoto et al., 2008; Smirkin et al., 2010). So far, the cell population of BINCs has been poorly characterized; however it

has been suggested that BINCs could be an activated form of resting microglia, expressing NG2 proteoglycan in response to injury ([Matsumoto et al., 2008](#); [Smirkin et al., 2010](#)).

Next we found that astrocytes, microglia and NG2 glia in the area of damage (CA1) expressed the markers of proliferation such as PCNA or nestin starting 1D after H/I prior to glial scar formation, with maximal expression at 7D after H/I at stage of permanent glial scar formation. Interestingly, we observed that dominantly proliferative cell types were NG2 glia and microglia, but not astrocytes. It was recently shown that increased proliferation of astrocytes was detected 3D and 7D after H/I, but reached only 8% of total number of astrocytes, while microglia increased to 37% with peak proliferation at 3D after H/I ([Anderova et al., 2011](#)). Nevertheless, we showed that proliferating NG2 glia already appear 1D after H/I (~20%) and their number is increased reaching 40% after 3D of reperfusion ([Pivonkova et al., 2010](#)). The proliferation activity of NG2 glia after global hypoxia/ischemia gives rise to several hypotheses. There is evidence that proliferating NG2 glia within damaged area could give rise to reactive astrocytes ([Zhao et al., 2009](#); [Alonso, 2005](#), [Honsa et al., 2012](#)) or oligodendrocytes ([Lytle et al., 2009](#)).

5.2 The correlation of TRPV4 gene expression with development of astrogliosis

It has been shown that TRPV4 is widely expressed in the brain, particularly in the neurons of the pyramidal hippocampal layer as well as in cortical and hippocampal astrocytes ([Lipski et al., 2006](#); [Shibasaki et al., 2007](#); [Benfenati et al., 2007](#)). However, there are no data demonstrating the expression of TRPV4 channels in astrocytes *in situ* under either physiological or pathophysiological conditions, such as ischemia. In agreement with previous studies ([Bai and Lipski, 2010](#); [Shibasaki et al., 2007](#)), we showed the expression of TRPV4 protein in hippocampal pyramidal neurons as well as in astrocytes of the CA1 region of the hippocampus in control rats. In addition, we found that TRPV4 immunoreactivity increases in hippocampal astrocytes starting 1H after ischemia and reaches maximal levels after 7D of reperfusion. Our immunohistochemical analyses revealed that CA1 pyramidal neurons express TRPV4 in sham-operated rats and rats in acute stage of reperfusion (1H and 6H after H/I) but not 7D after H/I. This decrease in neuronal TRPV4 expression over time is clearly due to extensive apoptosis in the hippocampal CA1 region, wiping out the majority of CA1 pyramidal neurons ([Anderova et al., 2011](#)). Hippocampal astrocytes in sham-operated animals showed very low TRPV4 expression, primarily detected in astrocytic processes enwrapping blood vessels. It is noteworthy that astrocytic TRPV4 immunoreactivity markedly increased

1H and achieved a peak 7D after H/I. Our Western blot analyses revealed an increase in total TRPV4 protein content 1H after ischemia, and quantitative RT-PCR analyses detected a ~2.4-fold increase in TRPV4 mRNA. A similar finding concerning astroglial acetylcholinesterase (AChE) gene expression (a two- to three-fold increase in readthrough-AChE within 1H post-ischemia) has been described previously (Bond et al., 2006). These authors suggested that the stress-induced increase in AChE release is due to the up-regulation of functional readthrough-AChE isoform expression, although it is possible that this increased release of AChE 1H post-ischemia may be attributed to increased readthrough-AChE mRNA transcript stability as well as to an increase in the rate of AChE transcription. Additionally, the increase in TRPV4 protein levels observed 1H after H/I might be, at least partially, due to the enhancement of TRPV4 post-transcriptional modifications occurring within hours after hypoxic/ischemic stress. This could lead to the appearance of additional bands after 1H and 6H corresponding to different isoforms of TRPV4, previously detected in astrocytes and shown by Benfenati and co-authors (Benfenati et al., 2007). Nevertheless, we hypothesize that slower TRPV4 protein degradation or protein stabilization might also contribute to the increased amount of TRPV4 protein 1H after H/I as well.

Curiously, a decline in the total content of TRPV4 protein was observed starting 1D after H/I. Since at this time point neurons are no longer present in the CA1 region of the hippocampus due to massive neuronal cell death, a decline in the levels of TRPV4 protein in the hippocampal CA1 region is to be expected. The remaining expression of TRPV4 protein is almost exclusively confined to reactive astrocytes. Of note, the enhanced TRPV4 expression coincided with maximal GFAP expression, astrocyte hypertrophy and increased astrocytic proliferation (Anderova et al., 2011), which might suggest that TRPV4-mediated Ca^{2+} signalling plays an important role in the formation of the gliotic scar. However, we cannot rule out that increased TRPV4 activity might be also linked to the initiation of delayed astrocytic cell death as described by Cao and co-authors (Cao et al., 2010).

5.3 The role of TRPV4-mediated Ca^{2+} signalling in astrocytes after hypoxia/ischemia

Considering that the physiological role of TRPV4 is mainly related to its permeability to Ca^{2+} (Nilius et al., 2004), any investigation of the functional expression of TRPV4 in astrocytes *in situ* must include an analysis of the role of TRPV4 in astroglial $[Ca^{2+}]_i$

signalling. In control astrocytes, we have recorded low frequency of spontaneous transient $[Ca^{2+}]_i$ oscillations, while in astrocytes 1H and 7D after H/I, these oscillations increased 7- and 20-fold, respectively. Under physiological conditions, similar low frequency of spontaneous transient $[Ca^{2+}]_i$ oscillations mediated mainly by the release of Ca^{2+} from internal stores were demonstrated in astrocytes *in situ* (Nett et al., 2002). During cerebral hypoxia/ischemia, astrocyte can be damaged by a rapid increase in $[Ca^{2+}]_i$ (Verkhatsky et al., 2009), which is in agreement with our data demonstrating augmented spontaneous $[Ca^{2+}]_i$ transients in ischemic astrocytes *in situ*. Our results are also corroborated by previous data showing enhanced spontaneous $[Ca^{2+}]_i$ oscillations in other models of ischemic injury in rodents (Takano et al., 2009), in human astrocytes of epileptic patients (Balazsi et al., 2003) and under pathophysiological conditions, such as Rasmussen's encephalitis (Manning and Sontheimer, 1997). Since the expression of a functional NMDA receptor subtype 2B was described in astrocytes following ischemia *in vivo* and anoxia *in vitro* (Krebs et al., 2003), we cannot rule out the possibility that the increased spontaneous Ca^{2+} oscillations in post-ischemic astrocytes in slices might be partially due to arachidonic acid-mediated potentiation of the current through the NMDA receptor channels, as previously demonstrated in cerebellar granule cells (Miller et al., 1992). Nevertheless, blocking spontaneous Ca^{2+} oscillations with RN1734 confirmed that these oscillations are also partially mediated by TRPV4 channels. The duration of reperfusion following H/I also altered the $[Ca^{2+}]_i$ dynamics. In control astrocytes and those 1H after H/I, we observed mainly an increased frequency of $[Ca^{2+}]_i$ transients, while 7D following ischemia we also detected sustained Ca^{2+} entry after 4 α PDD application in 57% of astrocytes, which was completely blocked by Ca^{2+} -free extracellular solution (Fig. 48, 49); however, it was insensitive to the specific TRPV4 inhibitor RN1734 (Fig. 50). In controls and 1H after H/I, only 3 and 15% of astrocytes showed sustained Ca^{2+} entry, respectively. We hypothesize that TRPV4-mediated Ca^{2+} entry could initiate an additional Ca^{2+} influx via the activation of other membrane proteins, such as sodium-calcium exchangers (NCX) (Meng et al., 2008). Meng and colleagues showed that hypoxia also induces Ca^{2+}/Na^+ influx via TRPC1, 3, 6 channels, resulting in the reversal of NCX and thus to an elevation of intracellular Ca^{2+} in PC12 cells. Such findings are supported by data demonstrating that the reverse mode of NCX contributes to astrocyte and neuronal pathology following experimental traumatic brain injury (Zhao et al., 2009). NCX-mediated fluxes of Ca^{2+} in both forward and reverse modes were found in astrocytes *in vitro* as well as those *in situ* (Kirischuk et al., 2007; Takuma et al., 1994) and moreover, the activation of astroglial ionotropic receptors or glutamate transporters induced a marked elevation of intracellular Na^+ , which switched the

exchanger to the reverse mode (Kirischuk et al., 1997; Kirischuk et al., 2007; Rojas et al., 2007). The reversal of NCX could be also triggered by mild depolarization (Paluzzi et al., 2007), which occurs in reactive astrocytes due to Kir4.1 down-regulation (Pivonkova et al., 2010).

The question arises as to what is the role of TRPV4 in the $[Ca^{2+}]_i$ signalling in astrocytes after ischemia. The possible implication of TRPV4 in enhancing the frequency of Ca^{2+} oscillations in astrocytes after H/I is plausible. In previous studies, a potential role for TRP channels in pathophysiological $[Ca^{2+}]_i$ rise in neurons has been suggested (Bae and Sun, 2011; Chen et al., 2010; Miller and Zhang, 2011; Runnels, 2011). In particular, TRPM7 and thermal-sensitive TRPV3 have been demonstrated to mediate a post-ischemic $[Ca^{2+}]_i$ elevations that ultimately lead to neuronal death (Lipski et al., 2006). Our data demonstrate that increased spontaneous $[Ca^{2+}]_i$ oscillations in astrocytes 1H and 7D after H/I are paralleled by a 2- to 3-fold increase in 4α PDD-induced Ca^{2+} influx. Our finding that spontaneous Ca^{2+} oscillations are partially carried by TRPV4 channels in astrocytes 7D after H/I contrasts with a large body of evidence documenting the involvement of Ca^{2+} release from intracellular stores during astrocytic Ca^{2+} oscillations rather than Ca^{2+} influx through the membrane (Takano et al., 2009). TRPV4 is a polymodal channel that is activated/modulated by different intracellular messengers comprising IP_3 (Fernandes et al., 2008), phosphorylation (Fan et al., 2009), changes in external and internal Ca^{2+} concentrations, PLC activity, and AA metabolites (Watanabe et al., 2003), which are generated via a PLA_2 pathway. Of note, in native ciliated epithelial cells, the IP_3 -mediated sensitization of TRPV4 positively modulates its ability to respond to osmotic stress via epoxyeicosatrienoic acid, a known PLA_2 secondary messenger (Fernandes et al., 2008). The latter signalling pathway is known to be up-regulated after ischemia and involved in augmented $[Ca^{2+}]_i$ oscillations. Intriguingly, in the same study functional coupling of TRPV4 and intracellular Ca^{2+} stores via IP_3 signalling was shown to trigger oscillatory $[Ca^{2+}]_i$ signals in native ciliated epithelial cells (Fernandes et al., 2008). The involvement of TRPV4 in increasing spontaneous $[Ca^{2+}]_i$ oscillations in astroglia after an ischemic insult is further corroborated by the observation that the specific TRPV4 activator 4α PDD increased the frequency of $[Ca^{2+}]_i$ transients and promoted sustained Ca^{2+} entry 7D after H/I.

Another explanation for TRPV4 up-regulation could originate from the proposed role of TRPV4 as a mechanosensor or an osmosensor in different cell types, including astrocytes (Benfenati et al., 2011; Liedtke, 2006). In the present study we showed that not all

hippocampal astrocytes responded to TRPV4 agonist in control rats, however, the number of responding cells significantly increased after ischemia. Since our previous studies demonstrated that astrocytes *in situ* respond differently to hypoosmotic stress, a condition simulating cell swelling frequently observed after ischemia (Chvatal et al., 2007), or to oxygen-glucose deprivation (Benesova et al., 2009), it could be envisaged that under physiological conditions only the subpopulation of astrocytes that is more capable of cell volume regulation expresses TRPV4. Therefore, the up-regulation of TRPV4 after ischemia could be linked to a required increase in the control of astrocytic volume under H/I, a pathological state characterized by impaired glial volume homeostasis (Kimmelberg, 2005). In addition, astrocytes release various bioactive substances via Ca^{2+} - and soluble N-ethylmaleimide-sensitive factor attachment protein receptor (SNARE)-dependent exocytosis, which functions as the main astroglial pathway in glia-neuron signalling (Evanko et al., 2004; Montana et al., 2006; Volterra and Meldolesi, 2005). Thus, we suggest that the increased expression/activation of TRPV4 channels in reactive astrocytes might also result in a Ca^{2+} -dependent release of cytokines or growth factors. Nevertheless, the mechanisms of exocytosis in astrocytes after ischemia are still poorly understood, and further studies using transgenic TRPV4-deficient mice could potentially clarify the role of this polymodal sensor in ischemic astrocytes.

Our study clearly shows that the increase in TRPV4-mediated $[\text{Ca}^{2+}]_i$ signalling was positively correlated with the time of reperfusion following H/I. An alteration in the activation of TRPV4 channels, possibly via a calmodulin (CaM) binding site or PLA_2 activation pathways as described previously (Watanabe et al., 2003; Strotmann et al., 2003), could be involved. Indeed, the activity of these enzymes is known to be increased during hypoxia (Clemens et al., 1996). However, the increased TRPV4 current amplitudes and $[\text{Ca}^{2+}]_i$ signals were paralleled by increased immunostaining for TRPV4 in astrocytes in the CA1 region of the hippocampus, thereby suggesting that the elevation in protein expression could account, at least partially, for the up-regulation of the TRPV4-mediated $[\text{Ca}^{2+}]_i$ signals observed after ischemia.

Despite the fact that our *in situ* experiments showed TRPV4-specific Ca^{2+} entry in astrocytes, one can argue that these Ca^{2+} transients might be evoked indirectly by the activation of TRPV4 in hippocampal neurons. It is in fact well established that astrocytes respond to enhanced neuronal activity by a rise in intracellular Ca^{2+} (Rao and Sikdar, 2006). However, TRPV4-mediated currents/ Ca^{2+} entry markedly increased when the neuronal loss

was maximal, i. e. 7D after ischemia, while 1H after ischemia, the changes were less pronounced. Moreover, the selective *in vitro* characterization of astroglial TRPV4-responses in adult primary astrocytes isolated from sham-operated as well as ischemic rats confirmed that both TRPV4-mediated currents and Ca^{2+} entry were astrocyte-specific and displayed a similar behavior as those *in situ*. Notably, the analyses we performed in astrocytes *in vitro* confirmed that 4 α PDD-evoked Ca^{2+} entry was due to the direct activation of TRPV4 on the astrocytic membrane and showed that 4 α PDD-evoked Ca^{2+} entry is also markedly increased 7D after H/I. Finally, we observed an increase in 4 α PDD current *in situ*, in cells that had been stained either with Alexa Fluor hydrazide or LY and that we had clearly identified as astrocytes by immunohistochemistry.

Our electrophysiological data are in agreement with the previous pharmacological characterization of TRPV4-mediated currents in astrocytes *in vitro* as well as that carried out in heterologous expression systems with respect to TRPV4 channel sensitivity to extracellular Ca^{2+} decrease and Ruthenium Red inhibition (Benfenati et al., 2007). Our data are also comparable with the pharmacological properties of TRPV4-specific currents described in hippocampal neurons (Shibasaki et al., 2007). However, Ruthenium Red symmetrically inhibits 4 α PDD-evoked outward and inward currents in astrocytes. Previously, it has been shown that Ruthenium Red is also inhibits two-pore domain K^+ channels such as TASK channels (Musset et al., 2006), which are expressed in astrocytes. During recording of TRPV4 currents we blocked K^+ conductance using Cs-contained solutions; however, residual K^+ conductance was still detected and might be carried by TASK channels. We hypothesize, that in our experiments Ruthenium Red could also inhibit TASK-mediated outward and inward current and to mask asymmetrical characteristic of TRPV4 current inhibition. Here, we also used a new TRPV4-specific antagonist, RN1734, which blocks 4 α PDD-evoked currents (Vincent et al., 2009). Interestingly, the 4 α PDD-evoked currents of adult astrocytes *in situ* (Fig. 54) as well as those *in vitro* (Fig. 65) displayed a rather linear current-voltage relationship, similar to that observed in striatal neurons and HEK293 cells transiently expressing rat TRPM2 (Hill et al., 2006); however, these channels are not expressed in astrocytes (Bai and Lipski, 2010). Even performing point-to-point digital subtraction of the current traces revealed a rather linear or weakly rectifying current-voltage relationship of 4 α PDD-currents in astrocytes *in situ* and *in vitro* (Fig. 68).

A similar current-voltage relationship was demonstrated in mutated TRPV4 channels (Voets et al., 2002), in which both aspartates in the TRPV4 pore region were neutralized,

causing a marked reduction in outward rectification. Moreover, a modest outward/inward rectification was also shown in HEK293 cells expressing human TRPV4 (Rock et al., 2008) and in human airway epithelial CFT1-LCFSN cells (Jung et al., 2009). Since it is not obvious what underlies the linear TRPV4 current-voltage relationship in adult astrocytes, we hypothesize that post-translational modifications, conformational changes of the TRPV4 protein or protein-protein interactions might contribute to such current behavior.

Generally, we observed marked heterogeneity in TRPV4 channel activity during 4 α PDD application even among astrocytes from sham-operated animals or those after H/I. Therefore, firstly, we performed 8 minute long application of 4 α PDD to understand the dynamics of TRPV4-mediated Ca²⁺ oscillation and cationic current (**Fig. 54**). However, in some cells during such long application TRPV4 current was spontaneously inactivated, thus the effect of antagonists, which were applied next 8 minutes was not evident, and therefore not shown in the Fig. 54. Heterogeneous responses of astrocytes to 4 α PDD application were previously described by Benfenati and colleagues (Benfenati et al., 2007), and more recently by Lanciotti and co-authors (Lanciotti et al., 2012). Both groups demonstrated marked differences in the activation/inactivation of TRPV4-mediated Ca²⁺ entry and the response onset within the recorded population of astrocytes. Such diversity in TRPV4 channel activity could possibly originate from alterations in extracellular/intracellular Ca²⁺ in the vicinity of the astrocytic membrane, as these have been shown to strongly regulate TRPV4 channels (Watanabe et al., 2003; Plant and Strotmann, 2007). In some astrocytes, 4 α PDD-evoked currents displayed either fast activation and inactivation, which have been reported to occur in high extracellular Ca²⁺ concentrations (Watanabe et al., 2003), or a slow rate of current decay, which might be attributed to [Ca²⁺]_i levels. Furthermore, an interaction between the C- and N-termini of the TRPV4 channel was found to control the Ca²⁺-dependent potentiation of the channel (Strotmann et al., 2010), and the presence of different splice variants, their homomerization/heteromerization or post-translational modifications of the TRPV4 protein might also contribute to the diversity in TRPV4 channel activation/desensitization following H/I. Until now, there are no published data describing TRPV4 splice variants in rats; however, the existence of different splice variants was described for the human TRPV4 channel (Arniges et al., 2006). Arniges and colleagues described five TRPV4 splice variants, three of which formed functional channels.

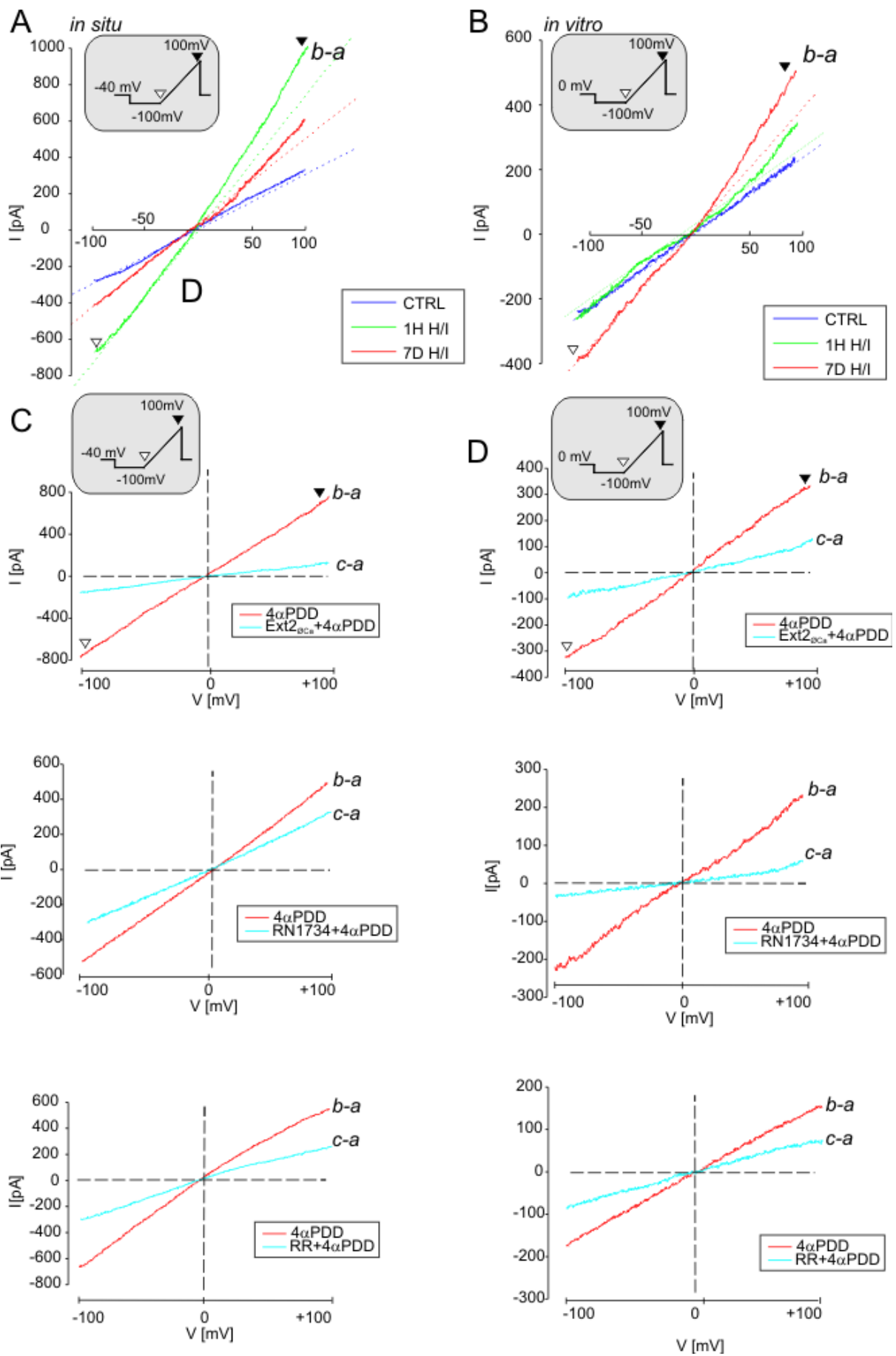


Figure 68. Isolation of 4 α PDD currents –point-to-point current subtraction. The 4 α PDD- current traces obtained after point-to-point subtraction of ramp current traces recorded prior to 4 α PDD application (*a*) and those recorded during 4 α PDD application (*b*) in astrocytes *in situ* (**A**) and astrocytes isolated from the adult rat hippocampal CA1 region (**B**) of sham-operated rats (CTRL) and rats 1 hour and 7 days after hypoxia/ischemia (1H, 7D H/I; see the voltage ramp protocol in the inset). Note the linear I-V relationship of the 4 α PDD-sensitive current (*b-a*) detected in astrocytes *in situ* as well as *in vitro* in sham-operated rats (blue trace), while a modest outward rectification of the 4 α PDD current was observed in post-ischemic astrocytes (red and green traces). Typical 4 α PDD-current traces obtained after point-to-point subtraction of ramp current traces recorded in astrocytes *in situ* (**C**) and astrocytes *in vitro* (**D**) prior to (*a*) and during 4 α PDD application (*b*) and in response to the removal of extracellular Ca²⁺ (Ext2_{0Ca}, top) or after the application of TRPV4 inhibitors, such as 10 μ M RN1734 (middle) or 10 μ M ruthenium red (RR, bottom, *c*). Red traces represent the 4 α PDD-sensitive current (*b-a*) and blue traces represent the remaining current after applying the inhibitors (*c-a*). Black and white arrowheads indicate the applied voltage protocol (see the insets) and the corresponding current traces.

Using qPCR method, we obtained preliminary data indicating that there are 3 isoforms of *Trpv4* present in rat hippocampus. To design splice variants of TRPV4 channel, rat *Trpv4* mRNA was aligned to the human and mice *Trpv4* mRNA in order to find theoretically possible exons. Based on the sequence alignment the suitable primers were designed to detect new theoretical splice variants. Thus, we identified the most common *Trpv4* isoform (full length) and also two *Trpv4* splice variants termed “isoB” (lacking exon number 1 and presents short deletions inside exons number 2 and 10) and “isoC” (lacking exon number 1 and presents short deletions inside exons number 2, 5 and 7) (**Fig. 69**). We found that expression levels of most common *Trpv4* and its 2 splice variants significantly change during reperfusion. We therefore hypothesize that the heterogeneity of TRPV4 channel activation might also depend on the presence/level of various *Trpv4* splice variants in particular time of reperfusion following ischemia.

Moreover, 4 α PDD might act on the lipid environment more efficiently *in vitro* than *in situ* and thus differentially modulate TRPV4 channels. The physiological relevance of such a lipid-modulated mechanism of activation has been suggested for other mechano-gated channels (Kim, 2005). Finally, astrocyte heterogeneity within the hippocampal CA1 region might be the reason for the observed variations in TRPV4 responses. A number of publications have appeared recently showing marked astrocyte heterogeneity even within an individual CNS region, with different astrocyte coupling or expression of ion channels, glutamate transporters or receptors (Benesova et al., 2012; Benesova et al., 2009; Matyash and Kettenmann, 2010). Moreover, the reactive astrocytes in post-ischemic tissue might

originate not only from proliferating astrocytes (Anderova et al., 2011), but also from polydendrocytes (Honsa et al., 2012), which might further contribute to the heterogeneity within the reactive astrocyte population.

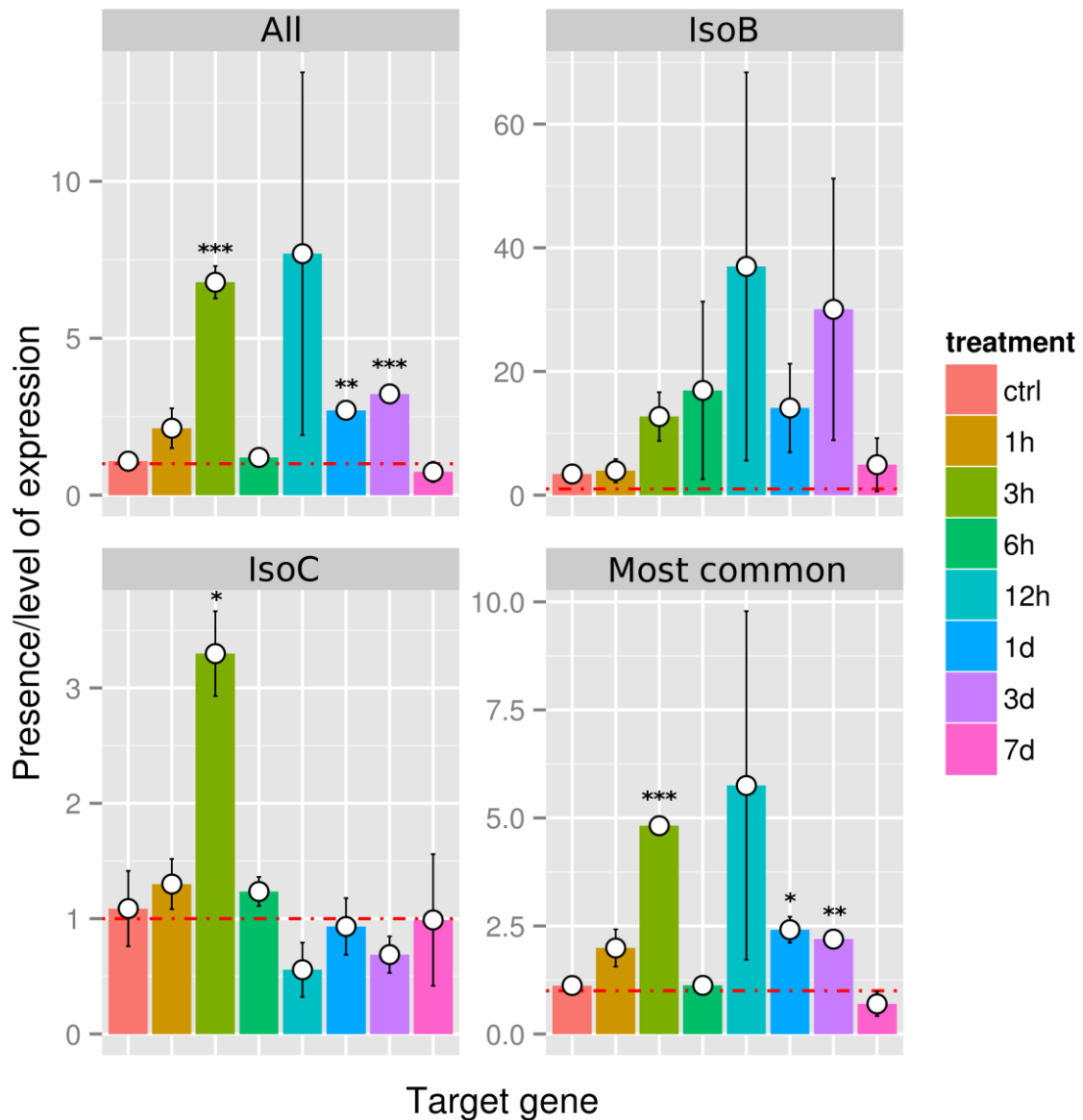


Figure 69. Time-dependent changes in the expression of TRPV4 receptor splice variants after hypoxia/ischemia in CA1 area of hippocampus. The dashed red line indicates the expression level of TRPV4 most common, isoB, isoC and all variants together in sham-operated rats (ctrl). Each experiment was prepared in triple replicate. Abbreviations: 1h - 1 hour; 3h - 3 hours, 6h - 6 hours; 12h - 12 hours, 1d - 1 day; 3d - 3 days; 7d - 7 days. The values are presented as mean \pm S.E.M. Statistical significance was calculated using one-way ANOVA. *p < 0.05, significant; **p < 0.01, very significant; ***p < 0.001, extremely significant.

In agreement with our Ca^{2+} imaging data, electrophysiological analysis also confirmed that after H/I, astrocytes display increased TRPV4 currents. These changes in TRPV4 current amplitude were not significant *in situ* (**Fig. 55**). However, this result is not surprising because the expression of passive conductance in astrocytes *in situ* makes the isolation of different currents in these cells quite difficult (Pivonkova et al., 2010). Importantly, we found that TRPV4-mediated currents in astrocytes *in vitro* are significantly increased 7D after H/I; however, 4 α PDD-evoked Ca^{2+} entry/currents were not enhanced in astrocytes isolated from the hippocampal CA1 region 1H after H/I. We hypothesize that astrocytes isolated during the acute stages of reperfusion could recover after their transfer into culture medium and therefore their responses to 4 α PDD were similar to those recorded in controls. In contrast, 7D after H/I, the changes in reactive astrocytes are rather permanent and therefore not reversible by the culturing.

In addition, we found that the incidence of astrocytes responding to 4 α PDD increases with the time of reperfusion and that the TRPV4-immunoreactivity of an individual reactive astrocyte in the CA1 region significantly increases, correlating well with the increasing number of TRPV4-positive astrocytes in the hippocampal CA1 region during reperfusion. Although we were not able to detect a significant increase in TRPV4-current amplitude *in situ* following ischemia, intracellular Ca^{2+} imaging revealed that Ca^{2+} entry mediated by TRPV4 channels is significantly augmented in astrocytes 1H and 7D after H/I. A significantly larger number of cells were analyzed by intracellular calcium imaging compared to patch-clamp recording *in situ*, which might result in the discrepancies between TRPV4-mediated Ca^{2+} entry and current amplitude. In contrast to intracellular Ca^{2+} measurements, where relatively intact cells are recorded, the patch-clamp technique in the whole-cell configuration significantly affects the astrocytic intracellular environment, possibly diluting the regulatory molecules required for enhanced TRPV4 activity.

Collectively, the data obtained *in vitro* validate the *in situ* analyses, thus identifying TRPV4 as one of the channels involved in the pathophysiological $[\text{Ca}^{2+}]_i$ signals in ischemic astroglia. Nevertheless, it still remains uncertain how astrocytic TRPV4 channels are activated under physiological or pathophysiological conditions. Generally, astrocytes play a significant role in ion/neurotransmitter and water homeostasis and therefore, neuronal activity leading to enhanced K^+ /glutamate uptake in astrocytes and resulting in the swelling of astrocytic processes enwrapping the synapses might be an initial trigger for TRPV4 activation, as these channels act as mechanosensors. Also, subtle changes in extracellular ion concentrations in

the vicinity of the astrocytic membrane might result in TRPV4 activation under physiological conditions, as these channels act as osmosensors. Recent data indicate that astrocytes contain a TRPV4/AQP4 complex (Benfenati et al., 2011) that constitutes a key element in the CNS volume homeostasis by acting as an osmosensor that couples osmotic stress to downstream signalling cascades. Additionally, the fact that several ion channels, such as Kir channels (specifically Kir4.1), AQP4 and TRPV4, are co-expressed in the astrocytic endfeet (Nagelhus et al., 2004; Seifert et al., 2009; Price et al., 2002) points to the importance of membrane protein interactions within membrane microdomains that are devoted to extracellular K⁺ buffering/glutamate uptake and water homeostasis. Thus, astrocytic swelling might activate TRPV4 channel via PLA₂ activation, the release of AA from membrane phospholipids followed by cytochrome P450 epoxygenase-dependent AA metabolism, producing 5', 6' epoxyeicosatrienoic acid. Under pathophysiological conditions, tissue damage and inflammation result in the release of pro-inflammatory mediators, which may in turn activate intracellular signalling pathways and downstream kinases, such as PKC and PKA, and consequently enhance the activation of TRPV4 ion channels by phosphorylation (Fan et al., 2009).

6. CONCLUSION

In the present study, we provide the first evidence of the functional expression of TRPV4 channels in CA1 hippocampal astrocytes *in situ*. Moreover, this is the first study describing the impact of global cerebral ischemia *in vivo* on TRPV4-mediated currents and intracellular Ca^{2+} signalling in hippocampal astrocytes. We found that following hypoxic/ischemic injury, the activity of TRPV4 channels markedly increases in astrocytes in the CA1 region of the adult rat hippocampus during the development of astrogliosis.

The main findings of this study are:

1. The cerebral hypoxia/ischemia is characterized by progressive neuronal death and subsequent development of astrogliosis in the CA1 area of the hippocampus, resulting in depletion of pyramidal neurons and formation of permanent glia scar 7D after H/I. Among reactive astrocytes, activated microglia and NG2 glia, which constitute the gliotic scar, the proliferation of microglia and NG2 glia strikingly prevails.
2. In response to cerebral hypoxia/ischemia, the levels of mRNA coding TRPV4 as well as the content of TRPV4 protein are significantly increased in the CA1 hippocampal astrocytes.
3. The hippocampal astrocytes *in situ* and those isolated from the hippocampus display enhanced TRPV4-mediated Ca^{2+} entry and cationic current 1H and 7D after hypoxia/ischemia. Moreover, the number of astrocytes showing TRPV4-specific responses significantly increases following ischemic injury.
4. Following hypoxia/ischemia, spontaneous Ca^{2+} oscillations in reactive astrocytes *in situ* are significantly augmented and they are partially mediated by TRPV4 channels.
5. The post-ischemic reactive hippocampal astrocytes *in situ* are characterized by time- and voltage-independent currents, predominantly carried by K^+ channels; however, they display significantly depolarized resting membrane potential, mainly due to down-regulation of Kir.4.1 channels.

6. We have developed a new method for isolation of adult astrocytes from hippocampal CA1 region of sham-operated as well as ischemic rats and characterized the properties of isolated astrocytes after 3-4 days of their culturing.

Taken together, we showed that TRPV4 channels are involved in the increase of Ca^{2+} signalling, which occurs after cerebral hypoxia/ischemia in the hippocampal astrocytes of adult rats. Because alterations in $[\text{Ca}^{2+}]_i$ dynamics in astroglia are associated with the modulation of physiological and pathophysiological processes ([Agulhon et al., 2008](#); [Cali et al., 2009](#)), our study identifies a novel molecular target to be explored in order to unravel astrocyte signalling after ischemia reperfusion and to define more clearly the astrocyte-mediated pathogenic processes in acute brain disorders. Furthermore, newly discovered participation of TRPV4 channels in astrocytic Ca^{2+} signalling after hypoxia/ischemia might lead to identification of TRPV4 as a possible target for the development of glia-oriented therapeutic strategies in post-ischemic patients.

7. REFERENCES

- Abe, K., M. Aoki, J. Kawagoe, T. Yoshida, A. Hattori, K. Kogure and Y. Itoyama (1995). Ischemic delayed neuronal death. A mitochondrial hypothesis. *Stroke* 26(8): 1478-1489.
- Acarin, L., S. Villapol, M. Faiz, T. T. Rohn, B. Castellano and B. Gonzalez (2007). Caspase-3 activation in astrocytes following postnatal excitotoxic damage correlates with cytoskeletal remodeling but not with cell death or proliferation. *Glia* 55(9): 954-965.
- Agulhon, C., J. Petravicz, A. B. McMullen, E. J. Sweger, S. K. Minton, S. R. Taves, K. B. Casper, T. A. Fiacco and K. D. McCarthy (2008). What is the role of astrocyte calcium in neurophysiology? *Neuron* 59(6): 932-946.
- Alberdi, E., M. V. Sanchez-Gomez and C. Matute (2005). Calcium and glial cell death. *Cell Calcium* 38(3-4): 417-425.
- Alonso, G. (2005). NG2 proteoglycan-expressing cells of the adult rat brain: possible involvement in the formation of glial scar astrocytes following stab wound. *Glia* 49(3): 318-338.
- Amiry-Moghaddam, M. and O. P. Ottersen (2003). The molecular basis of water transport in the brain. *Nat Rev Neurosci* 4(12): 991-1001.
- Anderova, M., I. Vorisek, H. Pivonkova, J. Benesova, L. Vargova, M. Cicanic, A. Chvatal and E. Sykova (2011). Cell death/proliferation and alterations in glial morphology contribute to changes in diffusivity in the rat hippocampus after hypoxia-ischemia. *J Cereb Blood Flow Metab* 31(3): 894-907.
- Arniges, M., J. M. Fernandez-Fernandez, N. Albrecht, M. Schaefer and M. A. Valverde (2006). Human TRPV4 channel splice variants revealed a key role of ankyrin domains in multimerization and trafficking. *J Biol Chem* 281(3): 1580-1586.
- Auer-Grumbach, M., A. Olschewski, L. Papic, H. Kremer, M. E. McEntagart, S. Uhrig, C. Fischer, E. Frohlich, Z. Balint, B. Tang, H. Strohmaier, H. Lochmuller, B. Schlotter-Weigel, J. Senderek, A. Krebs, K. J. Dick, R. Petty, C. Longman, N. E. Anderson, G. W. Padberg, H. J. Schelhaas, C. M. van Ravenswaaij-Arts, T. R. Pieber, A. H. Crosby and C. Guelly (2010). Alterations in the ankyrin domain of TRPV4 cause congenital distal SMA, scapuloperoneal SMA and HMSN2C. *Nat Genet* 42(2): 160-164.
- Badaut, J. (2010). Aquaglyceroporin 9 in brain pathologies. *Neuroscience* 168(4): 1047-1057.
- Badaut, J., F. Lasbennes, P. J. Magistretti and L. Regli (2002). Aquaporins in brain: distribution, physiology, and pathophysiology. *J Cereb Blood Flow Metab* 22(4): 367-378.
- Bae, C. Y. and H. S. Sun (2011). TRPM7 in cerebral ischemia and potential target for drug development in stroke. *Acta Pharmacol Sin* 32(6): 725-733.

- Bai, J. Z. and J. Lipski (2010). Differential expression of TRPM2 and TRPV4 channels and their potential role in oxidative stress-induced cell death in organotypic hippocampal culture. *Neurotoxicology* 31(2): 204-214.
- Balazsi, G., A. H. Cornell-Bell and F. Moss (2003). Increased phase synchronization of spontaneous calcium oscillations in epileptic human versus normal rat astrocyte cultures. *Chaos* 13(2): 515-518.
- Barreto, G., R. E. White, Y. Ouyang, L. Xu and R. G. Giffard (2011). Astrocytes: targets for neuroprotection in stroke. *Cent Nerv Syst Agents Med Chem* 11(2): 164-173.
- Barry, P. H. (1994). JPCalc, a software package for calculating liquid junction potential corrections in patch-clamp, intracellular, epithelial and bilayer measurements and for correcting junction potential measurements. *J Neurosci Methods* 51(1): 107-116.
- Ben Achour, S., L. Pont-Lezica, C. Bechade and O. Pascual (2010). Is astrocyte calcium signaling relevant for synaptic plasticity? *Neuron Glia Biol* 6(3): 147-155.
- Benesova, J., M. Hock, O. Butenko, I. Prajerova, M. Anderova and A. Chvatal (2009). Quantification of astrocyte volume changes during ischemia in situ reveals two populations of astrocytes in the cortex of GFAP/EGFP mice. *J Neurosci Res* 87(1): 96-111.
- Benesova, J., V. Rusnakova, P. Honsa, H. Pivonkova, D. Dzamba, M. Kubista and M. Anderova (2012). Distinct expression/function of potassium and chloride channels contributes to the diverse volume regulation in cortical astrocytes of GFAP/EGFP mice. *PLoS One* 7(1): e29725.
- Benfenati, V., M. Amiry-Moghaddam, M. Caprini, M. N. Mylonakou, C. Rapisarda, O. P. Ottersen and S. Ferroni (2007). Expression and functional characterization of transient receptor potential vanilloid-related channel 4 (TRPV4) in rat cortical astrocytes. *Neuroscience* 148(4): 876-892.
- Benfenati, V., M. Caprini, M. Dovizio, M. N. Mylonakou, S. Ferroni, O. P. Ottersen and M. Amiry-Moghaddam (2011). An aquaporin-4/transient receptor potential vanilloid 4 (AQP4/TRPV4) complex is essential for cell-volume control in astrocytes. *Proc Natl Acad Sci U S A* 108(6): 2563-2568.
- Benfenati, V. and S. Ferroni (2010). Water transport between CNS compartments: functional and molecular interactions between aquaporins and ion channels. *Neuroscience* 168(4): 926-940.
- Benjelloun, N., L. M. Joly, B. Palmier, M. Plotkine and C. Charriaut-Marlangue (2003). Apoptotic mitochondrial pathway in neurones and astrocytes after neonatal hypoxia-ischaemia in the rat brain. *Neuropathol Appl Neurobiol* 29(4): 350-360.
- Bond, C. E., P. Patel, L. Crouch, N. Tetlow, T. Day, S. Abu-Hayyeh, C. Williamson and S. A. Greenfield (2006). Astroglia up-regulate transcription and secretion of 'readthrough' acetylcholinesterase following oxidative stress. *Eur J Neurosci* 24(2): 381-386.
- Bordey, A. and H. Sontheimer (1997). Postnatal development of ionic currents in rat hippocampal astrocytes in situ. *J Neurophysiol* 78(1): 461-477.

- Brahmachari, S., Y. K. Fung and K. Pahan (2006). Induction of glial fibrillary acidic protein expression in astrocytes by nitric oxide. *Journal of Neuroscience* 26(18): 4930-4939.
- Brozzi, F., C. Arcuri, I. Giambanco and R. Donato (2009). S100B Protein Regulates Astrocyte Shape and Migration via Interaction with Src Kinase: IMPLICATIONS FOR ASTROCYTE DEVELOPMENT, ACTIVATION, AND TUMOR GROWTH. *J Biol Chem* 284(13): 8797-8811.
- Bushong, E. A., M. E. Marton and M. H. Ellisman (2004). Maturation of astrocyte morphology and the establishment of astrocyte domains during postnatal hippocampal development. *International Journal of Developmental Neuroscience* 22(2): 73-86.
- Cahoy, J. D., B. Emery, A. Kaushal, L. C. Foo, J. L. Zamanian, K. S. Christopherson, Y. Xing, J. L. Lubischer, P. A. Krieg, S. A. Krupenko, W. J. Thompson and B. A. Barres (2008). A transcriptome database for astrocytes, neurons, and oligodendrocytes: a new resource for understanding brain development and function. *Journal of Neuroscience* 28(1): 264-278.
- Cali, C., J. Marchaland, P. Spagnuolo, J. Gremion and P. Bezzi (2009). Regulated exocytosis from astrocytes physiological and pathological related aspects. *Int Rev Neurobiol* 85: 261-293.
- Cao, D. S., S. Q. Yu and L. S. Premkumar (2009). Modulation of transient receptor potential Vanilloid 4-mediated membrane currents and synaptic transmission by protein kinase C. *Mol Pain* 5: 5.
- Cao, X., Y. Zhang, L. Zou, H. Xiao, Y. Chu and X. Chu (2010). Persistent oxygen-glucose deprivation induces astrocytic death through two different pathways and calpain-mediated proteolysis of cytoskeletal proteins during astrocytic oncosis. *Neuroscience Letters* 479(2): 118-122.
- Chen, H. C., J. Xie, Z. Zhang, L. T. Su, L. Yue and L. W. Runnels (2010). Blockade of TRPM7 channel activity and cell death by inhibitors of 5-lipoxygenase. *PLoS One* 5(6): e11161.
- Chen, Y. and R. A. Swanson (2003). Astrocytes and brain injury. *J Cereb Blood Flow Metab* 23(2): 137-149.
- Chvatal, A., M. Anderova, M. Hock, I. Prajerova, H. Neprasova, V. Chvatal, F. Kirchhoff and E. Sykova (2007). Three-dimensional confocal morphometry reveals structural changes in astrocyte morphology in situ. *J Neurosci Res* 85(2): 260-271.
- Chvatal, A., M. Anderova, H. Neprasova, I. Prajerova, J. Benesova, O. Butenko and A. Verkhatsky (2008). Pathological potential of astroglia. *Physiol Res* 57 Suppl 3: S101-110.
- Clemens, J. A., D. T. Stephenson, E. B. Smalstig, E. F. Roberts, E. M. Johnstone, J. D. Sharp, S. P. Little and R. M. Kramer (1996). Reactive glia express cytosolic phospholipase A2 after transient global forebrain ischemia in the rat. *Stroke* 27(3): 527-535.
- Cornell-Bell, A. H., S. M. Finkbeiner, M. S. Cooper and S. J. Smith (1990). Glutamate induces calcium waves in cultured astrocytes: long-range glial signaling. *Science* 247(4941): 470-473.

- Cotrina, M. L. and M. Nedergaard (2009). Physiological and pathological functions of P2X7 receptor in the spinal cord. *Purinergic Signal* 5(2): 223-232.
- D'Ambrosio, R., D. S. Gordon and H. R. Winn (2002). Differential role of KIR channel and Na(+)/K(+)-pump in the regulation of extracellular K(+) in rat hippocampus. *J Neurophysiol* 87(1): 87-102.
- D'Ambrosio, R., J. Wenzel, P. A. Schwartzkroin, G. M. McKhann, 2nd and D. Janigro (1998). Functional specialization and topographic segregation of hippocampal astrocytes. *Journal of Neuroscience* 18(12): 4425-4438.
- Dani, J. W., A. Chernjavsky and S. J. Smith (1992). Neuronal activity triggers calcium waves in hippocampal astrocyte networks. *Neuron* 8(3): 429-440.
- Dijkhuizen, R. M., S. Knollema, H. B. van der Worp, G. J. Ter Horst, D. J. De Wildt, J. W. Berkelbach van der Sprengel, K. A. Tulleken and K. Nicolay (1998). Dynamics of cerebral tissue injury and perfusion after temporary hypoxia-ischemia in the rat: evidence for region-specific sensitivity and delayed damage. *Stroke* 29(3): 695-704.
- Doyle, K. P., R. P. Simon and M. P. Stenzel-Poore (2008). Mechanisms of ischemic brain damage. *Neuropharmacology* 55(3): 310-318.
- Dunn, K. M., D. C. Hill-Eubanks, W. B. Liedtke and M. T. Nelson (2013). TRPV4 channels stimulate Ca²⁺-induced Ca²⁺ release in astrocytic endfeet and amplify neurovascular coupling responses. *Proc Natl Acad Sci U S A* 110(15): 6157-6162.
- Durand, D., L. Carniglia, C. Caruso and M. Lasaga (2013). mGlu3 receptor and astrocytes: partners in neuroprotection. *Neuropharmacology* 66: 1-11.
- Eliasson, C., C. Sahlgren, C. H. Berthold, J. Stakeberg, J. E. Celis, C. Betsholtz, J. E. Eriksson and M. Pekny (1999). Intermediate filament protein partnership in astrocytes. *J Biol Chem* 274(34): 23996-24006.
- Eng, L. F., R. S. Ghirnikar and Y. L. Lee (2000). Glial fibrillary acidic protein: GFAP-thirty-one years (1969-2000). *Neurochem Res* 25(9-10): 1439-1451.
- Evanko, D. S., Q. Zhang, R. Zorec and P. G. Haydon (2004). Defining pathways of loss and secretion of chemical messengers from astrocytes. *Glia* 47(3): 233-240.
- Everaerts, W., B. Nilius and G. Owsianik (2010). The vanilloid transient receptor potential channel TRPV4: from structure to disease. *Prog Biophys Mol Biol* 103(1): 2-17.
- Everaerts, W., X. Zhen, D. Ghosh, J. Vriens, T. Gevaert, J. P. Gilbert, N. J. Hayward, C. R. McNamara, F. Xue, M. M. Moran, T. Strassmaier, E. Uykai, G. Owsianik, R. Vennekens, D. De Ridder, B. Nilius, C. M. Fanger and T. Voets (2010). Inhibition of the cation channel TRPV4 improves bladder function in mice and rats with cyclophosphamide-induced cystitis. *Proc Natl Acad Sci U S A* 107(44): 19084-19089.
- Fan, H. C., X. Zhang and P. A. McNaughton (2009). Activation of the TRPV4 ion channel is enhanced by phosphorylation. *J Biol Chem* 284(41): 27884-27891.
- Fernandes, J., I. M. Lorenzo, Y. N. Andrade, A. Garcia-Elias, S. A. Serra, J. M. Fernandez-Fernandez and M. A. Valverde (2008). IP3 sensitizes TRPV4 channel to the mechano-

- and osmotransducing messenger 5'-6'-epoxyeicosatrienoic acid. *J Gen Physiol* 131(5): i2.
- Fillenz, M. (2005). The role of lactate in brain metabolism. *Neurochem Int* 47(6): 413-417.
- Franke, H., A. Verkhratsky, G. Burnstock and P. Illes (2012). Pathophysiology of astroglial purinergic signalling. *Purinergic Signal* 8(3): 629-657.
- Garcia-Barcina, J. M. and C. Matute (1996). Expression of kainate-selective glutamate receptor subunits in glial cells of the adult bovine white matter. *Eur J Neurosci* 8(11): 2379-2387.
- García-Cáceres, C., E. Fuente-Matrín, J. Argente and J. A. Chowen (2012). Emerging role of glial cells in the control of body weight. *Molecular Metabolism* 1(1-2): 37-46.
- Gees, M., B. Colsoul and B. Nilius (2010). The role of transient receptor potential cation channels in Ca²⁺ signaling. *Cold Spring Harb Perspect Biol* 2(10): a003962.
- Grandl, J., S. E. Kim, V. Uzzell, B. Bursulaya, M. Petrus, M. Bandell and A. Patapoutian (2010). Temperature-induced opening of TRPV1 ion channel is stabilized by the pore domain. *Nat Neurosci* 13(6): 708-714.
- Gurer, G., Y. Gursoy-Ozdemir, E. Erdemli, A. Can and T. Dalkara (2009). Astrocytes are more resistant to focal cerebral ischemia than neurons and die by a delayed necrosis. *Brain Pathol* 19(4): 630-641.
- Harukuni, I. and A. Bhardwaj (2006). Mechanisms of brain injury after global cerebral ischemia. *Neurologic Clinics* 24(1): 1-+.
- Hendrickson, M. L., A. J. Rao, O. N. Demerdash and R. E. Kalil (2011). Expression of nestin by neural cells in the adult rat and human brain. *PLoS One* 6(4): e18535.
- Higashi, K., A. Fujita, A. Inanobe, M. Tanemoto, K. Doi, T. Kubo and Y. Kurachi (2001). An inwardly rectifying K(+) channel, Kir4.1, expressed in astrocytes surrounds synapses and blood vessels in brain. *Am J Physiol Cell Physiol* 281(3): C922-931.
- Hill, K., N. J. Tigue, R. E. Kelsell, C. D. Benham, S. McNulty, M. Schaefer and A. D. Randall (2006). Characterisation of recombinant rat TRPM2 and a TRPM2-like conductance in cultured rat striatal neurones. *Neuropharmacology* 50(1): 89-97.
- Honsa, P., H. Pivonkova, D. Dzamba, M. Filipova and M. Anderova (2012). Polydendrocytes display large lineage plasticity following focal cerebral ischemia. *PLoS One* 7(5): e36816.
- Imai, Y., I. Ibata, D. Ito, K. Ohsawa and S. Kohsaka (1996). A novel gene *iba1* in the major histocompatibility complex class III region encoding an EF hand protein expressed in a monocytic lineage. *Biochem Biophys Res Commun* 224(3): 855-862.
- Ito, D., K. Tanaka, S. Suzuki, T. Dembo and Y. Fukuuchi (2001). Enhanced expression of *Iba1*, ionized calcium-binding adapter molecule 1, after transient focal cerebral ischemia in rat brain. *Stroke* 32(5): 1208-1215.

- James, G. and A. M. Butt (2002). P2Y and P2X purinoceptor mediated Ca²⁺ signalling in glial cell pathology in the central nervous system. *Eur J Pharmacol* 447(2-3): 247-260.
- Jia, Y., X. Wang, L. Varty, C. A. Rizzo, R. Yang, C. C. Correll, P. T. Phelps, R. W. Egan and J. A. Hey (2004). Functional TRPV4 channels are expressed in human airway smooth muscle cells. *Am J Physiol Lung Cell Mol Physiol* 287(2): L272-278.
- Jin, R., G. Yang and G. Li (2010). Inflammatory mechanisms in ischemic stroke: role of inflammatory cells. *J Leukoc Biol* 87(5): 779-789.
- Jung, C., C. Fandos, I. M. Lorenzo, C. Plata, J. Fernandes, G. G. Gene, E. Vazquez and M. A. Valverde (2009). The progesterone receptor regulates the expression of TRPV4 channel. *Pflugers Arch* 459(1): 105-113.
- Kauer, J. A. and H. E. Gibson (2009). Hot flash: TRPV channels in the brain. *Trends in Neurosciences* 32(4): 215-224.
- Kim, D. (2005). Physiology and pharmacology of two-pore domain potassium channels. *Curr Pharm Des* 11(21): 2717-2736.
- Kimelberg, H. K. (2005). Astrocytic swelling in cerebral ischemia as a possible cause of injury and target for therapy. *Glia* 50(4): 389-397.
- Kimelberg, H. K., B. A. Macvicar and H. Sontheimer (2006). Anion channels in astrocytes: biophysics, pharmacology, and function. *Glia* 54(7): 747-757.
- Kimelberg, H. K. and M. Nedergaard (2010). Functions of astrocytes and their potential as therapeutic targets. *Neurotherapeutics* 7(4): 338-353.
- Kirischuk, S., H. Kettenmann and A. Verkhratsky (1997). Na⁺/Ca²⁺ exchanger modulates kainate-triggered Ca²⁺ signaling in Bergmann glial cells in situ. *Faseb Journal* 11(7): 566-572.
- Kirischuk, S., H. Kettenmann and A. Verkhratsky (2007). Membrane currents and cytoplasmic sodium transients generated by glutamate transport in Bergmann glial cells. *Pflugers Arch* 454(2): 245-252.
- Kirischuk, S., V. Parpura and A. Verkhratsky (2012). Sodium dynamics: another key to astroglial excitability? *Trends in Neurosciences* 35(8): 497-506.
- Kofuji, P. and E. A. Newman (2004). Potassium buffering in the central nervous system. *Neuroscience* 129(4): 1045-1056.
- Krebs, C., H. B. Fernandes, C. Sheldon, L. A. Raymond and K. G. Baimbridge (2003). Functional NMDA receptor subtype 2B is expressed in astrocytes after ischemia in vivo and anoxia in vitro. *Journal of Neuroscience* 23(8): 3364-3372.
- Kuan, C. Y., A. J. Schloemer, A. Lu, K. A. Burns, W. L. Weng, M. T. Williams, K. I. Strauss, C. V. Vorhees, R. A. Flavell, R. J. Davis, F. R. Sharp and P. Rakic (2004). Hypoxia-ischemia induces DNA synthesis without cell proliferation in dying neurons in adult rodent brain. *Journal of Neuroscience* 24(47): 10763-10772.

- Kuffler, S. W., J. G. Nicholls and R. K. Orkand (1966). Physiological properties of glial cells in the central nervous system of amphibia. *J Neurophysiol* 29(4): 768-787.
- Lalo, U., Y. Pankratov, F. Kirchhoff, R. A. North and A. Verkhratsky (2006). NMDA receptors mediate neuron-to-glia signaling in mouse cortical astrocytes. *Journal of Neuroscience* 26(10): 2673-2683.
- Lalo, U., A. Verkhratsky and Y. Pankratov (2011). Ionotropic ATP receptors in neuronal-glia communication. *Semin Cell Dev Biol* 22(2): 220-228.
- Lanciotti, A., M. S. Brignone, P. Molinari, S. Visentin, C. De Nuccio, G. Macchia, C. Aiello, E. Bertini, F. Aloisi, T. C. Petrucci and E. Ambrosini (2012). Megalencephalic leukoencephalopathy with subcortical cysts protein 1 functionally cooperates with the TRPV4 cation channel to activate the response of astrocytes to osmotic stress: dysregulation by pathological mutations. *Hum Mol Genet* 21(10): 2166-2180.
- Latour, I., J. Hamid, A. M. Beedle, G. W. Zamponi and B. A. Macvicar (2003). Expression of voltage-gated Ca²⁺ channel subtypes in cultured astrocytes. *Glia* 41(4): 347-353.
- Leffler, A., R. M. Linte, C. Nau, P. Reeh and A. Babes (2007). A high-threshold heat-activated channel in cultured rat dorsal root ganglion neurons resembles TRPV2 and is blocked by gadolinium. *European Journal of Neuroscience* 26(1): 12-22.
- Leis, J. A., L. K. Bekar and W. Walz (2005). Potassium homeostasis in the ischemic brain. *Glia* 50(4): 407-416.
- Li, L., W. Qu, L. Zhou, Z. Lu, P. Jie and L. Chen (2013). Activation of Transient Receptor Potential Vanilloid 4 Increases NMDA-Activated Current in Hippocampal Pyramidal Neurons. *Front Cell Neurosci* 7: 17.
- Li, Y., L. A. Holtzclaw and J. T. Russell (2001). Muller cell Ca²⁺ waves evoked by purinergic receptor agonists in slices of rat retina. *J Neurophysiol* 85(2): 986-994.
- Liedtke, W. (2006). Transient receptor potential vanilloid channels functioning in transduction of osmotic stimuli. *J Endocrinol* 191(3): 515-523.
- Lipski, J., T. I. Park, D. Li, S. C. Lee, A. J. Trevarton, K. K. Chung, P. S. Freestone and J. Z. Bai (2006). Involvement of TRP-like channels in the acute ischemic response of hippocampal CA1 neurons in brain slices. *Brain Research* 1077(1): 187-199.
- Lipton, P. (1999). Ischemic cell death in brain neurons. *Physiol Rev* 79(4): 1431-1568.
- Liu, W., Y. Tang and J. Feng (2011). Cross talk between activation of microglia and astrocytes in pathological conditions in the central nervous system. *Life Sci* 89(5-6): 141-146.
- Liu, X., B. C. Bandyopadhyay, T. Nakamoto, B. Singh, W. Liedtke, J. E. Melvin and I. Ambudkar (2006). A role for AQP5 in activation of TRPV4 by hypotonicity: concerted involvement of AQP5 and TRPV4 in regulation of cell volume recovery. *J Biol Chem* 281(22): 15485-15495.
- Lo, E. H., T. Dalkara and M. A. Moskowitz (2003). Mechanisms, challenges and opportunities in stroke. *Nature Reviews Neuroscience* 4(5): 399-415.

- Lukaszevicz, A. C., N. Sampaio, C. Guegan, A. Benchoua, C. Couriaud, E. Chevalier, B. Sola, P. Lacombe and B. Onteniente (2002). High sensitivity of protoplasmic cortical astroglia to focal ischemia. *J Cereb Blood Flow Metab* 22(3): 289-298.
- Lytle, J. M., R. Chittajallu, J. R. Wrathall and V. Gallo (2009). NG2 cell response in the CNP-EGFP mouse after contusive spinal cord injury. *Glia* 57(3): 270-285.
- Magistretti, P. J. (2006). Neuron-glia metabolic coupling and plasticity. *J Exp Biol* 209(Pt 12): 2304-2311.
- Makara, J. K., A. Rappert, K. Matthias, C. Steinhauser, A. Spat and H. Kettenmann (2003). Astrocytes from mouse brain slices express CIC-2-mediated Cl⁻ currents regulated during development and after injury. *Mol Cell Neurosci* 23(4): 521-530.
- Manning, T. J., Jr. and H. Sontheimer (1997). Spontaneous intracellular calcium oscillations in cortical astrocytes from a patient with intractable childhood epilepsy (Rasmussen's encephalitis). *Glia* 21(3): 332-337.
- Matsuda, T., N. Arakawa, K. Takuma, Y. Kishida, Y. Kawasaki, M. Sakaue, K. Takahashi, T. Takahashi, T. Suzuki, T. Ota, A. Hamano-Takahashi, M. Onishi, Y. Tanaka, K. Kameo and A. Baba (2001). SEA0400, a novel and selective inhibitor of the Na⁺-Ca²⁺ exchanger, attenuates reperfusion injury in the in vitro and in vivo cerebral ischemic models. *Journal of Pharmacology and Experimental Therapeutics* 298(1): 249-256.
- Matsumoto, H., Y. Kumon, H. Watanabe, T. Ohnishi, M. Shudou, M. Chuai, Y. Imai, H. Takahashi and J. Tanaka (2008). Accumulation of macrophage-like cells expressing NG2 proteoglycan and Ibal in ischemic core of rat brain after transient middle cerebral artery occlusion. *J Cereb Blood Flow Metab* 28(1): 149-163.
- Matthias, K., F. Kirchhoff, G. Seifert, K. Huttmann, M. Matyash, H. Kettenmann and C. Steinhauser (2003). Segregated expression of AMPA-type glutamate receptors and glutamate transporters defines distinct astrocyte populations in the mouse hippocampus. *Journal of Neuroscience* 23(5): 1750-1758.
- Matyash, V. and H. Kettenmann (2010). Heterogeneity in astrocyte morphology and physiology. *Brain Res Rev* 63(1-2): 2-10.
- McDermott, K. W., D. S. Barry and S. S. McMahon (2005). Role of radial glia in cytogenesis, patterning and boundary formation in the developing spinal cord. *Journal of Anatomy* 207(3): 241-250.
- Meng, F., W. K. To and Y. Gu (2008). Role of TRP channels and NCX in mediating hypoxia-induced [Ca²⁺]_i elevation in PC12 cells. *Respir Physiol Neurobiol* 164(3): 386-393.
- Metea, M. R. and E. A. Newman (2006). Calcium signaling in specialized glial cells. *Glia* 54(7): 650-655.
- Middeldorp, J. and E. M. Hol (2011). GFAP in health and disease. *Progress in Neurobiology* 93(3): 421-443.

- Miller, B., M. Sarantis, S. F. Traynelis and D. Attwell (1992). Potentiation of NMDA receptor currents by arachidonic acid. *Nature* 355(6362): 722-725.
- Miller, B. A. and W. Zhang (2011). TRP channels as mediators of oxidative stress. *Adv Exp Med Biol* 704: 531-544.
- Mitterauer, B. (2010). Significance of the astrocyte domain organization for qualitative information structuring in the brain. *Advances in Bioscience and Biotechnology* 1: 391-397.
- Mongin, A. A. and H. K. Kimelberg (2005). ATP regulates anion channel-mediated organic osmolyte release from cultured rat astrocytes via multiple Ca²⁺-sensitive mechanisms. *Am J Physiol Cell Physiol* 288(1): C204-213.
- Montana, V., E. B. Malarkey, C. Verderio, M. Matteoli and V. Parpura (2006). Vesicular transmitter release from astrocytes. *Glia* 54(7): 700-715.
- Montgomery, D. L. (1994). Astrocytes - Form, Functions, and Roles in Disease. *Veterinary Pathology* 31(2): 145-167.
- Musset, B., S. G. Meuth, G. X. Liu, C. Derst, S. Wegner, H. C. Pape, T. Budde, R. Preisig-Muller and J. Daut (2006). Effects of divalent cations and spermine on the K⁺ channel TASK-3 and on the outward current in thalamic neurons. *J Physiol* 572(Pt 3): 639-657.
- Nagelhus, E. A., T. M. Mathiesen and O. P. Ottersen (2004). Aquaporin-4 in the central nervous system: cellular and subcellular distribution and coexpression with KIR4.1. *Neuroscience* 129(4): 905-913.
- Nedergaard, M., B. Ransom and S. A. Goldman (2003). New roles for astrocytes: redefining the functional architecture of the brain. *Trends in Neurosciences* 26(10): 523-530.
- Nedergaard, M., J. J. Rodriguez and A. Verkhratsky (2010). Glial calcium and diseases of the nervous system. *Cell Calcium* 47(2): 140-149.
- Nedergaard, M., T. Takano and A. J. Hansen (2002). Beyond the role of glutamate as a neurotransmitter. *Nat Rev Neurosci* 3(9): 748-755.
- Nett, W. J., S. H. Oloff and K. D. McCarthy (2002). Hippocampal astrocytes in situ exhibit calcium oscillations that occur independent of neuronal activity. *J Neurophysiol* 87(1): 528-537.
- Nikonenko, A. G., L. Radenovic, P. R. Andjus and G. G. Skibo (2009). Structural features of ischemic damage in the hippocampus. *Anat Rec (Hoboken)* 292(12): 1914-1921.
- Nilius, B., G. Owsianik, T. Voets and J. A. Peters (2007). Transient receptor potential cation channels in disease. *Physiol Rev* 87(1): 165-217.
- Nilius, B., K. Talavera, G. Owsianik, J. Prenen, G. Droogmans and T. Voets (2005). Gating of TRP channels: a voltage connection? *J Physiol* 567(Pt 1): 35-44.

- Nilius, B., J. Vriens, J. Prenen, G. Droogmans and T. Voets (2004). TRPV4 calcium entry channel: a paradigm for gating diversity. *American Journal of Physiology-Cell Physiology* 286(2): C195-C205.
- Nimmerjahn, A., F. Kirchhoff, J. N. Kerr and F. Helmchen (2004). Sulforhodamine 101 as a specific marker of astroglia in the neocortex in vivo. *Nat Methods* 1(1): 31-37.
- O'Neil, R. G. and R. C. Brown (2003). The vanilloid receptor family of calcium-permeable channels: Molecular integrators of microenvironmental stimuli. *News in Physiological Sciences* 18: 226-231.
- O'Neil, R. G. and S. Heller (2005). The mechanosensitive nature of TRPV channels. *Pflugers Archiv-European Journal of Physiology* 451(1): 193-203.
- Oberheim, N. A., S. A. Goldman and M. Nedergaard (2012). Heterogeneity of astrocytic form and function. *Methods Mol Biol* 814: 23-45.
- Oberheim, N. A., G. F. Tian, X. Han, W. Peng, T. Takano, B. Ransom and M. Nedergaard (2008). Loss of astrocytic domain organization in the epileptic brain. *Journal of Neuroscience* 28(13): 3264-3276.
- Ordy, J. M., T. M. Wengenack, P. Bialobok, P. D. Coleman, P. Rodier, R. B. Baggs, W. P. Dunlap and B. Kates (1993). Selective vulnerability and early progression of hippocampal CA1 pyramidal cell degeneration and GFAP-positive astrocyte reactivity in the rat four-vessel occlusion model of transient global ischemia. *Exp Neurol* 119(1): 128-139.
- Owsianik, G., K. Talavera, T. Voets and B. Nilius (2006). Permeation and selectivity of TRP channels. *Annu Rev Physiol* 68: 685-717.
- Paluzzi, S., S. Alloisio, S. Zappettini, M. Milanese, L. Raiteri, M. Nobile and G. Bonanno (2007). Adult astroglia is competent for Na⁺/Ca²⁺ exchanger-operated exocytotic glutamate release triggered by mild depolarization. *Journal of Neurochemistry* 103(3): 1196-1207.
- Papadopoulos, M. C. and A. S. Verkman (2007). Aquaporin-4 and brain edema. *Pediatr Nephrol* 22(6): 778-784.
- Parkerson, K. A. and H. Sontheimer (2003). Contribution of chloride channels to volume regulation of cortical astrocytes. *Am J Physiol Cell Physiol* 284(6): C1460-1467.
- Parpura, V., V. Grubisic and A. Verkhratsky (2011). Ca²⁺ sources for the exocytotic release of glutamate from astrocytes. *Biochimica Et Biophysica Acta* 1813(5): 984-991.
- Parpura, V. and A. Verkhratsky (2012). The astrocyte excitability brief: from receptors to gliotransmission. *Neurochem Int* 61(4): 610-621.
- Pedersen, S. F., G. Owsianik and B. Nilius (2005). TRP channels: an overview. *Cell Calcium* 38(3-4): 233-252.
- Pekny, M., U. Wilhelmsson, Y. R. Bogestal and M. Pekna (2007). The role of astrocytes and complement system in neural plasticity. *Int Rev Neurobiol* 82: 95-111.

- Pforte, C., P. Henrich-Noack, K. Baldauf and K. G. Reymann (2005). Increase in proliferation and gliogenesis but decrease of early neurogenesis in the rat forebrain shortly after transient global ischemia. *Neuroscience* 136(4): 1133-1146.
- Pivonkova, H., J. Benesova, O. Butenko, A. Chvatal and M. Anderova (2010). Impact of global cerebral ischemia on K⁺ channel expression and membrane properties of glial cells in the rat hippocampus. *Neurochemistry International* 57(7): 783-794.
- Plant, T. D. and R. Strotmann (2007). TRPV4: A Multifunctional Nonselective Cation Channel with Complex Regulation.
- Porter, J. T. and K. D. McCarthy (1997). Astrocytic neurotransmitter receptors in situ and in vivo. *Progress in Neurobiology* 51(4): 439-455.
- Price, D. L., J. W. Ludwig, H. Mi, T. L. Schwarz and M. H. Ellisman (2002). Distribution of rSlo Ca²⁺-activated K⁺ channels in rat astrocyte perivascular endfeet. *Brain Research* 956(2): 183-193.
- Ramsey, I. S., M. Delling and D. E. Clapham (2006). An introduction to TRP channels. *Annu Rev Physiol* 68: 619-647.
- Rao, S. P. and S. K. Sikdar (2006). Astrocytes in 17beta-estradiol treated mixed hippocampal cultures show attenuated calcium response to neuronal activity. *Glia* 53(8): 817-826.
- Rock, M. J., J. Prenen, V. A. Funari, T. L. Funari, B. Merriman, S. F. Nelson, R. S. Lachman, W. R. Wilcox, S. Reyno, R. Quadrelli, A. Vaglio, G. Owsianik, A. Janssens, T. Voets, S. Ikegawa, T. Nagai, D. L. Rimoin, B. Nilius and D. H. Cohn (2008). Gain-of-function mutations in TRPV4 cause autosomal dominant brachyolmia. *Nat Genet* 40(8): 999-1003.
- Rojas, H., C. Colina, M. Ramos, G. Benaim, E. H. Jaffe, C. Caputo and R. DiPolo (2007). Na⁺ entry via glutamate transporter activates the reverse Na⁺/Ca²⁺ exchange and triggers Ca²⁺-induced Ca²⁺ release in rat cerebellar Type-1 astrocytes. *Journal of Neurochemistry* 100(5): 1188-1202.
- Rossi, D. J., J. D. Brady and C. Mohr (2007). Astrocyte metabolism and signaling during brain ischemia. *Nat Neurosci* 10(11): 1377-1386.
- Rothermundt, M., M. Peters, J. H. Prehn and V. Arolt (2003). S100B in brain damage and neurodegeneration. *Microsc Res Tech* 60(6): 614-632.
- Runnels, L. W. (2011). TRPM6 and TRPM7: A Mul-TRP-PLIK-cation of channel functions. *Curr Pharm Biotechnol* 12(1): 42-53.
- Sas, K., H. Robotka, E. Rozsa, M. Agoston, G. Szenasi, G. Gigler, M. Marosi, Z. Kis, T. Farkas, L. Vecsei and J. Toldi (2008). Kynurenine diminishes the ischemia-induced histological and electrophysiological deficits in the rat hippocampus. *Neurobiol Dis* 32(2): 302-308.
- Scemes, E. and C. Giaume (2006). Astrocyte calcium waves: what they are and what they do. *Glia* 54(7): 716-725.

- Schmidt-Kastner, R., K. Wietasch, H. Weigel and U. T. Eysel (1993). Immunohistochemical staining for glial fibrillary acidic protein (GFAP) after deafferentation or ischemic infarction in rat visual system: features of reactive and damaged astrocytes. *International Journal of Developmental Neuroscience* 11(2): 157-174.
- Seifert, G., K. Huttmann, D. K. Binder, C. Hartmann, A. Wyczynski, C. Neusch and C. Steinhauser (2009). Analysis of astroglial K⁺ channel expression in the developing hippocampus reveals a predominant role of the Kir4.1 subunit. *Journal of Neuroscience* 29(23): 7474-7488.
- Seifert, G., K. Schilling and C. Steinhauser (2006). Astrocyte dysfunction in neurological disorders: a molecular perspective. *Nat Rev Neurosci* 7(3): 194-206.
- Sen, J. and A. Belli (2007). S100B in neuropathologic states: the CRP of the brain? *J Neurosci Res* 85(7): 1373-1380.
- Shibasaki, K., Y. Ishizaki and S. Mandadi (2013). Astrocytes express functional TRPV2 ion channels. *Biochem Biophys Res Commun* 441(2): 327-332.
- Shibasaki, K., M. Suzuki, A. Mizuno and M. Tominaga (2007). Effects of body temperature on neural activity in the hippocampus: regulation of resting membrane potentials by transient receptor potential vanilloid 4. *Journal of Neuroscience* 27(7): 1566-1575.
- Sik, A., R. L. Smith and T. F. Freund (2000). Distribution of chloride channel-2-immunoreactive neuronal and astrocytic processes in the hippocampus. *Neuroscience* 101(1): 51-65.
- Simard, M. and M. Nedergaard (2004). The neurobiology of glia in the context of water and ion homeostasis. *Neuroscience* 129(4): 877-896.
- Sizonenko, S. V., E. J. Camm, A. Dayer and J. Z. Kiss (2008). Glial responses to neonatal hypoxic-ischemic injury in the rat cerebral cortex. *International Journal of Developmental Neuroscience* 26(1): 37-45.
- Small, D. L., P. Morley and A. M. Buchan (1999). Biology of ischemic cerebral cell death. *Prog Cardiovasc Dis* 42(3): 185-207.
- Smirkin, A., H. Matsumoto, H. Takahashi, A. Inoue, M. Tagawa, S. Ohue, H. Watanabe, H. Yano, Y. Kumon, T. Ohnishi and J. Tanaka (2010). Iba1(+)/NG2(+) macrophage-like cells expressing a variety of neuroprotective factors ameliorate ischemic damage of the brain. *J Cereb Blood Flow Metab* 30(3): 603-615.
- Smith, G. D., J. Gunthorpe, R. E. Kelsell, P. D. Hayes, P. Reilly, P. Facer, J. E. Wright, J. C. Jerman, J. P. Walhin, L. Ooi, J. Egerton, K. J. Charles, D. Smart, A. D. Randall, P. Anand and J. B. Davis (2002). TRPV3 is a temperature-sensitive vanilloid receptor-like protein. *Nature* 418(6894): 186-190.
- Sofroniew, M. V. and H. V. Vinters (2010). Astrocytes: biology and pathology. *Acta Neuropathol* 119(1): 7-35.
- Sontheimer, H., J. A. Black and S. G. Waxman (1996). Voltage-gated Na⁺ channels in glia: properties and possible functions. *Trends in Neurosciences* 19(8): 325-331.

- Steinhauser, C., R. Jabs and H. Kettenmann (1994). Properties of GABA and glutamate responses in identified glial cells of the mouse hippocampal slice. *Hippocampus* 4(1): 19-35.
- Straub, S. V. and M. T. Nelson (2007). Astrocytic calcium signaling: The information currency coupling neuronal activity to the cerebral microcirculation. *Trends in Cardiovascular Medicine* 17(6): 183-190.
- Strotmann, R., G. Schultz and T. D. Plant (2003). Ca²⁺-dependent potentiation of the nonselective cation channel TRPV4 is mediated by a C-terminal calmodulin binding site. *J Biol Chem* 278(29): 26541-26549.
- Strotmann, R., M. Semtner, F. Kepura, T. D. Plant and T. Schoneberg (2010). Interdomain interactions control Ca²⁺-dependent potentiation in the cation channel TRPV4. *PLoS One* 5(5): e10580.
- Sugawara, T., A. Lewen, N. Noshita, Y. Gasche and P. H. Chan (2002). Effects of global ischemia duration on neuronal, astroglial, oligodendroglial, and microglial reactions in the vulnerable hippocampal CA1 subregion in rats. *J Neurotrauma* 19(1): 85-98.
- Sun, M. C., C. R. Honey, C. Berk, N. L. Wong and J. K. Tsui (2003). Regulation of aquaporin-4 in a traumatic brain injury model in rats. *J Neurosurg* 98(3): 565-569.
- Syntichaki, P. and N. Tavernarakis (2002). Death by necrosis. Uncontrollable catastrophe, or is there order behind the chaos? *EMBO Rep* 3(7): 604-609.
- Szeto, H. H. (2006). Cell-permeable, mitochondrial-targeted, peptide antioxidants. *AAPS J* 8(2): E277-283.
- Takano, T., N. Oberheim, M. L. Cotrina and M. Nedergaard (2009). Astrocytes and ischemic injury. *Stroke* 40(3 Suppl): S8-12.
- Takuma, K., T. Matsuda, H. Hashimoto, S. Asano and A. Baba (1994). Cultured rat astrocytes possess Na⁽⁺⁾-Ca²⁺ exchanger. *Glia* 12(4): 336-342.
- Tang, X., K. Taniguchi and P. Kofuji (2009). Heterogeneity of Kir4.1 channel expression in glia revealed by mouse transgenesis. *Glia* 57(16): 1706-1715.
- Tao, Y. X., J. Gu and R. L. Stephens, Jr. (2005). Role of spinal cord glutamate transporter during normal sensory transmission and pathological pain states. *Mol Pain* 1: 30.
- Thorneloe, K. S., A. C. Sulpizio, Z. J. Lin, D. J. Figueroa, A. K. Clouse, G. P. McCafferty, T. P. Chendrimada, E. S. R. Lashinger, E. Gordon, L. Evans, B. A. Misajet, D. J. DeMarini, J. H. Nation, L. N. Casillas, R. W. Marquis, B. J. Votta, S. A. Sheardown, X. P. Xu, D. P. Brooks, N. J. Laping and T. D. Westfall (2008). N-((1S)-1-[[4-((2S)-2-[[[(2,4-dichlorophenyl)sulfonyl]amino]-3-hydroxypropanoyl]-1-piperazinyl]carbonyl]-3-methylbutyl)-1-benzothiophene-2-carboxamide (GSK1016790A), a novel and potent transient receptor potential vanilloid 4 channel agonist induces urinary bladder contraction and hyperactivity: Part I. *Journal of Pharmacology and Experimental Therapeutics* 326(2): 432-442.
- VanGilder, R. L., J. D. Huber, C. L. Rosen and T. L. Barr (2012). The transcriptome of cerebral ischemia. *Brain Research Bulletin* 88(4): 313-319.

- Verkhatsky, A., M. Anderova and A. Chvatal (2009). Differential calcium signalling in neuronal-glia networks. *Front Biosci* 14: 2004-2016.
- Verkhatsky, A. and A. Butt (2007). *Glial Neurobiology*, John Wiley & Sons Ltd.
- Verkhatsky, A., O. A. Krishtal and G. Burnstock (2009). Purinoceptors on neuroglia. *Mol Neurobiol* 39(3): 190-208.
- Verkhatsky, A. and C. Steinhäuser (2000). Ion channels in glial cells. *Brain Res Brain Res Rev* 32(2-3): 380-412.
- Vincent, F., A. Acevedo, M. T. Nguyen, M. Dourado, J. DeFalco, A. Gustafson, P. Spiro, D. E. Emerling, M. G. Kelly and M. A. Duncton (2009). Identification and characterization of novel TRPV4 modulators. *Biochem Biophys Res Commun* 389(3): 490-494.
- Voets, T., J. Prenen, J. Vriens, H. Watanabe, A. Janssens, U. Wissenbach, M. Boddling, G. Droogmans and B. Nilius (2002). Molecular determinants of permeation through the cation channel TRPV4. *J Biol Chem* 277(37): 33704-33710.
- Voets, T., K. Talavera, G. Owsianik and B. Nilius (2005). Sensing with TRP channels. *Nat Chem Biol* 1(2): 85-92.
- Volterra, A. and J. Meldolesi (2005). Astrocytes, from brain glue to communication elements: the revolution continues. *Nat Rev Neurosci* 6(8): 626-640.
- Vriens, J., G. Appendino and B. Nilius (2009). Pharmacology of vanilloid transient receptor potential cation channels. *Molecular Pharmacology* 75(6): 1262-1279.
- Walz, W. (2000). Role of astrocytes in the clearance of excess extracellular potassium. *Neurochem Int* 36(4-5): 291-300.
- Walz, W. (2002). Chloride/anion channels in glial cell membranes. *Glia* 40(1): 1-10.
- Walz, W. and W. A. Wuttke (1999). Independent mechanisms of potassium clearance by astrocytes in gliotic tissue. *J Neurosci Res* 56(6): 595-603.
- Wang, D. D. and A. Bordey (2008). The astrocyte odyssey. *Progress in Neurobiology* 86(4): 342-367.
- Wang, X., N. Lou, Q. Xu, G. F. Tian, W. G. Peng, X. Han, J. Kang, T. Takano and M. Nedergaard (2006). Astrocytic Ca²⁺ signaling evoked by sensory stimulation in vivo. *Nat Neurosci* 9(6): 816-823.
- Watanabe, H., J. Vriens, A. Janssens, R. Wondergem, G. Droogmans and B. Nilius (2003). Modulation of TRPV4 gating by intra- and extracellular Ca²⁺. *Cell Calcium* 33(5-6): 489-495.
- Watanabe, H., J. Vriens, J. Prenen, G. Droogmans, T. Voets and B. Nilius (2003). Anandamide and arachidonic acid use epoxyeicosatrienoic acids to activate TRPV4 channels. *Nature* 424(6947): 434-438.

- Wei, L., D. J. Ying, L. Cui, J. Langsdorf and S. P. Yu (2004). Necrosis, apoptosis and hybrid death in the cortex and thalamus after barrel cortex ischemia in rats. *Brain Research* 1022(1-2): 54-61.
- Yang, B., Z. Zador and A. S. Verkman (2008). Glial cell aquaporin-4 overexpression in transgenic mice accelerates cytotoxic brain swelling. *J Biol Chem* 283(22): 15280-15286.
- Zelenina, M. (2010). Regulation of brain aquaporins. *Neurochem Int* 57(4): 468-488.
- Zhao, J. W., R. Raha-Chowdhury, J. W. Fawcett and C. Watts (2009). Astrocytes and oligodendrocytes can be generated from NG2+ progenitors after acute brain injury: intracellular localization of oligodendrocyte transcription factor 2 is associated with their fate choice. *Eur J Neurosci* 29(9): 1853-1869.
- Zhou, M. and H. K. Kimelberg (2000). Freshly isolated astrocytes from rat hippocampus show two distinct current patterns and different [K⁺]_o uptake capabilities. *J Neurophysiol* 84(6): 2746-2757.
- Zhou, M., G. P. Schools and H. K. Kimelberg (2006). Development of GLAST(+) astrocytes and NG2(+) glia in rat hippocampus CA1: mature astrocytes are electrophysiologically passive. *J Neurophysiol* 95(1): 134-143.
- Zhou, M., G. Xu, M. Xie, X. Zhang, G. P. Schools, L. Ma, H. K. Kimelberg and H. Chen (2009). TWIK-1 and TREK-1 are potassium channels contributing significantly to astrocyte passive conductance in rat hippocampal slices. *Journal of Neuroscience* 29(26): 8551-8564.
- Zonta, M., M. C. Angulo, S. Gobbo, B. Rosengarten, K. A. Hossmann, T. Pozzan and G. Carmignoto (2003). Neuron-to-astrocyte signaling is central to the dynamic control of brain microcirculation. *Nature Neuroscience* 6(1): 43-50.

8. ATTACHMENTS

1. **Butenko O**, Dzamba D, Benesova J, Honsa P, Benfenati V, V. Rusnakova, S. Ferroni, M. Anderova. (2012) The Increased Activity of TRPV4 Channel in the Astrocytes of the Adult Rat Hippocampus after Cerebral Hypoxia/Ischemia. PLoS ONE. 7(6), IF 4.04
2. Pivonkova H., Benesova J., **Butenko O.**, Chvatal A., Anderova M. (2010) Impact of global cerebral ischemia on K(+) channel expression and membrane properties of glial cells in the rat hippocampus. *Neurochem Int.* 57 783-794, IF 3.54
3. Chvátal A., Anděrová M., Neprašová H., Prajerová I., Benešová J., **Butenko O.**, Verkhatsky A. (2008) Pathological potential of astroglia. *Physiol Res.* 2008; 57(3), IF 1.65
4. Benesova. J., Hock M., **Butenko O.**, Prajerova I., Anderova M., Chvatal A. (2009) Quantification of Astrocyte Volume Changes During Ischemia In Situ Reveals Two Populations of Astrocytes in the Cortex of GFAP/EGFP Mice. *Journal of Neuroscience Research* 87:96–111, IF 3.38